Aus dem Institut für Immunologie im Biomedizinischen Centrum

Institut der Ludwig-Maximilians-Universität München

Vorstand: Prof. Dr. rer. nat. Thomas Brocker

Reciprocal regulation of mTORC1 and ribosomal biosynthesis determines cell cycle progression in activated T cells

Dissertation

zum Erwerb des Doktorgrades der Naturwissenschaften

an der Medizinischen Fakultät der

Ludwig-Maximilians-Universität München

vorgelegt von

Teresa Rosenlehner, geb. Scheibenzuber

aus Gräfelfing

2023

Mit Genehmigung der Medizinischen Fakultät
der Ludwig-Maximilians-Universität München

Betreuer:	PD Dr. rer. nat. Reinhard Obst
Zweitgutachter:	PD Dr. rer. nat. Christof Geldmacher
Dekan:	Prof. Dr. med. Thomas Gudermann
Tag der mündlichen Prüfung:	10. Oktober 2024

Abstract

Anabolic metabolism of antigen-stimulated T cells is coordinated by mechanistic target of rapamycin (mTOR) which is activated by T cell receptor (TCR) and interleukin-2 (IL-2) signals. T cells rapidly shift their metabolism following activation and highly increase their protein and RNA production to prepare and maintain cellular proliferation and differentiation. mTOR is known to be a key transmitter of many of these processes, however, it remains unclear, how this massive biomass production and proliferation are coregulated and what role ribosomal RNA (rRNA) transcription plays in this process.

mTOR is a serine/threonine kinase that functions in the two complexes mTORC1 and mTORC2 with their main proteins Raptor and Rictor, respectively. Previous work in our lab showed that mTORC1 regulates both the exit of quiescence and later divisions as Raptor-deficient T cells proceed 3x slower through each cell division in vivo. This led to further questions that were investigated in this thesis by use of conditional knockout mice, as well as cell- and cytometry-based functional assays. We noticed that following stimulation the amount of RNA per cell increases 9-40x and is reduced to ~50% in Raptor, but not Rictor-deficient T cells. Using Coulter volume measurements, RNA-, FISH- and imaging flow cytometry we determined that following stimulation the cell volume increases five-fold. It consists of the increase of nuclear volume and nucleolar rRNA synthesis on day 1 and a further increase of cytoplasmic volume on day 2. Raptor-deficiency delays and reduces the growth of these cellular compartments, of ribosomal biosynthesis and the cell volume. Inhibitors of rRNA transcription block cell cycle progression at the G1/S and G2/M checkpoints. The lack of Raptor and Torin inhibition showed similar effects, suggesting a common mechanism. In experiments with rRNA transcription inhibitors we found that mTORC1 activity depends on RNA polymerase I activity in early T cell activation and that the two pathways are tightly linked.

Our data show that mTORC1-adjusted cell physiology and the biosynthesis of ribosomal 'hardware' are reciprocally regulated during clonal T cell expansion.

Zusammenfassung

Anaboler Stoffwechsel von Antigen-stimulierten T-Zellen wird von mechanistic target of rapamycin (mTOR) koordiniert, welches durch T-Zell-Rezeptor (TZR) und Interleukin-2 (IL-2) Signale aktiviert wird. T-Zellen verändern ihren Stoffwechsel schnell nach Aktivierung und erhöhen ihre Protein- und RNA-Produktion stark, um zelluläre Teilung und Differenzierung vorzubereiten und aufrechtzuerhalten. mTOR ist bekannt als ein Schlüssel-Transmitter bei vielen dieser Prozesse; dennoch bleibt unklar, wie diese massive Biomasseproduktion und Zellteilung koreguliert sind, und welche Rolle ribosomale RNA (rRNA) Transkription in diesem Prozess spielt.

mTOR ist eine Serin/Threonin-Kinase, die in den beiden Komplexen mTORC1 und mTORC2 mit ihren Hauptproteinen Raptor bzw. Rictor arbeitet. Vorherige Arbeit in unserem Labor zeigte, dass mTORC1 sowohl den „exit of quiescence“, als auch spätere Zellteilungen reguliert, da Raptor-defiziente T-Zellen 3x langsamer durch jede Zellteilung in vivo schreiten. Dies führte zu weiteren Fragen, die in dieser Arbeit untersucht wurden durch die Nutzung von konditionellen Knockout-Mäusen, sowie Zell- und Zytometrie-basierten funktionellen Methoden. Wir bemerkten, dass die RNA-Menge pro Zelle nach Stimulation 9-40x ansteigt und um 50% reduziert ist in Raptor-, aber nicht in Rictor-defizienten T-Zellen. Anhand von Volumenmessungen nach dem Coulter-Prinzip, RNA-, FISH- und bildgebender Durchflusszytometrie stellten wir fest, dass nach Stimulation das Zellvolumen fünffach ansteigt. Es besteht aus einem Anstieg des Nukleusvolumens und nucleolarer rRNA-Synthese and Tag 1, sowie einem weiteren Anstieg des Zytoplasmavolumens an Tag 2. Ein Raptordefizit verzögert und reduziert das Wachstum dieser zellulären Kompartimente, die ribosomale Biosynthese und das Zellvolumen. Inhibitoren von rRNA-Transkription blockieren den Zellzyklusfortlauf am G1/S und am G2/M Kontrollpunkt. Ein Raptordefizit und Torininhibierung zeigten ähnliche Effekte, was einen gemeinsamen Mechanismus andeutet. In Experimenten mit rRNA Transkriptionsinhibitoren fanden wir heraus, dass die Aktivität von mTORC1 abhängig ist von RNA Polymerase I Aktivität in früher T Zell Aktivierung und dass die beiden Wege eng miteinander verbunden sind.

Unsere Daten zeigen, dass die mTORC1-angepasste Zellphysiologie und die Biosynthese der ribosomalen Hardware wechselseitig während der klonalen T-Zell Expansion reguliert werden.

Table of Content

List of Figures

List of Tables

List of abbreviations

4E-BP	Eukaryotic translation initiation factor 4E-binding protein
ALL	Acute lymphatic leukemia
APC	Allophycocyanine
APS	Ammonium persulfate
BSA	Bovine serum albumin
CD	Cluster of differentiation
CDK	Cyclin-dependent kinase
CHH	Cartilage hair Hyploplasia
CTL	Cytotoxic T lymphocyte
CTR	CellTracker Red
CTV	CellTrace Violet
DAPI	4',6-Diamidino-2-phenylindole
DBA	Diamond Blackfan Anemia
DEPTOR	DEP domain containing mTOR interacting protein
DFC	Dense fibrillar component
DMEM	Dulbecco's modified Eagle medium
DMSO	Dimethylsulfoxide
DNA	Deoxyribonucleic acid
dNTP	Deoxynucleotide triphosphate
ECL	Enhanced chemiluminescence
EDTA	Ethylenediaminetetraacetic acid
EdU	5-ethynyl-2'-deoxyuridine
EGTA	Ethylene Glycol tetra acetic acid
Erk1/2	Extracellular-signal regulated kinase 1/2
ETS	External transcribed spacer
FACS	Fluorescence-activated cell sorting
FC	Fibrillar Center
FCS	Fetal calf serum
FDA	Food and Drug Administration
FISH	Fluorescence in situ hybridization
FITC	Fluorescein-5-isothiocyanate
FKBP	FK506 binding protein
FSC-A	Forward scatter area
FSC-H	Forward scatter height
FVD	Fixable viability dye
GC	Granular component

GFP	Green fluorescent protein
gMFI	Geometric mean fluorescence intensity
HPG	Homopropargylglycine
HRP	Horseradish peroxidase
i.p.	Intraperitoneal
i.v.	Intravenous
IKKß	Inhibitor of nuclear factor kappa B kinase subunit ß
IL	Interleukin
IL-2R	IL2 Receptor
kDa	Kilo Dalton
LCMV	Lymphocytic choriomeningitis virus
MACS	Magnetic-activated cell sorting
MHC	Major histocompatibility complex
mLST8	Mammalian lethal with SEC13 protein 8
mRNA	Messenger RNA
mSin1	mammalian stress-activated map kinase-interacting protein 1
mTOR	Mechanistic target of rapamycin
mTORC1	mTOR Complex 1
mTORC2	mTOR Complex 2
NK cells	Natural Killer cells
NPM1	Nucleophosmin 1
OVA	Ovalbumin
PBS	Phosphate buffered saline
PCR	Polymerase chain reaction
PE	Phycoerythrin
PFA	Paraformaldehyde
PI3K	Phosphoinositid-3-kinase
PIP_2	Phosphatidylinositol-4,5-bisphosphate
PIP_3	Phosphatidylinositol-3,4,5-trisphosphate
PKB	Protein kinase B
Pol I	Polymerase I
PRAS40	Proline-rich AKT substrate of 40 kDa
Protor1/2	protein observed with rictor 1 and 2
pS6	Phospho-S6
PTEN	Phosphatase and Tensin homolog
PY	Pyronin Y
QF	Quarfloxin
RA	Rheumatoid Arthritis
Raptor	Regulatory-associated protein of mTOR

Rb	Retinoblastoma
Rheb	Ras homolog enriched in brain
Rictor	Rapamycin-insensitive companion of mTOR
RMRP	RNA component of mitochondrial RNA processing endoribonuclease
RNA	Ribonucleic acid
RP	Ribosomal protein
RPMI	Roswell Park Memorial Institute Medium
rRNA	Ribosomal RNA
S6K	S6 Kinase
SA	Streptavidin
SDS	Sodium dodecylsulfate
SGK1	Serum/glucocorticoid regulated kinase 1
SREBP	Sterol regulatory element-binding protein
SSC	Side Scatter
Stat5	Signal transducer and activator of transcription 5
TAE	TRIS-acetate-EDTA
TBS	TRIS-buffered saline
TBS-T	TRIS-buffered saline with Tween20
TCR	T cell receptor
Tif1a	Transcription intermediary factor 1-alpha
TNF-a	Tumor necrosis factor alpha
TSC1	Tuberous sclerosis 1
UBF	Upstream binding transcription factor
UTR	Untranslated region

1. Introduction

1.1 Adaptive immune system

The immune system evolved in order to protect the host from pathogenic microbes, toxins and allergens, and at the same time tolerate beneficial and non-pathogenic microbes (Chaplin, 2010; Finlay and McFadden, 2006). It is comprised of an innate and an adaptive immune response which strongly work together and are essential for an intact and effective immune response.

The adaptive immune system consists mostly of T and B lymphocytes and is defined by specific immune responses that become effective several days post infection. After stimulation with a specific antigen, the cells become activated and undergo clonal expansion.

B cells derive from hematopoietic stem cell in the bone marrow and make up to 15% of peripheral blood leukocytes. They are defined by their B cell receptor and the production of Immunoglobulins. T cells develop as well from hematopoietic stem cells in the bone marrow and mature in the thymus where they undergo positive and negative selection to prevent the generation of autoimmune reactive cells (Klein et al., 2014). Besides this, each T cell is equipped with its specific T cell receptor (TCR) with single specificity before the cell is released into the periphery. A huge repertoire of T cells is required to cover the enormous range of microbes. The T cells recognize peptides bound to major histocompatibility complex (MHC) via their TCR and then proliferate by differentiating into subsets including $CD8^+$ T cells to kill infected target cells and $CD4^+$ T cells which are essential to regulate cellular and humoral immune responses (Chaplin, 2010). The activation and clonal expansion of T cells is a major topic of this thesis and will be introduced in detail in the following sections.

One specific characteristic of the adaptive immune response is the generation of an immune memory which is further introduced in section 1.2.2.

1.2 T cells

1.2.1 TCR signaling and activation

1.2.1.1 T cell receptor – pMHC interaction

T cell receptors (TCRs) recognize peptides bound to major histocompatibility complex (MHC) molecules leading to the activation of T cells. MHC class I molecules are expressed on the surface of all cells and can be recognized by $CD8^+$ T cells, while MHC class II is expressed on antigen-presenting cells such as B cells, dendritic cells and macrophages and are recognized by $CD4^+$ T cells. To avoid autoimmune defects, T cells are selected to distinguish self and non-self peptides which are presented by MHC with a high selectivity (Chakraborty and Weiss, 2014). Following stimulation by the TCR, several cascades of signaling pathways are engaged, causing changes at the membrane, the cytoplasm and in the nucleus to facilitate clonal expansion and differentiation to effector cells (Cantrell, 2002; Samelson, 2002).

One can distinguish between early signaling events taking place at the TCR in the first seconds after pMHC binding, and distal signaling events, resulting in the activation of various transcription factors and thus gene transcription.

The most important early TCR signaling components are the CD4-/CD8 coreceptor, to a lesser degree bound src family kinases LCK and FYN which phosphorylate immunoreceptor tyrosin-based activation motifs (ITAMs) at the intracellular tails of the CD3 molecules. Phosphorylation of ITAMs then further leads to the phosphorylation and activation of ZAP-70, which completes proximal early signaling (Shah et al., 2021).

These early signaling events result in the activation of various distal signaling pathways, including the PKC-IKK-NFkB, RAS-RAF-ERK1/2 and Ca^{2+}-calcineurin-NFAT cascade, as depicted schematically in Figure 1. Different adaptor proteins, second messengers and enzymes are required for these signaling cascades, whereas Phospholipase Cγ1 (PLCγ1) connects proximal to distal signaling (Beach et al., 2007). Beside those three signaling pathways, PI3K-TSC1/2-mTOR signaling plays an important role in T cell activation as well and will be further described in chapter 1.4.2.

Activated PLCγ1 cleaves membrane-bound phosphatidylinositol-4,5-bisphosphate (PIP_2) into inositol-3-phosphate (IP_3) and diacylglycerol (DAG) (Zhong et al., 2008). Both act as second messengers and initiate further signaling cascades such as PKC, RASGRPS1 and PDK1-mediated pathways by DAG, and the Ca^{2+}-dependent calcineurin NFAT pathway by IP_3 (Berridge, 2009; Oh-hora and Rao, 2008; Zhong et al., 2008).

Following TCR stimulation, intracellular Ca^{2+} levels are increased, which leads to the activation of calcineurin, a protein phosphatase. Calcineurin dephosphorylates nuclear factor of activated T cells (NFAT), which then translocates into the nucleus (Figure 1).

Protein kinase C (PKC) is a serine/threonine kinase which gets activated by diacylglycerin (DAG) and thus initiates the formation of the CBM complex which consists of the three proteins CARMA1, BCL10 and MALT1 (Lu et al., 2018; Meininger and Krappmann, 2016; Ruland and Hartjes, 2019). First, PKC phosphorylates CARMA1 (Matsumoto et al., 2005) which then enables the association with BCL10 (Weil and Israel, 2006) which is required to bind MALT1. As soon as the complex is formed, it associates with the tumor necrosis factor receptor-associated factor 6 (TRAF6) and subsequently IKKy, the inhibitory molecule of the Ikß pathway, is degraded (Sun et al., 2004). NF-kB is released from its inhibitory complex and translocates into the nucleus (Hayden et al., 2006; Hoffmann et al., 2006; So and Croft, 2012). The PKC-CBM-NF-kB pathway regulates the activation, homeostasis and survival of T cells and is thus an important pathway in T cell activation (Schulze-Luehrmann and Ghosh, 2006).

The third major signaling cascade is the Ras-Raf-Erk1/2 pathway which controls T cell differentiation, development, and TCR-induced signal strength (Bertin et al., 2015). RAS guanyl nucleotide-releasing protein (RASGRP1) is activated by DAG and recruited to the plasma membrane (Ebinu et al., 1998). There, RAS activates the serine/threonine kinase Raf1, which is a MAPK kinase kinase (MAPKKK) (Janknecht et al., 1993). It further phosphorylates MAPK kinases like MEK1/2 which in turn phosphorylate the MAPK extracellular signal-regulated kinase 1&2 (ERK1/2) (Janknecht et al., 1993; Kolch, 2005). Additionally, AP1-transcription factors JUN and FOS are activated and translocate into the nucleus (Kaminuma et al., 2001), where they form a complex with NFAT and start the transcription of genes that are essential for effector functions as well as IL-2 transcription, which is further sustained by the DAG-RAS pathway (Gorentla and Zhong, 2012; Samelson, 2002).

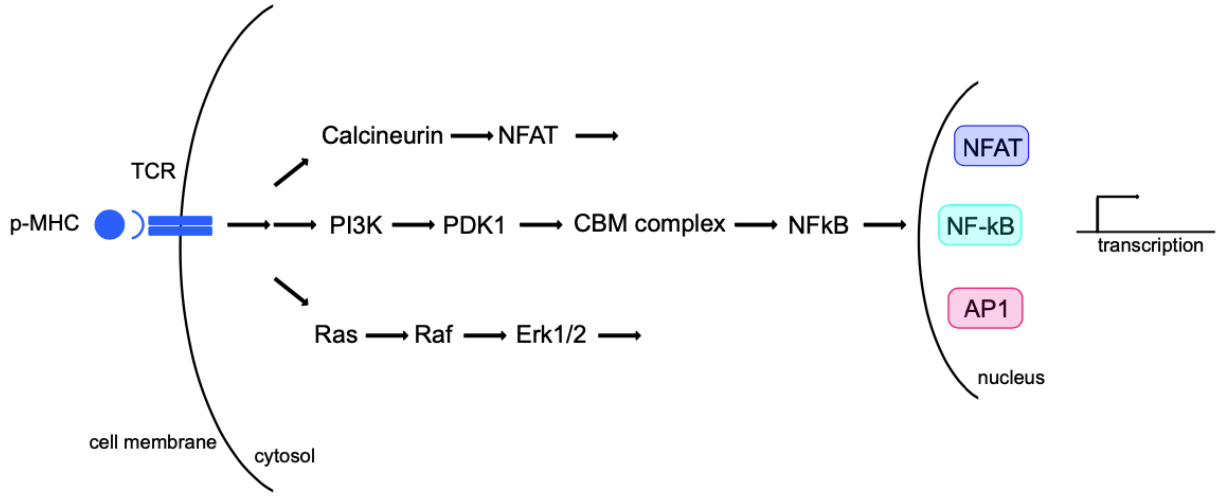

Figure 1: Schematic overview of TCR signaling.
When a peptide-MHC complex binds to the TCR, a signaling cascade is initiated in the T cell. The three classical TCR signaling pathways are shown – on top Calcineurin which activates NFAT and leads to its translocation into the nucleus. In the middle signaling via PI3K which leads to the activation of NF-kB via the CBM complex. On the bottom the Ras/Raf pathway which leads to the translocation of AP1 into the nucleus. Inside the nucleus, the transcription factors NFAT, NF-kB and AP1 start transcription.

1.2.1.2 Co-stimulation with CD28

Naïve T cells require a second signal for their full activation, which is mediated by costimulatory receptors. CD28 is constitutively expressed on naïve T cells and is a major costimulatory receptor expressed by T cells. Especially weak TCR signals are amplified by CD28, enabling differentiation and proliferation of the cell. Without co-stimulation, the T cells would undergo cell death or become anergic (Shah et al., 2021) due to a defect in the MAPK signaling pathway (ElTanbouly and Noelle, 2021; Fields et al., 1996; Li et al., 1996). Without productive costimulation, the transcription factor AP1 cannot translocate into the nucleus (Kang et al., 1992) which leads to an imbalance in downstream TCR signaling. Thereby, the activation of NFAT1 alone results in higher levels of proteins such as diacylglycerol kinase-α which is involved in the induction of anergy (Macian et al., 2002). However, it was shown that CD28 stimulation alone does not activate the cell as it initiates only the expression of a few irrelevant genes (Xia et al., 2018). Following stimulation of CD28 by binding to CD80/CD86, its cytoplasmic tail gets phosphorylated, which recruits PI3K and thus cleaves PIP_2 to Phosphatidylinositol-3,4,5-trisphosphate (PIP_3). AKT then associates with PIP_3 and further acts on various downstream targets. For example, AKT ensures the extended localization of NFAT inside the nucleus and thus contributes to sustained IL-2 transcription. Also, the formation of

the CBM complex is regulated by AKT which allows nuclear translocation of NF-kB (Narayan et al., 2006). Besides NFAT and NF-kB and MAPK pathways, also PI3K-AKT-mTOR signaling is strongly sustained by co-stimulation due to the increased presence of AKT.

1.2.1.3 IL-2 signaling

IL-2, first described as a T cell growth factor, is an important regulator of T cell metabolism and effector differentiation (Ross and Cantrell, 2018). IL-2 signaling is mediated by the IL-2 receptor, which consists of an α chain (CD25), β chain (CD122) and γ chain (CD132). β and γ chains are constitutively expressed in naïve T cells and form an IL-2R complex. Together with the α chain, a heterotrimeric high- affinity IL-2R is formed, whereas the α chain is mainly essential fo the species specificity. This receptor is induced by T cell activation and is constitutively expressed by regulatory T (T_{reg}) cells (Damoiseaux, 2020).

Following TCR stimulation and CD28 co-stimulation, IL-2 transcription is induced by the transcription factors NFAT, NFkB and AP1, leading to the upregulation of IL-2Rα on the cell surface. Activation of the IL-2R complex is required for the differentiation and proliferation of $CD4^+$ and $CD8^+$ T cells (Liao et al., 2013). Clonal expansion in cytotoxic $CD8^+$ T cells is promoted by IL-2, as it activates the transcriptional program for cell cycle and proliferation (Boyman and Sprent, 2012; Liao et al., 2013). Furthermore, it promotes trafficking of $CD8^+$ T cells to peripheral tissues due to increased production if interferon γ (IFN-γ), granzyme and perforin (Kalia et al., 2010; Pipkin et al., 2010). mTORC1 signaling is also induced by IL-2 signaling, leading to metabolic changes within the cell to support rapid T cell proliferation (Hukelmann et al., 2016; Powell et al., 2012; Sinclair et al., 2008). Many nutrient transporters for amino acid and glucose uptake are also regulated by IL-2 likely coordinated with mTORC1 activity (Rollings et al., 2018). Besides mTOR, MAPK and STAT5 signaling can be activated by IL-2R signaling.

IL-2 signaling is sustained by paracrine and autocrine IL-2 signaling which boosts the CD25 and CD122 expression (Liao et al., 2013). It signals through the tyrosine kinases JAK1 and JAK3, which can be targeted by inhibitors such as tofacitinib to modulate immune responses (Furumoto and Gadina, 2013; Rollings et al., 2018; Schwartz et al., 2017). Due to its central role in the regulation of T cell fate and immune responses, IL-2 became a target for immunotherapies, aiming to increase the T cell response, or to promote the proliferation of tumor-specific T cells (Hernandez et al., 2022; Saxton et al., 2023).

It was shown that Raptor-deficient T cells also lack CD25 and Stat5 expression and produce lower levels of IL-2 indicating that mTORC1 promotes autocrine IL-2 signaling (Yang et al.,

2013). In this thesis we further investigated the induction of mTORC1 activity in dependence of IL-2 and JAK1 and JAK3 signaling.

1.2.2 Memory T cells

Naïve $CD8^+$ T cells are activated upon acute infection or vaccination and undergo clonal expansion to become T effector cells. The differentiation towards T_{eff} cells is marked by transcriptional adaptations and metabolic reprogramming as well as the production of cytokines. $CD8^+$ effector T cells directly kill infected target cells and thereby control the infection. After antigen clearance, most of the T cells die. However, a small subset of T cells differentiates further into memory T cells, which are able to persist long after the intial antigen stimulation (Barber et al., 2003; Lalvani et al., 1997). The T memory cell stage is characterized by a downregulated effector program and the ability to survive as long-lived antigen-experienced cell through stem cell-like features. Especially metabolic reprogramming is responsible for promoting persistence (O'Sullivan, 2019).

Upon rechallenge with antigen, memory T cells can produce effector cytokines and kill immediately, unlike naïve cells. It is known that memory cells have many characteristics in common with naïve T cells but are able to rapidly re-gain effector functions and are marked by a higher metabolic activity. (Gubser et al., 2013; Pearce et al., 2013; Youngblood et al., 2017).

Another understanding of this process is that memory precursor cells de-differentiate from effector to memory T cells. It was shown that effector T cells that became memory cells demethylate effector-associated genes, while naïve-associated genes acquired de novo DNA methylation (Youngblood et al., 2017). The epigenetic signature of their effector history is stored in mouse and human memory T cells (Akondy et al., 2017).

mTOR signaling downstream of TCR activation is known to induce and regulate the transcriptional and translational program required for the efficient resolution of infection (Pollizzi and Powell, 2015). Thereby, mTORC1 was shown to favor the generation of $CD8^+$ effector T cells and mTORC2 to inhibit the generation of memory T cells. Thus, mTOR activation contributes to the generation of both effector T cells and memory T cells in an immune response (Pollizzi et al., 2015). It was shown in several studies that transient rapamycin treatment of T cells results in enhanced memory generation, whereas metabolic changes and effector T cell differentiation are inhibited (Araki et al., 2009; Rao et al., 2010; Sowell et al., 2014). However, it is still unknown how RNA synthesis is regulated in memory cells and whether the rapid immune response induced by memory cells after re-challenge is accompanied by an increased rate of RNA synthesis and mTORC1 signals which was thus investigated in this thesis.

1.3 Ribosomal RNA biosynthesis

1.3.1 Structure and function of the nucleolus

Initially lymphocytes were identified as immunologically compentent cells which rapidly adapt their morphological characteristics in graft-versus-host reactions. Thereby, the lymphocytes were shown to increase in size and develop large nucleoli (Gowans et al., 1962). Nucleoli are membrane-less organelles which are located within the nucleus. Their size and appearance differ between different cell types depending on their transcriptional activity, as key steps of the ribosomal biosynthesis occur in the nucleoli of a cell. The nucleolus is comprised of Fibrillar Centers (FCs), Dense Fibrillar Components (DFCs) and the granular component (GC), as shown in Figure 2. Thereby, transcription of the rDNA genes happens in the FC and DFCs, while processing and assembly occurs in the granular component (Frottin et al., 2019; Thiry et al., 2011). This structure of nucleolar components can easily be disturbed by RNA Pol I inhibition, leading to alterations in the proteome as well as impaired transcription and DNA repair (Nemeth and Grummt, 2018). The nucleolus is known to play a key role in regulation of stress response, cell growth and survival (Boulon et al., 2010). The absence of a lipid membrane allows the nucleolus to react dynamically to cell stresses. The number and size of nucleoli within a cell can vary in different disease such as cancer. Therefore, the nucleolus represents an important biomarker and target for cancer therapy (Derenzini et al., 2009; Hein et al., 2013). The three compartments are defined by the expression of upstream binding factor (UBF) in FCs, Fibrillarin in DFCs and nucleophosmin (NPM1) for the GC which are all essential regulators of rRNA maturation (Farley et al., 2015; Frottin et al., 2019; Grummt and Langst, 2013; Hamperl et al., 2013). The assembly and disassembly are dynamic processes that happen cell-cycle dependent (Nemeth and Grummt, 2018). However, all these findings are based on experiments in tumor cells and not much is known about the function of the nucleolus in T cells and is thus addressed in this thesis.

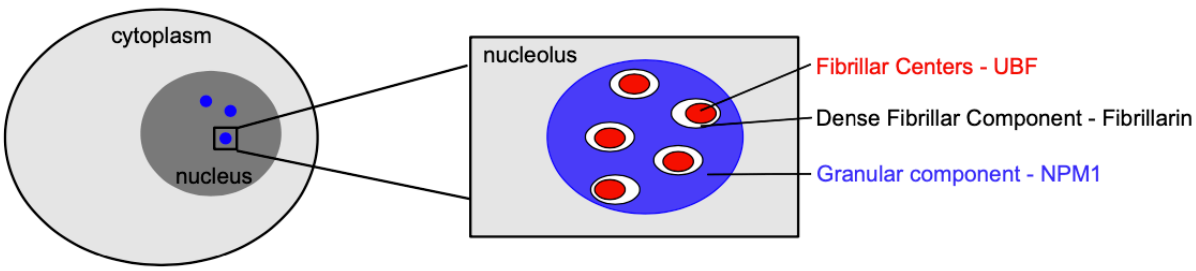

Figure 2: Schematic view of nucleoli structures.
Nucleoli are the sites of rRNA transcription. The nucleolus consists of fibrillar centers (FCs), Dense Fibrillar Components (DFCs) and the granular component (GC). The compartments are marked by the expression of UBF, Fibrillarin and NPM1, respectively. Modified from Frottin et al. (Frottin et al., 2019).

1.3.2 Ribosome biogenesis

Ribosomal RNA synthesis is a major essential cellular process which consumes the largest part of cellular energy (Warner, 1999) and consists of the three steps pre-RNA transcription, processing and ribosomal subunit assembly. The human ribosome contains 4 ribosomal RNAs, which are organized in 2 subunits. The whole process of assembly, cleavage and maturation of pre-RNA occurs first in the nucleolus, then in the nucleus and in the cytoplasm (Hernandez-Verdun et al., 2010; Klinge and Woolford, 2019).

The process starts in the nucleolus, where the 47S pre-ribososmal RNA is synthesized, containing the three 18S, 5.8S and 28S rRNAs as well as a 5' external transcribed spacer (ETS) site and a 3' untranslated region (UTR) end as depicted in Figure 3 (1). The three RNAs are separated by internal transcribed spacers 1 (ITS1) and 2 (ITS2) and are transcribed by RNA Polymerase I (RNA Pol I) as one pre-RNA transcript. The subsequent pre-rRNA associates with many ribosomal proteins (RPs) and pre-ribosomal factors, which support structural formations, correct folding and modification (2). The generated pre-RNA is further processed into the mature RNA species which assemble into two subunits (3). Therefore, the 5' ETS site gets removed and after cleavage at the ITS1, the small pre-40S subunit containing the 18S rRNA is formed, while 5.8S and 28S assemble in the newly formed pre-60S subunit. The smallest RNA, the 5S RNA, is transcribed from multiple genes by RNA Polymerase III in the nucleoplasm (Henras et al., 2015), is then transported into the nucleolus, gets processed and incorporated into the pre-60S subunit. The two pre-subunits are then exported into the cytoplasm for further maturation. In the cytoplasm, the two subunits incorporate further RPs and remove unnecessary pre-ribosomal and accessory factors. After final maturation, the 40S subunit binds transcribed mRNA, which associates the 60S subunit and represent the functional ribosome (4). The main function of the small subunit (40S) that includes 18S rRNA and 33 RPs, is the decoding of mRNA (Steitz, 2008). The big subunit (60S) contains 5S, 5.8S and 28S rRNAs and 47 RPs and its main function is the formation of proteins (Melnikov et al., 2012).

Since macromolecular biosynthesis is one of the primary tasks of activated T cells, we asked how cellular RNA is affected by mTORC1 and -C2 deletion and visualized dsRNA by flow cytometry with Pyronin Y (Darzynkiewicz et al., 2004; Shapiro, 1981). To visualize de novo 47S rRNA synthesis, we established a new technique and designed oligonucleotide FISH probes that bind to the 5'ETS site, which is cleaved and destroyed within minutes after rRNA synthesis in tumor cells (Popov et al., 2013).

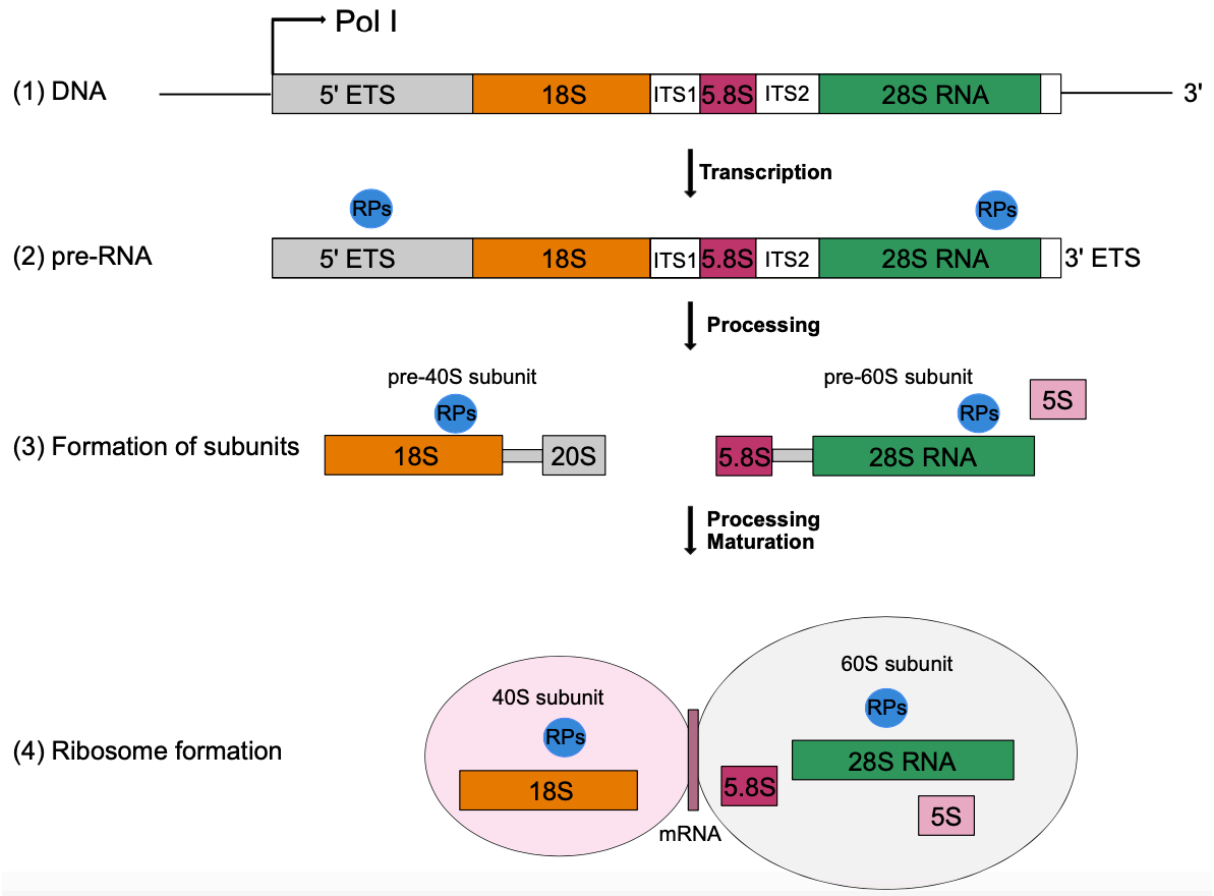

Figure 3: Schematic view of ribosome biogenesis.
(1) Structure of the 47S pre-ribosomal DNA (Grummt, 2013). 18S, 5.8S and 28S are transcribed by RNA Polymerase I. (2) The transcribed pre-RNA associates with ribosomal proteins and other accessory factors. (3) After cleaving the 5'ETS and 3'ETS sites and ITS1, the pre-40S, containing 18S and 20S rRNA, and pre-60S subunit, containing the 28S and 5S rRNA, are formed. 5S rRNA is transcribed by Pol III independently. (4) After final maturation, the complete mature ribosome is formed when mRNA binds to the 40S subunit, which leads to assembly of the 60S subunit to the whole complex. Modified from Danilova and Gazda (Danilova and Gazda, 2015).

1.3.3 RNA Polymerase I complex

RNA Pol I is responsible for the transcription of ribosomal RNA as described in chapter 1.3.2. It functions in a protein complex, consisting of several subunits and its main factors UBF, SL-1 and Tif1a. The upstream binding factor (UBF) initially binds to the rDNA promoter and subsequently recruits SL-1 to the promoter. This complex of UBF/SL-1 then binds Tif1a, which is associated with RNA Pol I. The transcription factor Tif1a facilitates the interaction and subsequent binding of SL-1 and RNA Pol I, altogether building the pre-initiation complex as shown in Figure 4 (Drygin et al., 2010; Grummt, 2003; Hein et al., 2013; Jin and Zhou, 2016). Rate-limiting factor in this process is the protein Tif1a, which is as well aberrantly activated by cancer cells and facilitates increased rate of RNA synthesis and subsequent cell cycle

progression. Its function in this process is conserved among other species, from yeast to mammals (Moorefield et al., 2000).

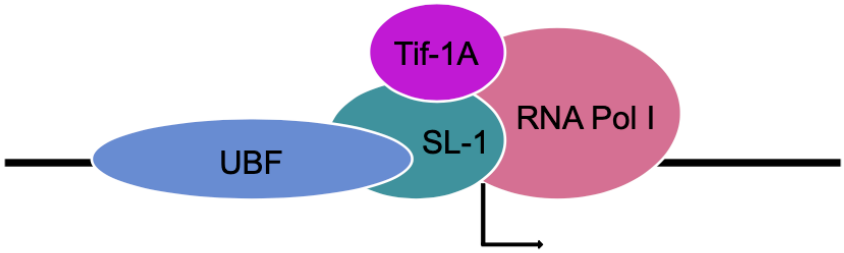

Figure 4: Factors associated with the rDNA promoter and Pol I.
Binding of UBF and SL1 (Tif-1B) to the rDNA promoter is essential for the recruitment of RNA Pol I and Tif-1A, a Pol I-associated factor, to the transcription start site. Based on Grummt (2013).

Tif1a is ubiquitously expressed (Bodem et al., 2000) and its expression levels can be influenced by environmental factors such as nutrient availability. Due to its function in ribosomal RNA synthesis, it is mostly found in cytoplasm, nucleolus and nucleoplasm. The highest concentration of Tif1a can be found in the nucleolus, although only 7% of total Tif1a is in the nucleoli (Szymanski et al., 2009). It was shown that rapamycin treatment of Hela cells resulted in a higher proportion of Tif1a levels in the cytoplasm (Mayer et al., 2004). In genetically modified mice with a homozygous Tif1a gene deletion, no pre-rRNA could be detected and such mice show impaired growth and development, resulting in early embryonic lethality. Conditional deletion in MEF cells resulted in cell cycle arrest and promoted p53-mediated cell death (Parlato et al., 2008; Yuan et al., 2005).

mTORC1 plays an important role in ribosomal synthesis as well and contributes in multiple ways. On the one hand, it induces the expression of Tif1a, which then interacts with RNA Pol I (Iadevaia et al., 2014; Mayer and Grummt, 2006; Mayer et al., 2004; Schnapp et al., 1993). Additionally, mTORC1 induces the phosphorylation of Maf1, a RNA Pol III repressor, and thus inhibits it. Thereby, 5S rRNA and tRNA transcription are induced (Iadevaia et al., 2014; Kantidakis et al., 2010; Mayer and Grummt, 2006; Shor et al., 2010).

1.3.4 Nucleolar stress

The nucleolus is known to be a cellular stress regulator and controls the abundance of tumor suppressor protein p53 (Budde and Grummt, 1999; Klein and Grummt, 1999). Nucleolar stress is marked by changes in nucleolar morphology such as nucleolar segmentation or disruption, and by impaired function of ribosomal biosynthesis. Besides rRNA synthesis, the

nucleolar has additional functions, including signal recognition, DNA repair and cell cycle regulation (Andersen et al., 2005; Boisvert et al., 2007). Nucleolar disruption was observed the first time when ribosome biosynthesis was blocked by actinomycin D (Yung et al., 1985). Later studies showed similar effects through treatments with cytotoxic agents (Chan et al., 1999), radiation (Colombo et al., 2002; Thielmann et al., 1999), DNA damage (Yogev et al., 2008), heat shock (Chan et al., 1999), starvation or chemotherapeutic agents and others. These cellular stressors lead to the activation of p53 and other stress signaling pathways (Rubbi and Milner, 2003). Nucleophosmin (NPM1) is the most prominent marker of nucleolar stress and, together with other nucleolar proteins, translocates to the nucleoplasm in response to cellular stress (Yang et al., 2016). This shuttle between the nucleolus and the nucleoplasm is highly increased upon stress conditions. In the nucleoplasm, NPM1 interacts with p53 and prevents its binding to murine double minute 2 (MDM2), its main negative regulator, and subsequent ubiquitination and proteasomal degradation (Kurki et al., 2004). P53 is thus stabilized, and its levels increase in the nucleoplasm and induce cell cycle arrest at the G1/S and G2/M checkpoints and promote apoptosis (el-Deiry et al., 1994). It was demonstrated in p53 knockout cells that cell cycle arrest and apoptosis can be induced through nucleolar stress independently of p53 activation (Russo and Russo, 2017). Impaired ribosomal biogenesis by chemical inhibition or in ribosomopathies lead to p53-dependent cell cycle arrest. Thereby, Tif1a plays an important role, as its deletion was shown to disrupt the nucleolus and lead to cell cycle arrest and p53-dependent apoptosis (Yuan et al., 2005). In addition to p53, other transcription factors respond to ribosomal stress, like c-Myc or E2F (Dai et al., 2007; Russo and Russo, 2017). Some ribosomal proteins function as negative regulator of c-myc and are released upon nucleolar stress, which thus leads to a suppression of c-myc and subsequent cell cycle arrest and reduced ribosomal biosynthesis (van Riggelen et al., 2010; Zhou et al., 2013).

1.3.5 Ribosomopathies

Defective ribosome function or production leads to various disorders in humans, the so called ribosomopathies (Robertson et al., 2022). This group of rare diseases is caused by reduced expression or mutations of ribosomal proteins, RNA Pol I transcription machinery or pre-ribosome maturation factors. The effects of ribosomopathies are mostly tissue-specific (Robertson et al., 2022). For instance, Cartilage Hair Hyploplasia (CHH) is a ribosomopathy which results in skeletal abnormalities and immunodeficiency, mainly characterized by an impaired T cell activation (Vakkilainen et al., 2020). These patients are more prone to malignant and autoimmune diseases and recurrent infections. T cells of CHH patients show reduced proliferative capacity following stimulation and have an increased rate of activation-induced cell death (de la Fuente et al., 2011; Kostjukovits et al., 2017). It was shown that

mutations in RNA component of mitochondrial RNA processing endoribonuclease (RMRP), as in CHH, show a delay of pre-RNA processing (Robertson et al., 2022). An example for a ribosomopathy with a haploinsufficient mutation of ribosomal proteins is Diamond Blackfan Anemia (DBA) which is defined by reduced ribosome numbers and reduced translational activity (Khajuria et al., 2018). This defect in processing of ribosomal pre-rRNA (Choesmel et al., 2007) causes a defective erythropoiesis, leading to anemia as well as physical malformation. The patients have an increased risk for cancer, but do not suffer from immunodeficiency (Halperin and Freedman, 1989; Vlachos et al., 2012). Although the aetiology of both diseases is similar, the clinical manifestations differ. The mechanism for this discrepancy is still unclear and how ribosomopathies contribute to ribosomal stress in a tissue-specific manner is under investigation.

Some Ribosomopathies like the DBA can be studied in mouse models with a mutation in Rps19 and Rps20. These mice show an impaired erythropoiesis, anemia, decreased number of leukocytes and a reduced size (Jaako et al., 2011; McGowan et al., 2008).

Many ribosomopathies share an increase in p53 activation. RpS6 deletion in mice leads to p53 activation in T cells (Sulic et al., 2005). Further studies showed p53 activation as a general response to ribosomal protein (RP) deficiency (Barlow et al., 2010; Danilova et al., 2008; McGowan et al., 2008; Taylor et al., 2012). Several reasons for an increase of p53 levels were suggested, including the disruption of the nucleolus and subsequent cell cycle arrest in response to cellular stress including DNA damage or hypoxia. As the nucleolus is not always affected by RP deficiency (Fumagalli and Thomas, 2011), other mechanisms are involved as well such as p53 stabilization through RPs by binding to Mdm2. This mechanism indicates that a balance between synthesis of rRNA and RPs is important and disruption of one of them can lead to imbalance and trigger stress responses. RP-deficient cells have an altered nucleotide metabolism and imbalance of nucleotides in the cell can disrupt DNA synthesis and thus lead to increased p53 (Austin et al., 2012).

1.4 mTOR

1.4.1 Structure and function of the two mTOR complexes

Mechanistic target of rapamycin (mTOR) is a serine-threonine protein kinase (Laplante and Sabatini, 2012) and occurs in two complexes, mTORC1 and mTORC2, whereas both complexes contain the mTOR protein, mammalian lethal with sec-13 protein 8 (mLST8, GβL) (Jacinto et al., 2004; Kim et al., 2003), DEP domain containing mTOR interacting protein (DEPTOR) (Peterson et al., 2009) and Tti1/Tel2 complex (Kaizuka et al., 2010), as shown in Figure 5. mTORC1 additionally contains the regulatory-associated protein of mammalian

target of rapamycin (Raptor) (Hara et al., 2002; Kim et al., 2002) and the proline-rich Akt substrate 40kDa PRAS40 (Sancak et al., 2007; Thedieck et al., 2007; Vander Haar et al., 2007; Wang et al., 2007) (Figure 5, left).

On the other hand, mTORC2 contains as unique component the rapamycin-insensitive companion of mTOR (Rictor) (Jacinto et al., 2004; Sarbassov et al., 2004), mammalian stress-activated map kinase-interacting protein 1 (mSin1) (Frias et al., 2006; Jacinto et al., 2006) and protein observed with rictor 1 and 2 (protor1/2) (Pearce et al., 2007; Pearce et al., 2011; Thedieck et al., 2007) (Figure 5, right).

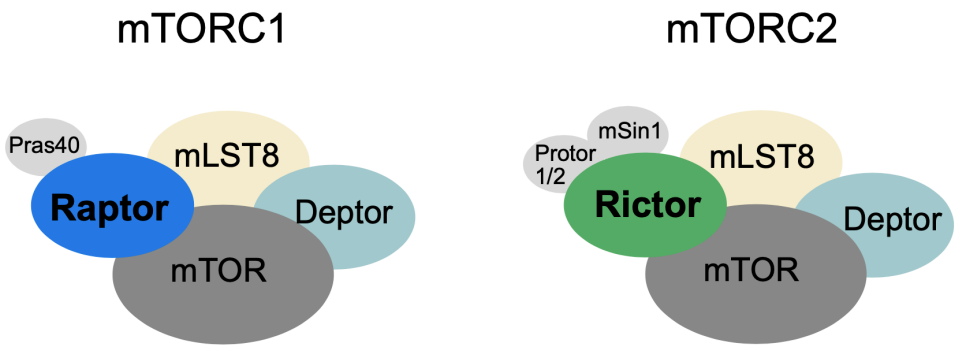

Figure 5: Schematic view of the two mTOR complexes.
Left: mTOR Complex 1 containing mTOR, Deptor, mLST8, Pras40 and its main protein Raptor. Right: mTOR Complex 2, containing mTOR; Deptor, mLST8, Protor1/2, mSin1 and its main protein Rictor.

Although both complexes share most of its proteins and a Ser/Thr kinase activity, each of them has a different sensitivity towards rapamycin, as well as different upstream regulators and downstream targets (Laplante and Sabatini, 2012). Early results suggested that mTORC1 exerts its function mainly through its two known downstream targets p70 ribosomal protein S6 kinase 1 (S6K1) and initiation factor 4E-binding proteins (4EBPs). S6K1 is known to be a key regulator for cellular metabolism and functions by phosphorylation of its substrate ribosomal S6 protein in some cell types (Fumagalli and Pende, 2022; Um et al., 2006). However, while the S6 protein is indispensable for T cell differentiation (Sulic et al., 2005), its phosphorylation is not required for T cell development and responses to TCR stimulation in vitro (Salmond et al., 2015). The most investigated process regulated by mTORC1 is protein synthesis, which is achieved by the phosphorylation of eIF4E binding protein 1 (4E-BP1) (Ma and Blenis, 2009).

mTORC2 regulates the kinases Akt and serum-and-glucocorticoid-induced protein kinase 1 (SGK1) (Garcia-Martinez and Alessi, 2008) and protein kinase Ca (PKCa). Thus, mTORC2 contributes to mTORC1 activity by regulating Akt. Besides that, Akt is involved in many cellular processes including survival, growth, metabolism and proliferation through phosphoryla-

tion of downstream effectors. More recent proteomic analyses have identified many more targets of both mTORC1 and mTORC2 (Battaglioni et al., 2022). In activated T cells, 547 mTORC1-dependent phosphopeptides have been identified (Tan et al., 2017).

1.4.2 Signaling via the PI3K/Akt/mTORC1 axis

Besides the three classical TCR signaling pathways which lead to the induction of gene transcription mTOR signaling plays an important role for the rapid activation of T cells. mTOR signaling is induced through PI3K which activates AKT and this negatively regulates Tuberous sclerosis 1 and 2 (TSC1/2). TSC1/2 is a key upstream activator of mTORC1. It regulates mTOR by transforming Rheb into its inactive form and thus releases mTOR. (Inoki et al., 2003; Tee et al., 2003). mTORC1 functions through its two downstream targets 4EBP1/2 and S6K1/2. S6K phosphorylates the S6 protein quickly after activation and leads to an increase of pS6, which can be used as a marker for mTOR activity. A schematic view of mTORC1 activation is shown in Figure 6. WAVE2 was recently identified as a new mTORC1 regulator which directly inhibits mTOR activity by disrupting the interaction of mTOR with Raptor and Rictor effector proteins (Liu et al., 2021). The signaling via mTORC1 and its downstream effects in T cells is a central topic of this thesis.

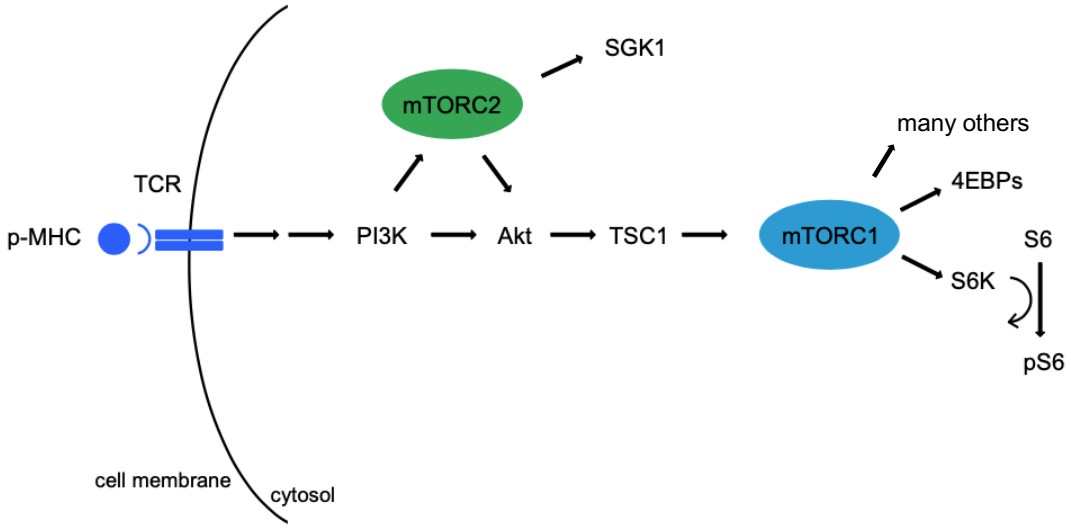

Figure 6: Schematic view of the PI3K/Akt/mTOR axis.
Following TCR stimulation, PI3K activates mTORC1 via Akt and TSC1, as well as mTORC2. Downstream targets of mTORC1, besides others 4EBPs and S6K, and mTORC2, SGK1 and Akt, are shown.

1.4.3 Functions of mTORC1 in T cells

The major functions of mTORC1 in T cells include the induction of key anabolic processes as protein, nucleotide and lipid synthesis, cell cycle progression, proliferation and cell growth.

It was shown in vitro that mTORC1 activity is required for the cell cycle entry (G0/G1 transition) but is less essential for later divisions (Hukelmann et al., 2016; Terada et al., 1993a; Terada et al., 1993b; Yang et al., 2013). Genetic deletion of Raptor, the main protein of mTORC1, or mTOR itself, results in impaired proliferation and differentiation of $CD4^+$ T cells (Yang et al., 2011). Upstream deletion of the negative regulator TSC1 leads to spontaneous activation and proliferation of $CD4^+$ and $CD8^+$ T cells (Delgoffe et al., 2009; Delgoffe et al., 2011; Yang et al., 2011; Yang et al., 2013). Mechanistically, mTORC1 induces the expression of c-myc (Wang et al., 2011b; Yang et al., 2013), an important transcription factor for cell growth and proliferation. Since c-myc contributes to the cell cycle entry by promoting the expression of relevant CDKs and cyclins (Otto and Sicinski, 2017) it might mediate several mTORC1-dependent effects on T cell proliferation.

Another characteristic function is cell growth, which starts during the exit of quiescence and coincides with an increase in RNA and protein levels (Chapman and Chi, 2018). Studies with rapamycin showed that $CD4^+$ T cells had reduced growth and delayed cell cycle entry (Mondino and Mueller 2007; Colombetti et al. 2006). In order to prepare for cell growth, the T cells rapidly increase their biomass which is characterized by an increase in amino acid, lipid, cholesterol and protein synthesis (Ben-Sahra and Manning, 2017). To do so, the T cell adapts its metabolism towards an anabolic metabolism by increasing aerobic glycolysis, called Warburg effect, which is also observed in fast growing cancer cells (Chapman and Chi, 2018). mTORC1 is known to induce the expression of hypoxia inducible factor 1a (Hif1a), which contributes to an increased glycolytic flux (Brugarolas et al., 2003; Duvel et al., 2010; Hudson et al., 2002; Laughner et al., 2001). To further support cell growth, mTORC1 negatively regulates autophagy, which is an important mechanism for cellular adaptation and recycling of damaged cell organelles (Laplante and Sabatini, 2012).

The upregulation of lipid synthesis is mainly essential for the generation of cell membranes (Laplante and Sabatini, 2009; Otto and Sicinski, 2017; Wells and Morawski, 2014). Essential for fatty acid and cholesterol synthesis is transcription via the sterol regulatory element binding protein 1/2 (SREBP1/2), which is regulated by mTORC1 through S6K1 (Duvel et al., 2010; Li et al., 2010; Li et al., 2011b; Wang et al., 2011a).

One of the most important functions of mTORC1 signaling is the induction of ribosome biogenesis and protein translation through S6K1 and 4E-BP1 (Saxton and Sabatini, 2017) as has been described in chapter 1.3.2.

1.4.4 Nucleotide metabolism

Proliferating cells require the synthesis of essential macromolecules to be able to generate biomass for replication and cell growth. mTORC1 is an important regulator of these anabolic processes, including the synthesis of nucleotides, proteins and lipids (Ben-Sahra and Manning, 2017). Signaling via mTORC1 induces the de novo synthesis of purine and pyrimidine nucleotides to meet the increased demand during rRNA synthesis (Ben-Sahra et al., 2013; Ben-Sahra et al., 2016; Robitaille et al., 2013; Valvezan et al., 2017). Amino acids are required as essential precursor of purine and pyrimidine synthesis and derive from the pentose phosphate pathway. As mTORC1 promotes glycolysis and the pentose phosphate way, it also supplies the cell with the essential precursors (Duvel et al., 2010). mTORC1 was shown to regulate the de novo pyrimidine synthesis through its downstream target S6K1 which phosphorylates the carbamoyl-phosphate synthetase 2, aspartate transcarbamylase and dihydroorotase (CAD) in tumor cell lines. CAD is the rate limiting enzyme in the first steps of the de novo pyrimidine synthesis (Ben-Sahra et al., 2013). Phosphorylated CAD persists in the cell even after mTOR activity has decreased to baseline which suggests that CAD plays a role in the rapid immune response in memory T cells (Claiborne et al., 2022). Enhanced purine synthesis through mTORC1 is induced by the expression of the mitochondrial tetrahydrofolate cycle enzyme methylenetetrahydrofolate dehydrogenase 2 (MTHFD2), which catalyzes the generation of one-carbon units (Ben-Sahra et al., 2016). MTHFD2, as well as other enzymes in nucleotide synthesis, like the inosine monophosphate dehydrogenase (IMPDH), became common therapeutic targets in cancer therapy and immunosuppression (Ishikawa, 1999; Valvezan et al., 2017; Zhu and Leung, 2020).

1.5 Cell cycle

mTORC1 is a known regulator of the cell cycle, especially the G1/S transition (Yang et al., 2013). Following stimulation, the T cell exits the quiescent state and enters the cell cycle, which is divided into interphase, where DNA synthesis takes place, mitosis, and cytokinesis, when the cell finally divides into two cells. This entry into the cell cycle influences the differentiation and effector function of the cell, as well as the metabolic fitness and proliferative capacity. The regulation of the cell cycle by mTORC1 at several checkpoints is further investigated in this thesis.

The progression through each cycle is mediated by phase-specific cyclin-dependent kinases (CDKs) and cyclins, which are induced by growth factors. Cyclins are bound by CDKs in order to activate them and thus lead to the phosphorylation of cell cycle inhibitors like Retinoblastoma (Rb) (Chapman and Chi, 2018). For G1 entry specifically, the complex of CDK4/6 and cyclin D is required, as shown in Figure 7. For the progression through the cell

cycle, this complex becomes less important, and CDK2-cyclin E expression is increased to promote the transition into S phase (Otto and Sicinski, 2017; Wells and Morawski, 2014). Therefore, an increased phosphorylation of the Rb protein is essential (Yoon et al., 2010). In a naïve quiescent state, the CDK2-cyclin E complex is blocked by p27, however, following TCR signaling with CD28 co-stimulation leads to p27 degradation which allows the induction of cyclin E (Appleman et al., 2000; Boussiotis et al., 2000; Rowell et al., 2006; Wells and Morawski, 2014).

Interestingly, it was shown that CDK2 is neglectable for T cell proliferation and might be compensated by other CDKs to promote clonal expansion (Chunder et al., 2012).

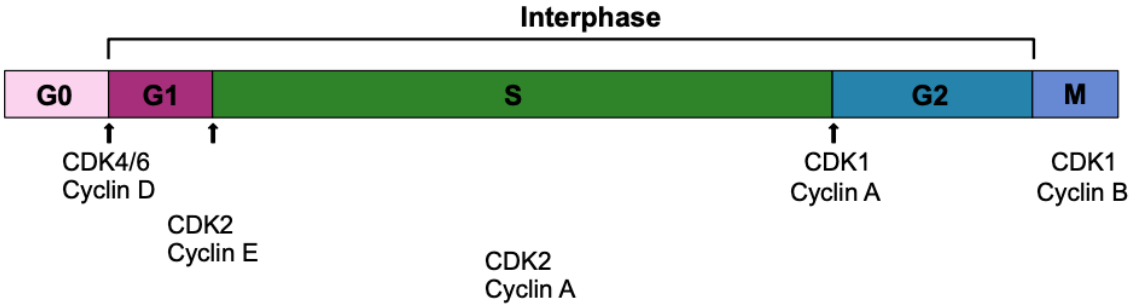

Figure 7: Schematic view of the cell cycle stages.
Naïve T cells occur in the periphery in a quiescent stage (G0 phase). Following stimulation, T cells enter the G1 phase by upregulating the expression of CDK4/6 and Cyclin D. To enter S phase CDK2 forms a complex with Cyclin E to allow transition. Throughout S phase the expression of cyclin E decreases, while Cyclin A expression increases and forms a complex with CDK2. To enter G2/M phase of the cell cycle, CDK1/Cyclin A are required (Aleem and Arceci, 2015).

1.6 Chemical inhibitors of mTOR and RNA synthesis

1.6.1 Rapamycin as mTOR inhibitor

Rapamycin is a macrolide antibiotic, that was found to exert its function via TOR1 and TOR2 in yeast in the early 90s. It is produced from Streptomyces Hygroscopius bacteria and got famous for its antiproliferative capacities (Cafferkey et al., 1993; Kunz et al., 1993). mTOR was then discovered as a target of rapamycin (Brown et al., 1994; Sabatini et al., 1994; Sabers et al., 1995). The effects of rapamycin are known to be dose-dependent, as high doses completely inhibit the $CD8^+$ T cell responses to LCMV infection, while low doses were shown to have positive effects on memory cell generation (Araki et al., 2009).

Due to its immunosuppressive function, which was discovered in the 1970s (Chi, 2012), rapamycin was approved by the FDA in the 1990s to prevent tissue rejection in kidney transplant patients. However, the effect of prevention was only weak and could be increased by the addition of Calcium signaling blocking agents such as Cyclosporin and FK506. Rapamy-

cin was known to reduce autoimmune disorders and to affect the functionality of T cells (Chi, 2012).

These immunomodulatory effects on $CD8^+$ T cells were also investigated in other infectious models (Ferrer et al., 2010; Turner et al., 2011) and tumor models (Li et al., 2011a; Wang et al., 2011c). However, despite some clinical success, rapamycin and rapalogs show only limited effects in cancer prevention or treatment (Guo et al., 2011; Laplante and Sabatini, 2012). A reason for the limited efficacy could be a high number of negative feedback loops, that are regulated by mTOR (Laplante and Sabatini, 2012). As rapamycin prevents mTORC1-induced feedback inhibition of the PI3K signaling axis, it leads to an enhancement of AKT signaling, which might explain the limited therapeutic efficacy of mTOR inhibition in cancer patients (O'Reilly et al., 2006).

1.6.2 Second generation mTOR inhibitors

Rapamycin belongs to the group of first generation mTOR inhibitors and does so by interacting with FKBP12 by allosteric inhibition. This leads to an immense functional loss of S6 kinases, but other downstream targets like 4EBPs are hardly affected (Choo et al., 2008). The second generation of mTOR inhibitors include ATP competitive molecules like Torin-1 and PP242, which block mTORC1 activity completely. Torin-1 and PP242 were shown to also inhibit mTORC2 and thus do not result in increased ATP levels (Apsel et al., 2008; Feldman et al., 2009; Thoreen et al., 2009). These newly developed generation of mTOR inhibitors exhibit more promising effects in cancer treatment and prevention probably due to its complete inhibition (Hsieh et al., 2010; Janes et al., 2010) and are tested in clinical trials (Benjamin et al., 2011). In this work, Torin-1 was used to fully inhibit mTOR activity.

1.6.3 Inhibitors of ribosomal biosynthesis

Excessive ribosomal biosynthesis is a major hallmark of cancer cells which leads to an increased rate of cell proliferation and cell growth. Therefore, ribosomal biosynthesis became a common therapeutic target for cancer therapy or ribosomopathies. There are different classes of inhibitors, which target various parts during this complex process. Many of them directly target RNA Pol I due to its central function in rRNA synthesis, like chemotherapeutic drugs, alkylating agents, antibiotics, or via targeting topoisomerases or G-quadruplexes (Burger et al., 2010; Pitts and Laiho, 2022).

CX-3543 (Quarfloxin) is a small molecule deriving from fluoroquinolone. Quarfloxin functions by disrupting the interaction of G-quadruplex rDNA complexes and the nucleolin protein at the rDNA strand and thus blocks the activity of RNA Pol I. G-quadruplex DNA structures are formed in the non-template strands in the presence of G-rich templates, such as rDNA

(Duquette et al., 2004). These G-quadruplex structures stabilize the template strand and prevent renaturation. Additionally, it promotes the dense intervals of Pol I molecules (French et al., 2003). The nucleolar protein nucleolin associates with G-quadruplex structures and further stabilizes them, which leads to increased Pol-I driven transcription (Srivastava and Pollard, 1999). Nucleolin is an essential part of RNA synthesis, as its deletion was demonstrated to inhibit Pol I transcription (Rickards et al., 2007; Storck et al., 2009). Quarfloxin was shown to induce a rapid redistribution of nucleolin within the nucleolus, leading to the inhibition of rRNA synthesis, and as well to apoptotic death which makes it an innovative therapeutic approach (Drygin et al., 2009). However, Quarfloxin turned out to have limited bioavailability and was thus unsuccessful in clinical trials. Instead CX-5461 (Pidnarulex) was developed by the same company as another small molecule and was shown to inhibit topoisomerase 2 (TOP2) instead of G4 complexes (Bossaert et al., 2021; Bruno et al., 2020; Pan et al., 2021). CX-5461 was used in clinial trials and completed phase 1 and 2 (Hilton et al., 2022).

Recently, a new first-in-class inhibitor named BMH-21 was discovered, which is unique in its mechanism to inhibit RNA Pol I (Peltonen et al., 2010; Peltonen et al., 2014). It intercalates into DNA and binds to GC-rich regions without interacting with TOP2 (Bruno et al., 2020) and without inducing DNA damage (Colis et al., 2014; Peltonen et al., 2010; Peltonen et al., 2014). BMH-21 inhibits rDNA synthesis during initiation, promoter escape and elongation (Wei et al., 2018). One mode of action is the induction of proteasome-mediated degradation of one of the subunits of Pol I, RPA1 (Peltonen et al., 2014; Pitts et al., 2022). Compared to the other classes of ribosomal biosynthesis inhibitors, BMH-21 selectively inhibits RNA Pol I and has no off-target effects, which makes it a promising therapeutic target (Pitts and Laiho, 2022).

Transcriptional inhibition leads to major changes including the segregation of nucleolar substructures (Boulon et al., 2010) and reorganization of the nucleolus (Bensaude, 2011), altogether described as the transcriptional stress response (Ljungman, 2007) or nucleolar stress response. When using inhibitors, one must consider the selectivity, efficiency, reversibility and rapidity. Ribosomal biosynthesis and transcription inhibition became an attractive target for cancer therapeutic intervention, although, each of them has advantages and disadvantages regarding their physiological effects on the cell.

1.7 Aim of the Thesis

mTOR is a key metabolic sensor and is essential for the regulation of T cell growth, differentiation, and expansion following antigen stimulation of naïve T cells. Its immunomodulatory effects led to clinical applications for immunosuppression. However, understanding how mTOR mediates its effects on proliferation and ribosomal RNA synthesis, would lead to advanced therapeutic opportunities in the clinic.

Several studies have shown the correlation between mTORC1 and proliferation, but the precise mechanism is unclear. Previous in vivo data in our lab have demonstrated that mTORC1 is essential for ongoing proliferation during each consecutive cell division.

An important downstream effect of mTORC1 activation is the regulation of multiple steps during ribosomal RNA biogenesis by upregulating RNA Polymerase I. However, the molecular mechanism is still unclear. Furthermore, it is not clear if and to what extent ribosome biogenesis affects the activation state and cell cycle progression of T cells.

The aim of this thesis was on the one hand to investigate the effect of mTORC1 on T cell proliferation in relation to the RNA synthesis. On the other hand, we investigated whether cell cycle progression in T cells is dependent on ribosomal RNA transcription. To answer these questions, conditional knockout mouse models for mTORC1, mTORC2 or both were used, as well as inhibitors for mTORC1/2 and rRNA transcription in functional T cell assays. A novel assay for the visualization of rRNA synthesis was established to analyze quantitative effects of mTORC1 and -C2 deficiencies on rRNA transcription and nucleolar anatomy.

2. Material and Methods

2.1 Material

2.1.1 Antibodies for Flow Cytometry

Antibody	Clone	Species	Conjugate	Company
CD11b	M1/70	rat	Biotin	Biolegend
CD11c	N418	Armenian hamster	Biotin	Biolegend
CD19	6D5	rat	Biotin	Biolegend
CD25	3C7	Rat	PE	Biolegend
CD28	37.51	Syrian hamster	-	Biolegend/BioXCell
CD3	2C11	Armenian hamster	-	Biolegend/BioXCell
CD4	RM4-5	rat	FITC, PeCy7, biotin	Biolegend
CD4	GK1.5	rat	PE, APC	Biolegend
CD44	IM7	rat	Pe-Cy7	Biolegend
CD45.1	A20	Mouse	APC	Biolegend
CD45.2	104	Mouse	PE, APC	Biolegend
CD45R/B220	RA3-6B2	rat	Biotin	Biolegend
CD49b	DX5	rat	Biotin	Biolegend
CD62L	MEL-14	rat	PE	Biolegend
CD69	H1.2F3	Armenian Hamster	PE	Biolegend
CD69	H1.2F3	Armenian Hamster	V450	BD Horizon, BD Biosciences
CD8a	53-6.7	rat	FITC, PE, PerCp, Pe-Cy7, APC, biotin	Biolegend
Gr-1 (Ly-6G/Ly-6C)	RB6-8C5	rat	Biotin	Biolegend
H3 Phospho	HTA28	rat	Alexa Fluor 488	Biolegend
P-S6 Ribo. Prot. (S235/236)	2F9	rabbit	Alexa-Fluor 488	Cell Signaling
P-S6 Ribo. Prot. (S235/236)	D57.2.2E	rabbit	Pe-Cy7	Cell Signaling
Streptavidin	-	-	PE	ebioscience
TCRß	H57-597	Armenian hamster	FITC	Biolegend

TER119	TER-119	rat	Biotin	Biolegend
Va2	B20.1	rat	FITC	BD Pharmingen, BD Biosciences
Vb5.1, 5.2	MR9-4	mouse	PE	BD Pharmingen, BD Biosciences

2.1.2 Antibodies for Western Blotting

Antibody	**Species**	**Label**	**Dilution**	**Company**
Alpha-tubulin	Rabbit	-	1:2000	Cell Signaling
Alpha-tubulin	Mouse	-	1:10000	V. Heissmeyer, Helmholtz Zentrum München
Anti-mouse IgG	Horse	HRP	1:3000	V. Heissmeyer, Helmholtz Zentrum München
anti-rabbit IgG	Goat	HRP	1:2000	Cell Signaling
mTOR	Rabbit	-	1:1000	Cell Signaling
Phospho-mTOR (Ser2448)	Rabbit	-	1:1000	Cell Signaling
Phospho-mTOR (Ser2481)	Rabbit	-	1:1000	Cell Signaling
Phospho-S6	Rabbit	-	1:1000	Cell Signaling
Raptor	Rabbit	-	1:1000	Cell Signaling
Rictor	Rabbit	-	1:1000	Cell Signaling

2.1.3 Chemicals, Reagents and Medium

Reagent	**Company**
2’-Desoxyribonucleosid-5’-triphosphate (dNTPs)	Peqlab/VWR
4’,6-Diamidin-2-phenylindol (DAPI)	Biolegend
47S RNA FISH probe	Stellaris
Acrylamide 30%	PanReac
Agarose	Sigma-Aldrich
Ammoniumpersulfate (APS)	Diagonal
Anti-biotin Microbeads	Miltenyi Biotech
Anti-mouse CD40 (Clone FGK4.5)	BioXCell
Antibiotic/Antimycotic	Sigma-Aldrich

Aprotinin	PanReac Applichem
Bovine Serum Albumin (BSA)	PanReac
Bradford Reagent	PanReac Applichem
Bromophenolblue	PanReac Applichem
Carboxyfluorescein succinimidyl ester (CFSE)	Thermo Fisher
CASYton	Omni Life Science
Cell Trace Violet (CTV)	Invitrogen
CellTracker Red (CTR)	Invitrogen
CHAPS	PanReac Applichem
Deionized formamide	PanReac AppliChem
DMSO	PanReac AppliChem
Dulbecco's Modified Eagle Medium (DMEM), Powder	Diagonal
ECL Prime Western-Blot-Detektionsreagenz (ECL Solution 1)	GE Healthcare
EdU (5-ethynyl-2′-deoxyuridine)	Thermo Fisher
EGTA	PanReac Applichem
Enhancer	VWR
Ethanol	PanReac Applichem
Ethidiumbromide	BioFroxx
Ethylenediaminetetraacetic acid (EDTA)	Diagonal
Fetal Calf Serum (FCS)	PAN Biotech
Fixable Viability Dye (eFluor780)	Thermo Fisher
Gelatin	Sigma-Aldrich
GeneRuler 1 kb DNA Ladder	Thermo Fisher
Glycerin	Applichem GmbH
Glycine	PanReac Applichem
HCl	Roth
HEPES	Sigma-Aldrich
Hoechst-33342	Thermo Fisher
Immobilon-p^{SQ} Transfer Membrane PVDF 0.2 µm	Millipore, Sigma
Incuwater Clean	PanReac Applichem
Interleukine 2 (rm IL-2)	Immunotools
Interleukine 7 (rm IL-7)	Immunotools
Isopropanol	PanReac Applichem
Leupeptin	PanReac Applichem
Magnesium Sulfate	PanReac Applichem; Merck

Methanol	J.T. Baker
Mineral oil	Sigma-Aldrich
Oligo dt RNA FISH	Stellaris
Orange G	Sigma-Aldrich
OVA-peptide	Peptides and Elephants
Pancoll	PAN Biotech
Paraformaldehyde (PFA)	PanReac Applichem
PCR Buffer	VWR
Perm Buffer III	BD Biosciences
Proteinase K	Diagonal
Pyronin Y	Sigma-Aldrich
Red blood cell (RBC) Lysis Buffer	Biolegend
Roswell Park Memorial Institute (RPMI) 1640 + GlutaMAX	Thermo Fisher
RPMI Methionine free	Thermo Fisher
SDS 10% in solution	PanReac
Sodium azide 10%	Morphisto
Sodium chloride	J.T. Baker
Sodium Fluorid	PanReac Applichem
Sodium orthovanadate	Sigma-Aldrich
Spectra Multicolor High Range Protein Ladder	Thermo Fisher
ß-Mercaptoethanol	Roth
Stellaris RNA FISH Hybridisation Buffer	LGC Biosearch Technologies
Stellaris RNA FISH Wash Buffer A	LGC Biosearch Technologies
Taq Polymerase	VWR
TEMED	PanReac
Tris	PanReac
Triton-X-100	Sigma
Tween20	Sigma, PanReac Applichem
UltraPure DEPC Treated Water	Invitrogen
Water for molecular biology	Panreac Applichem
Whatman Filter	Merck

2.1.4 Inhibitors

Inhibitor	Solution	Target	Company
BAY11-7082	DMSO	NFkB	LKT Laboratories, Inc.
BMH-21	DMSO	RNA Polymerase	Selleck Chemicals
CX3543	DMSO	RNA Polymerase	Hölzl; MCE
Cyclosporin A	DMSO	Calcineurin	AdipoGen Life Science
GDC0941	DMSO	PI3K	LKT Laboratories, Inc.
GDC0973	DMSO	MEK	LKT Laboratories, Inc.
LY2584702	DMSO	S6K1/2	MCE
PF4708671	DMSO	S6K1	Sigma Aldrich
Tigecyclin	DMSO	Mit. ribosome	Sigma Aldrich
Tofacitinib	DMSO	Jak/Stat	Selleck Chemicals
Torin-1	DMSO	mTOR	Selleck Chemicals

2.1.5 Mice

Linie	Official Line Name	Background	Source
ANDx45.1	Tg(TcrAND)53Hed;Ptprca	B10.BR/Ifi	C. Benoist, D. Mathis, Harvard Medical School, Boston, USA
B10.BR	B10.BR-H2^{k2};H2-T18^{a}/SgSnJJrep	B10.BR/Jax	The Jackson Laboratory
B10.BR	B10.BR-H2^{k}/OlaHsd		Envigo
B6	C57BL/6	C57BL/6	The Jackson Laboratory; Institute for Immunology
CD4-cre	Tg(Cd4-cre)1Cwi	C57BL/6	The Jackson Laboratory
H-2A$^{b/bm12}$	H2-Ab1^{bm12}	B6KhEgJ	The Jackson Laboratory
H-2K$^{b/bm1}$	H2-K^{bm1}	C57BL/6	V. Buchholz, Technische Universität München
OT1x45.1	Tg(TcraTcrb)1100Mjb;Ptprc^{a}	C57BL/6	The Jackson Laboratory
OT1xNR4	Tg(TcraTcrb)1100Mjb;Tg(Nr4a1-EGFP/cre)820Khog	C57BL/6	The Jackson Laboratory
OT1xRaptor	Tg(TcraTcrb)1100Mjb;Tg(Cd	C57BL/6	The Jackson Laborato-

	4-cre)1Cwi;Rptor$^{tm1.1Dmsa}$		ry
OT1xRictor	Tg(TcraTcrb)1100Mjb;Tg(Cd 4-cre)1Cwi;Rictor$^{tm1.1Klg}$	C57BL/6	The Jackson Laboratory
OT1xRR	Tg(TcraTcrb)1100Mjb;Tg(Cd 4-cre)1Cwi;Rptor$^{tm1.1Dmsa}$; Rictor$^{tm1.1Klg}$	C57BL/6	The Jackson Laboratory

2.1.6 Primer

Number	Gene	Sequence
RO289	CD4-cre	TGTGGCTGATGATCCGAATA
RO290	CD4-cre	GCTTGCATGATCTCCGGTAT
RO291	Raptor loxP	ATGGTAGCAGGCACACTCTTCATG
RO292	Raptor loxP	GCTAAACATTCAGTCCCTAATC
RO293	Rictor loxP	TTATTAACTGTGTGTGGGTTG
RO294	Rictor loxP	CGTCTTAGTGTTGCTGTCTAG
RO445	NR4	CGGGTCAGAAAGAATGGTGT
RO446	NR4	CAGTTTCAGTCCCCATCCTC
RO459	OT1	CAGCAGCAGGTGAGACAAAGT
RO460	OT1	GGCTTTATAATTAGCTTGGTCC
RO488	CD45.2 (reverse)	CATGGGGTTTAGATGCAGAC
RO489	CD45.1 (reverse)	CATGGGGTTTAGATGCAGGA
RO490	CD45 (forward)	GCAAGGCAGGATGCTAGAAA
RO559	H-2K^{b}	GCTGGTGAAGCAGAGAGACT
RO560	H-2K^{bm1}	GGCTGGTGCTGCAGAGTATTA
RO561	H-2K$^{b/bm1}$ (reverse)	GATGAGGGATCAGGAGACCA
RO625	H-2A$^{b/bm12}$ (forward)	AGACGCCGAGTACTGGAAC
RO626	H-2A^{b}	CGGAGATCCTGGAGCGAAC
RO627	H-2A^{bm12}	CGGAGTTCCTGGAGCCAAA
RO628	H-2A$^{b/bm12}$ (reverse)	AGAGGTGAGACAGGAGGGA

2.1.7 Buffers

Buffer	Amount/vol	Substance	End concentration
35% BSA	200 ml	PBS	-
	70 g	BSA	35%
	1 ml	Sodium azide	10%
Blotting Buffer	15 g	Tris	
	72.1 g	Glycine	
	1 L	Methanol	
	Fill up to 5L	ddH_20	
CTV Labeling Buffer	100 mL	PBS	-
	0.1 g	BSA	0.1%
FACS Medium	500 ml	DMEM	-
	5 ml	HEPES	1%
	14,3 ml (35%)	BSA	1%
Gel loading Buffer	250 mg	Orange G	2.5 mg/ml
	30 ml	Glycerin	30%
	70 ml	ddH_2O	-
Gene Ruler Mix	100 µl	Gene Ruler	
	700 µl	TAE	
	200 µl	Gel loading buffer	
Gitocher Buffer 10x		Tris, pH 8.8	670 mM
		Ammonium sulfate	166 mM
		Magnesium chloride	65 mM
		Gelatin	0.1%
		ddH_2O	
Laemmli Buffer 4x	1.514 g	Tris	
	4 g	SDS	
	20 ml	Glycerol	
	10 ml	ß-Mercaptoethanol 50 µM	
	200 mg	Bromophenolblue	
	Fill up to 50 mL	ddH_2O	
MACS Buffer	1x	PBS	-
		EDTA	1 mM
		BSA	0.5%
Paraformaldehyde 4%	4 g	Paraformaldehyde	4%
	10 ml	10x PBS	1x

	Adjust to pH 7.4	HCl	-
	Fill up to 100 mL	ddH_2O	-
PBS, selfmade (10x)	180 g	NaCl	
	28.66 g	Dinatriumhydrogenphosphat	
		Kaliumdihydrogenphosphate	
	5.34 g	ddH_2O	
	Fill up to 2L		
Protein lysis Buffer		HEPES	50 mM
		NaCl	150 mM
		Glycerol	10%
		CHAPS	0.3%
		Magnesium chloride	1.5 mM
		EGTA	1 mM
		Sodium Fluoride	100 mM
		Sodium orthovanadate	500 µM
		Aprotinin	10 µg/ml
		Leupeptin	10 µg/ml
SDS Running Buffer 10x	30.28 g	Tris	
	187.75g	Glycine	
	10g	SDS	
	Fill up to 1L	ddH_2O	-
Selfmade ECL Solution 2	3 ml	H_2O_2	3%
	100 ml	ddH_2O	-
T cell Medium	500 ml	RPMI + Glutamax	
	50 ml	FCS, heat-inactivated	10%
	5 ml	Antimycotic/Antibiotic	1%
	2 µl	ß-Mercaptoethanol 50 µM	50 µM
TAE 1x	4.9 l	ddH_2O	-
	100 ml	TAE (50x)	1x
TAE 50x	242 g	Tris	
	27.1 ml	Acetic acid (99%)	
	100 ml	EDTA (pH 8.0), 0.5M	0.05M
	Fill up to 1L	ddH_2O	-
TBS 10x	12.1 g	Tris	
	87.7 g	NaCl	
	Adjust pH to 8.0	HCl	-
	Fill up to 1L	ddH_2O	-
TBS-T 1x	900 ml	ddH_2O	-

	100 ml	TBS (10x)	1x
	500 µl	Tween20	0.05%
Tissue Digestion Buffer	82 µl	ddH_2O	
	10 µl	Gitocher Buffer	
	3 µl	PK	
	5 µl	Triton-X	

2.1.8 Consumables

Consumable	Company
1.5 ml tubes	Eppendorf
10 ml snap cap tubes	Greiner bio-one
14 ml snap cap tubes	Falcon
15 ml tubes	Greiner bio-one
2 ml tubes	Eppendorf
50 ml Luerlock syringe	BD Plastipak
50 ml tubes	Greiner bio-one
CASY tubes	OLS Omni Life Science
Cell strainer	Miltenyi Biotech
Cover foil for PCR plates Easy Seal	Greiner Bio-one
Disposable cuvettes 1.5 ml semi-micro	Brand
FACS tubes	Falcon
Falcon tubes 15ml and 50ml	Falcon
Filter tips 1-10 µl	Starlab TipOne
Filter tips 2-20 µl	Starlab TipOne
Flüssigkeitsreservoir 60 ml	Diagonal
Gel holder cassette	BioRad
Glass plates	BioRad
Gloves	Meditrade
Hypercassette	Dr. Goos Suprema
Insulin syringe 1 ml	Diagonal
Insulin syringes 0.5 ml	Diagonal
LS column	Miltenyi Biotech
MACS magnet	Miltenyi Biotech
Medical X-ray film, blauempfindlich	Röntgen Bender GmbH & Co. KG
Millex GP Filter unit 0.22 µm	Millipore Express

Multichannel 1-10 µl (8 channel)	Brand
Multichannel pipette 20-200 µl (12 channel)	Brand
Objektträger	Diagonal
Pasteurpipetten 3 ml, steril	Diagonal
PCR plates	Sapphire, Greiner bio-one
Petri dishes	Diagonal
Pipetboy	Accu-jet pro
Pipette 0.1-2 µl	Brand
Pipette 100-1000 µl	Brand
Pipette 2-20 µl	Brand
Pipette 20-200 µl	Brand
Pipette tips	Brand
Polyamid Siebgewebe 120 µm	Klein & Wieler OHG
Polyamid Siebgewebe 80 µm	Diagonal
RP New, Medical X-ray films, blue	CEA
Restrainer mice	Sigma
Scissors	WPI-europe
Serologische Einmalpipetten	Ratiolab
Staining plates (96-well)	Diagonal
Sterile pipettes 2 ml, 5 ml, 10 ml, 25 ml	Diagonal, Greiner bio-one
Tweezers, small	A.Dumont &FILS
Tweezers, large	WPI-europe
U-bottom 96-well plates	Sarstedt

2.1.9 Kits

Kit	**Company**
Click-iT™ EdU Alexa Fluor™ 488 Flow Cytometry Assay Kit	Thermo Fisher
Click-iT™ HPG Alexa Fluor™ 488 Protein Synthesis Assay Kit	Thermo Fisher
mTOR Pathway Antibody Sampler Kit	Cell Signaling
Pierce BCA Protein Assay Kit	Thermo Fisher

2.1.10 Machines

Machine	Company
-80°C Herafreeze HFU T series	Thermo Scientific
Amnis Imagestream	Merck
autoMACS	Miltenyi
CASY Counter	OLS Omni Life Science
Cell culture hood Flow Safe B-(MaxPro)^2-190	Berner
Centrifuge Heraeus Multifuge X3R	Thermo Scientific
Centrifuge klein 5417 R	Eppendorf
Centrifuge Rotanta 460R	Hettich
Electrophoresis Power Supply EPS200	Pharmacia Biotech
Eppendorf BioSpectrometer	Eppendorf
Eppendorf ThermoMixer C	Eppendorf
FACS Aria III	BD
FACS Aria Fusion	BD
FACS Canto	BD
FACS Fortessa	BD
Freezer	Liebherr
Fridge	Liebherr
Gel Doc XR+	BioRad
Incubator New Brunswick, Galaxy 170R	eppendorf
Microscope	Leica
Microwave	Bosch
Mini Protean Tetra System	BioRad
Optimax Developer	Protec
Orbital Rocking Motion Shaker (Taumelschüttler)	GFL
PCR Cycler T Advanced	Biometra
PCR Cycler T1 Thermocycler	Biometra
pH meter	WTW inoLab
Schüttelplatte WB (Wippschüttler) ST5 CAT	NeoLab
Vortex 54119 REAX 2000	Heidolph
Waage Scout	Ohaus
Water bath JB Series	Grant Instruments
WB Power Supply	BioRad

2.1.11 Softwares

Program	Company
Affinity Designer	Serif (Europe) Ltd
CASYworX	OLS, Omni Life Science
Endnote 20.6	Clarivate Analytics
FACS Diva	BD
FlowJo 10	BD
Gel documentation	Intas
GraphPad Prism 7, 10	Graphpad Software, Inc.
IDEAS	Merck KGaA
Microsoft Office (Word, Excel, Powerpoint)	Microsoft
tick@lab	a-tune software

2.2 Methods

2.2.1 Mice

2.2.1.1 Breeding and housing of the mice

Mice were bred and maintained at the animal core facility of the BMC, Ludwig-Maximilians-University Munich, Germany. All experiments were conducted in compliance with the German federal guidelines under the protocols ROB-55.2-2532.Vet_02-22-53 and ROB-55.2-1-54-2532-84-2015 approved by the government of Upper Bavaria.

2.2.1.2 Wildtype mice

Wildtype mice with B6 (C57Bl/6) and B10.BR (B10.BR/Jax) background were purchased from The Jackson Laboratory and bred at the animal core facility of the BMC.

2.2.1.3 TCR transgenic mice

TCR transgenic mice which carry an OT1 (Tg(TcraTcrb)1100Mjb;Ptprca) or AND (Tg(TcrAND)53Hed;Ptprca) transgenic T cell receptor were used for antigen-specific stimulation experiments in vivo and in vitro (Hogquist et al., 1994; Kaye et al., 1989). OT1 mice were purchased from The Jackson Laboratory. AND mice were obtained from C. Benoist and D. Mathis from the Harvard Medical School, USA.

The TCR of $OT1^+$ transgenic T cells mainly consists of the Vα2 and Vβ5 chain, which recognizes the peptide ovalbumin ($OVA_{257-264}$/SIINFEKL). The AND transgenic T cell receptor mainly consists of the Vα11 and Vβ3 chain, which recognizes a peptide derived from moth cytochrome C. The OT1 and AND transgenic mice were crossed with mice expressing the congenic marker CD45.1 to obtain the OT1x45.1 and ANDx45.1 mouse lines.

2.2.1.4 Congenic marker

The congenic marker CD45.1 was used to distinguish adoptively transferred cells from endogenous cells. CD45.1 originally derives from Ptprca mice which were purchased from The Jackson Laboratory.

2.2.1.5 NR4 reporter mice

In order to visualize early TCR signaling, a mouse line was used that carries a Nur77-GFP reporter cassette (Moran et al., 2011). NR4 mice (Tg(Nr4a1-EGFP/cre)820Khog) were purchased from The Jackson Laboratory and visualize early Nur77 (Nr4a1) expression after TCR stimulation. The NR4 mice were crossed to OT1 and AND transgenic mice to obtain OT1xNR4 and ANDxNR4 mouse lines.

2.2.1.6 mTORC1 and mTORC2-deficient mice

To investigate the function of mTORC1 and mTORC2, specific knockouts for each complex were used; Raptor (Tg(Cd4-cre)1Cwi;Rptor$^{tm1.1Dmsa}$) for mTORC1 (Sengupta et al., 2010) and Rictor (Tg(Cd4-cre)1Cwi;Rictor$^{tm1.1Klg}$) for mTORC2 (Tang et al., 2012). Both Raptor and Rictor lines were crossed to the transgene CD4-cre which drives the expression of a Cre recombinase gene. The Cre rembinase is mainly expressed in CD4$^+$ T cells during different stages during T cell development in the thymus and results in deletion of loxP flanked genes. (Sawada et al., 1994). Both lines were purchased from The Jackson Laboratory and crossed to OT1 transgenic mice carrying the congenic marker CD45.1. Another line which carries both deletions at the same time, Rap/Ric, was created as well to see effects of both Raptor and Rictor deletion.

2.2.1.7 Bm1 and Bm12 mice

H2-A$^{b/bm12}$ mice were purchased from The Jackson Laboratory and H2-K$^{b/bm1}$ were obtained from V. Buchholz (Technische Universität München). The bm1 mutation (MGI ID: 3618114) contains seven different nucleotides, resulting in three amino acid exchanges (McKenzie et al., 1977). Therefore, a different repertoire of self-peptides is presented in the context of MHC-I. The bm12 mutation (MGI ID: 3586447) as well contains different nucleotides, leading to three amino acid substitutions and thus, binding and presenting a different repertoire in the context of MHC-II (McKenzie et al., 1979).

2.2.2 Adoptive Transfer

Mice were treated with 20 µg anti-CD40 to activate dendritic cells for immunogenic antigen presentation to T cells (Obst et al., 2007). Sterile solutions of anti-CD40 in PBS were prepared and injected intraperitoneally (i.p.) with a maximum of 100 µL per mouse on day -1. For in vivo stimulation assays, lymphocytes were harvested from lymph nodes (axillary, inguinal, brachial, cervical) in DMEM without BSA. For details on lymphocyte isolation refer to chapter 2.2.8. If indicated, cells were labeled with CTV (chapter 2.2.11) and injected in a maximal volume of 100 µL DMEM without BSA intravenously (i.v.). Cell numbers varied between 0.1 x 10^6 and 2 x 10^6 cells per mouse depending on the experimental setup.

2.2.3 Immunization of B10.BR or B6 mice to generate memory T cells

For memory experiments, lymph nodes and spleen were taken from one B6 mouse and erythrocytes depleted by addition of 1 ml Red blood cell lysis buffer (RBC Lysis Buffer). After 5 minutes incubation at room temperature, cells were spun down and resuspended in fresh FACS Buffer without BSA and washed twice. 10x10^6 splenocytes in 100 µl buffer were injected intraperitoneally (i.p.) into 4 B10.BR mice. Two weeks later there was a second im-

munization with freshly isolated splenocytes. 4 weeks after the second injection, spleens were harvested and processed for cell sorting and reculture. Animals were scored following the protocols listed under 2.2.1.1 regarding weight, behaviour and health condition regularly on the first 3 days post immunization, later once per week.

2.2.4 Tissue digestion

Biopsies were taken from the mice (ear tags or tails) by the animal caretakers in the Core Facility Animal Models (CAM) for genotyping. The biopsies were transferred into PCR tubes and 100 µl of DNA digestion buffer was added, freshly prepared according to the following table:

Table 1: Ingredients of Tissue digestion buffer

Reagent	**Volume**
H_2O	82 µl
Gitocher Buffer	10 µl
PK	3 µl
Triton-X	5 µl
Total	**100 µl**

Samples were spun down shortly on a mini centrifuge to make sure the biopsies are fully immersed by the buffer and incubated at 56°C on a PCR cycler for 6 hours, followed by 10 min at 95°C step to inactivate the PK. DNA samples were then stored at -20°C until further processing.

2.2.5 Polymerase Chain Reaction (PCR)

2.2.5.1 General Procedure

The primers (stock: 100 µM) used for PCR were diluted 1:10 (working conc.: 10 µM) in UltraPure DEPC treated water under the cell culture hood. A mastermix was prepared on ice for each primer pair according to the following scheme:

Table 2: PCR mix

Component	**c(stock)**	**c(end)**	**µl per reaction**
H_2O	-	-	13.375
PCR buffer	10x	1x	2.5
Enhancer	5x	1x	5

Oligo 1	10 µM	0.5 µM	1.25
Oligo 2	10 µM	0.5 µM	1.25
dNTPs	10 mM	0.2 mM	0.5
Taq	5 U/µl	0.125 U/reaction	0.125
Total	-	-	**24**

1 µl DNA/reaction was pipetted into a PCR tube or a 96-well plate, spun down for 1 minute and 24 µl of Mastermix was added to each tube or well. The samples were centrifuged again for 1 minute and each sample was overlayed with 1 drop of mineral oil to prevent condensation. The plate was covered with a transparent foil and put into the PCR cycler as soon as 95°C were reached. The program ran according to this scheme:

Table 3: Overview of PCR program sequence

Denaturation	95°C	5 min	
Annealing	95°C	30 sec	35x
	55°C	30 sec	
	72°C	45 sec	
Extension	72°C	5 min	

2.2.6 Agarose gel electrophoresis

For gel electrophoresis a 1.5% agarose gel was prepared. 3 g of agarose were dissolved in 200 ml TAE Buffer by heating in the microwave at 800V for 4 minutes. The solution was shaken carefully in between until it was completely transparent. The solution was then cooled down under running tap water. 1 drop of ethidiumbromide was added under a hood and the agarose poured into a prepared chamber. After 20-30 minutes the gel was solid and transferred in an electrophoresis chamber, which was filled up with TAE buffer. 10 µl of a Gene Ruler was loaded into the first and last lane of each row, and in between 15 µl of PCR product, mixed with 2-3 µl of Orange G. The electrophoresis was run at 120V for 30-60 minutes, depending on the genotype. Afterwards the gel was measured by Geldoku. In Figure 8 representative genotyping results for samples from mouse lines OT1xRa (A) and OT1xNR4 (B) are shown with the associated genes to be determined.

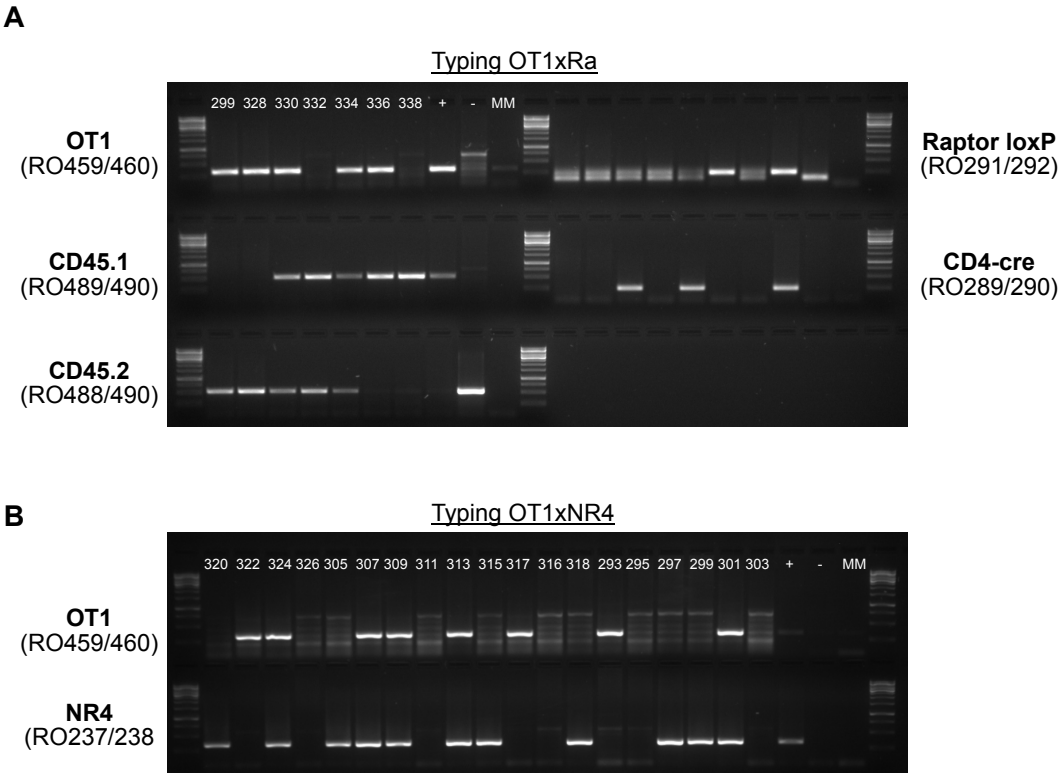

Figure 8: Genotyping of several mouse lines.
(A), (B) and (C) show examples for gel electrophoresis of PCR products from (A) OT1xRaptor$^{fl/fl}$ mice, (B) OT1xNR4. Numbers in () indicate the used primer pair.

2.2.7 Blood genotyping

Some genes, such as OT1 and CD45.1 and CD45.2, were occasionally also typed by blood. Animal caretakers provided 2-3 drops of blood, mixed with Heparin containing PBS. The blood was transferred into 1.5 ml tubes and centrifuged at 1500 rpm for 1 minute. The supernatant was discarded and 1 ml of Red blood cell lysis buffer, diluted 1:10 with water, added and incubated for 5 minutes at room temperature. After incubation time, samples were centrifuged as before and the supernatant removed. The cell pellet was resuspended in 200 µl FACS Buffer and transferred into a 96-well staining plate. For OT1 typing, cells were stained with Va2-FITC, Vb5-PE, CD4-PerCp and CD8-APC. For CD45 congenic marker, cells were stained with CD45.1-PeCy7 and CD45.2-APC. For details on surface marker staining, see chapter 2.2.16. Samples were then measured with a BD Canto II and analyzed by FlowJo. A representative FACS plot is shown below in Figure 9 for two samples.

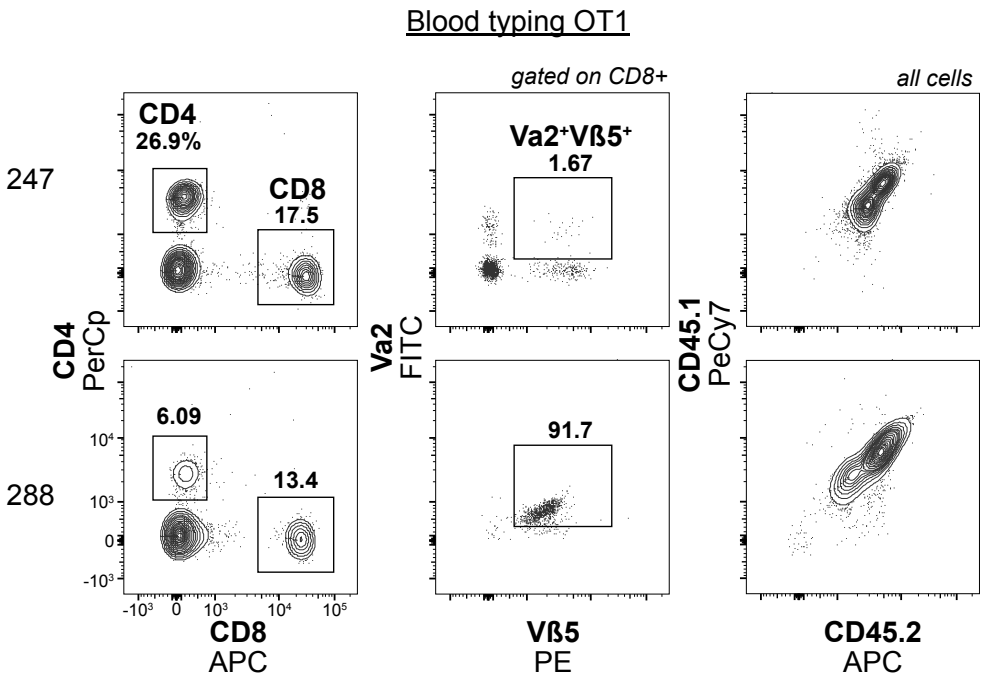

Figure 9: FACS plots of 2 blood samples from the OT1x45.1 mouse line.
Upper row shows an OT1 negative mouse (247). The lower row shows an OT1 positive mouse (288). Both animals were CD45.1/2.

2.2.8 Organ removal and cell isolation

Spleen, axillary, inguinal, brachial and cervical lymph nodes were isolated with scissors and tweezers and stored in FACS Buffer. By using sterile glass cover slides, the organs were carefully ground and washed off with 5 ml of FACS buffer and transferred into 14 ml tubes under sterile conditions. 3 ml Ficoll was added on the bottom of the tube with Pasteur pipettes. The cell suspension was then centrifuged through the Ficoll cushion for 10 minutes at 1500 rpm with reduced brake to remove erythrocytes. The intermediate phase containing the lymphocytes was transferred into a fresh tube and washed again with FACS Buffer.

2.2.9 Cell counting by CASY Cell counter

The CASY Cell counter determines the viability, volume, and number of cells in a defined solution by Electronic Current Exclusion (ECE) and Pulse Field Analysis (Product description Omni Life Science, www.ols-bio.de). Therefore, 10 µl of a cell suspension was diluted in 10 ml Casyton solution. The tube was put on the CASY Cell Counter, which measured the conductivity between the two electrodes between a defined pore. The cell number/ml was determined by the Counter. If required, the cell suspension was diluted in Casyton and the result calculated considering the dilution factor. Cell volume and diameter could be exported from the CASY software and imported into Excel for visualization.

2.2.10 Titration and use of inhibitors

All inhibitors were resolved in DMSO according to the manufacturer's protocol. Titrations were performed for all inhibitors in 1:3 or 1:2 dilutions steps in a 96-well plate to display the range of the response.

Torin-1 was used to block mTORC1 and mTORC2 activity completely (Thoreen et al., 2009). Quarfloxin (CX3543, Hölzel) and BMH21 (Selleckchem) were used as RNA Pol I inhibitors (Colis et al., 2014; Drygin et al., 2009; Peltonen et al., 2014). Tigecyclin was used as an inhibitor of mitochondrial RNA synthesis (Livermore, 2005).

To investigate the effects of blocking single TCR signaling pathways we used Cyclosporin A (Flanagan et al., 1991; Liu et al., 1991), GDC0973 (Hoeflich et al., 2012) and BAY117082 (Melisi and Chiao, 2007) to block Calcineurin (NFAT), MEK and NFkB signaling pathways, respectively. GDC0941 was used as a downstream inhibitor for PI3K to block mTOR activation (Folkes et al., 2008).

Tofacitinib (Selleckchem) was used to investigate the effect of JAK/Stat signaling in restimulation experiments (Flanagan et al., 2010).

2.2.11 CellTrackerViolet (CTV)/ CellTrackerRed (CTR) Labeling

To visualize cell proliferation, naïve T cells/lymphocytes were labeled with CellTracker Violet or CellTracker Deep Red (Thermo Fisher). $2x10^6$ cells were resuspended in pre-warmed PBS+0.5% BSA and 1 µl CTV/CTR was added during vortexing. Cells were incubated for 10' in the waterbath and then washed twice with FACS Buffer. The number of divisions was calculated as follows: $N = \log_2(\text{CTV MFI}_{ctrl}/\text{CTV MFI}_{sample})$ (Obst et al., 2007).

2.2.12 MACS sorting of T cells

Sample preparation

For isolation of T cells, a cell suspension containing splenocytes was spun through a Ficoll cushion as described in chapter 2.2.8. Afterwards the cell pellet was resuspended in a mixture of 180 µl FACS buffer plus biotinylated antibodies per sample, according to Table 4:

Table 4: Mix of biotinylated antibodies for negative selection by MACS

Antibody	Fluorochrome	Target	µl/mouse
CD45R	Biotin	B cells	8
CD49	Biotin	NK cells	5
Gr-1	Biotin	Granulocytes	5

CD11b	Biotin	Macrophages	5
CD11c	Biotin	Dendritic cells	5
TER119	Biotin	Erythrocytes	5
CD19	Biotin	B cells	5
CD4 (if required)	Biotin	CD4 T cells	5
CD8 (if required)	Biotin	CD8 T cells	5

Cells incubated for 15 min in the biotinylated antibody mix on ice. Then, 3 ml FACS Buffer was added to each tube to wash off unbound antibodies. Samples were centrifuged as described before and washed twice. Then, the pellet was resuspended in 100 µl FACS Buffer containing 10 µl anti-biotin mAb magnetic beads and incubated for 20 minutes on ice.

Magnetic sorting – LS columns

For manually magnetic sorting, cells were washed again twice in MACS Buffer and finally resuspended in 2 ml MACS Buffer. LS columns (Miltenyi) were placed in a magnet and fresh 14 ml tubes placed below. The complete 2 ml suspension was pipetted onto the column. By running through the column, labeled cells stick to the magnet, while unlabeled cells (CD4 or CD8 T cells or both) are collected into the tube. The column was eluted twice with 3 ml MACS buffer. The complete flow-through was then centrifuged and resuspended in FACS buffer. Post-sort purity was checked by FACS as shown in Figure 10. Generally, purities were between 95-100% (lower panel).

Magnetic sorting – autoMACS

With the same principle, T cells were sorted at the autoMACS (Miltenyi). Cell suspensions were transferred into 15 ml Falcon tubes in 100 µl FACS buffer containing Streptavidin (SA)-magnetic beads. The tubes were placed in a pre-cooled rack and put into the machine. The program DEPLETES, supplied by the manufacturer, was chosen and cells were automatically sorted into fresh 15 ml tubes.

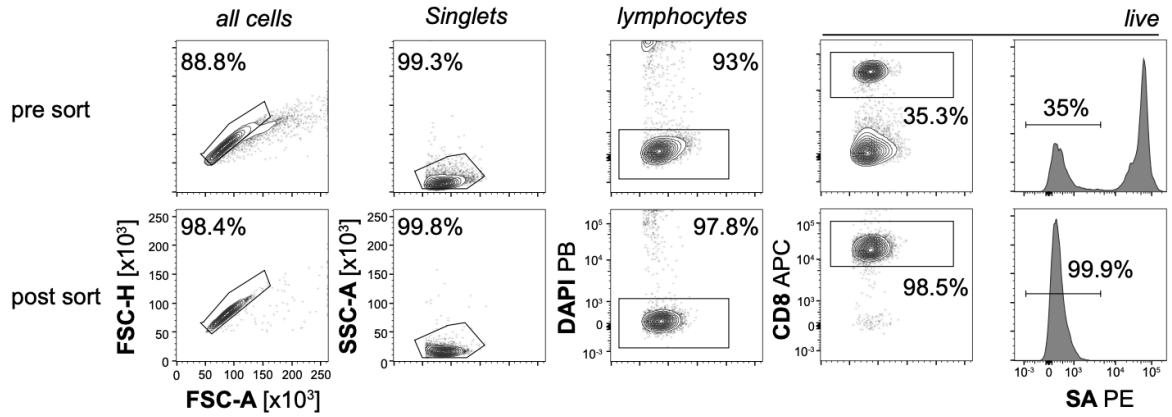

Figure 10: Purity check post MACS enrichment of CD8⁺ T cells.
Upper panels show cells pre-sort, gated on Singlets, lymphocytes and live CD8⁺ T cells. Lower panels show cells post sorting. The amount of Streptavidin (SA) is shown in the panels on the right, indicating that levels of SA-bound cells before and after enrichment.

2.2.13 Culturing and stimulation of T cells

2.2.13.1 Purified T cells

MACS-enriched non-TCR transgenic T cells were stimulated with plate-bound anti-CD3 (10 µg/ml) and anti-CD28 (10 µg/ml) mAbs. For plate coating, µl/plate anti-CD3 and anti-CD28 antibodies were diluted in 7 ml PBS/plate and 70 µl distributed in the wells of a 96-well round bottom plate (Sarstedt, type suspension). The plates were incubated for 90 minutes at 37°C, 5% CO_2 in a tissue culture incubator. 100 µl ice-cold PBS were then added to each well and removed. The plates were washed again with 100 µl PBS. Then $1x10^6$ cells/well were plated in 200 µl T cell medium/well. 10 µg/ml IL-7 was added to the medium to increase survival.

2.2.13.2 OT1 transgenic splenocytes

OT1 splenocytes were cultured at $2x10^6$ cells per well in a 96-well round bottom plate (Sarstedt, type suspension) in T cell medium and stimulated with 10 ng/ml OVA peptide (SIINFEKL) for the indicated time points. 10 µg/ml IL-7 was added to the culture to increase survival. All cells were stained and measured by FACS to confirm their naïve phenotype and OT1 genotype, as shown in Figure 11. CD4, CD8 and Va2 staining confirms that the T cells are OT^+, while $CD44^{int}$ and $CD62L^{high}$ stainings confirm that the cells are naïve.

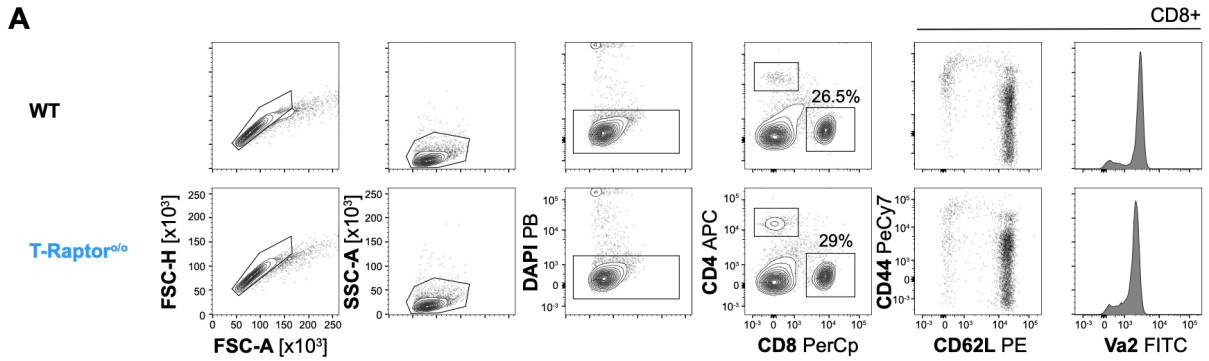

Figure 11: Control staining of OT1 T cells from WT and T-Rap$^{o/o}$ mice.
T cells are gated for Single cells, separated by FSC-H and FSC-A, lymphocytes by SSC-A and FSC-A gating, live cells (DAPI-) and CD4$^+$ and CD8$^+$ T cells. CD62L^{high} CD44^{int} staining confirms naïve state of cells. Va2 staining confirms presence of OT1 TCR.

2.2.13.3 Generation of memory-like T cells in vitro

OT1 splenocytes were stimulated with 10 ng/ml OVA peptide and 10 ng/ml IL-2 for three days. On day 3, the cells were washed twice in T cell medium and re-cultured with either 10 µg/ml IL-2 for effector T cells or 10 ng/ml IL-15 for T cells with phenotypic properties of memory T cells for four more days (Carrio et al., 2004). On day 7 post stimulation the T cells were further analyzed by flow cytometry.

2.2.14 5-ethynyl-2'deoxyuridine (EdU) assay

For 5-ethynyl-2'-deoxyuridine (EdU) pulse/chase experiments, 10 µM EdU was added to the stimulation cultures described in chapter 2.2.13.1 on day 2 and incubated for 1 hour. Then EdU was washed away, and samples taken after indicated time points (Figure 15). EdU was visualized using the Click-iT EdU Flow Cytometry Cell Proliferation Assay Kit according to the manufacturer's protocol (Thermo Fisher). EdU is a nucleoside analog to thymidine which is incorporated into the DNA during S phase. By click chemistry, the incorporation is visualized by the reaction between an azide and an alkyne. The alkyne is part of the EdU moiety, and the azide is coupled to an Al488 dye. Cells were harvested and labeled for surface markers including a live/dead dye (see chapter 2.2.16) and fixed and permeabilized with the reagents offered in the kit. For the Click-iT reaction a mix was prepared according to the following table (Table 5):

Table 5: Reaction mix for EdU detection

Reaction components	**For 1 reaction**
PBS	438 µl
CuSO4 (Component F)	10 µl
Fluorescent dye azide	2.5 µl
Reaction Buffer Additive	50 µl
Total volume	500 µl

The cells were transferred into 14 ml tubes or 1.5 ml tubes and 500 µl of the Click-iT reaction mix added and mixed well. After 30 minutes incubation at room temperature the cells were washed twice and counterstained with Hoechst33342 to differentiate cell cycle stages. Samples were then acquired on a BD LSR Fortessa.

2.2.15 L-Homopropargylglycine (HPG) assay

The de novo protein synthesis was measured with the Click-iT HPG Alexa Fluor 488 Assay-Kit from Thermo Fisher, according to the manufacturer's protocol. L-Homopropargylglycine (HPG) is an amino acid analog to methionine which contains an alkyne part. The azide for the Click reaction is included in the Al488 dye.

On day 2 post stimulation, the cells were harvested, washed twice and re-cultured in methionine-free RPMI culture medium. HPG was added in a 1:1000 dilution and incubated for 1 hour. Afterwards cells were harvested and stained for surface markers. According to the protocol, cells were fixed and permeabilized. For the Click-iT reaction the same reaction mix as described in 2.2.14 (see Table 5) was prepared and added. HPG incorporation was then measured by flow cytometry with a BD LSR Fortessa.

2.2.16 Cell surface staining

T lymphocytes were harvested at indicated time points, washed twice and transferred into 96-well plates. An antibody mix was prepared in PBS, containing a live/dead dye such as FVD780 (1:4000 diluted) or DAPI for live cells (1:1000 diluted). Surface markers for distinguishing $CD4^+$ and $CD8^+$ populations as well as other surface antibodies were added in a 1:400 dilution. 50 µl of the mix were added to the cells and incubated for 20 minutes in the fridge. After the incubation time, the cells were washed twice and transferred through a filter into FACS tubes. Data were then acquired with a Canto II or LSR Fortessa.

2.2.17 Intracellular staining

2.2.17.1 5’ external transcribed spacer (ETS) staining

For 5’ ETS staining cells were fixed in 200 µl 2% paraformaldehyde (PFA)/PBS for 10 min at room temperature, followed by two washing steps with FACS buffer. Then the cells were permeabilized in 100 µl Perm Buffer III (BD Bioscience) for 5 minutes at room temperature and washed twice. Cells were washed once in Wash Buffer A (Stellaris), followed by an overnight incubation in 100 µl Hybridization buffer (Stellaris) containing 1 µl probe/sample at 37°C. The probe consists of 48 Oligos. After incubation time, cells were washed again with Wash Buffer A and FACS buffer and then stained with Hoechst33342. Samples were measured using an LSR Fortessa (BD) or an MK II Imaging Flow cytometer (Amnis, Merck).

2.2.17.2 RNA and DNA staining

T cells were harvested at the indicated time points post stimulation and counted. $1x10^6$ cells were used for each experiment and stained for surface markers and fixed in 2% PFA. Then the cells were permeabilized with Perm Buffer III (BD Bioscience), washed twice and resuspended in 100 µl Hoechst33342 (stock: 10 mg/mL; diluted 1:1000 in PBS) and incubated for 10’ at room temperature. After the incubation time, 100 µl Pyronin Y solution (stock: 1 mg/mL; diluted 1:200 in PBS) was added on top and incubated for further 10’. The cells were centrifuged and resuspended in FACS buffer and immediately measured with LSR Fortessa or Canto II cytometers (BD).

2.2.17.3 Phospho-antibody staining

For intracellular staining with phospho-S6 (pS6) or phospho-H3 (pH3) antibodies, T cells were first surface stained with CD8 and fixable viability dye and then fixed in 2% PFA. For pS6 staining, the cells were permeabilized in Perm Buffer III, washed twice, and incubated with the pS6 antibody (diluted 1:100) for 20 min at room temperature. For pH3 staining, the cells were washed after permeabilization in PBS/3% FCS and the antibody added 1:10 diluted in PBS/3% FCS and incubated for 2 hours at room temperature. Cells were washed twice in PBS/3% FCS and counterstained with Hoechst33342.

2.2.18 Flow cytometry

Flow cytometry allows rapid analysis of cells at single cell level by scattering of light and measuring the fluorescence. The fluorescent-labeled cells move in a fluid stream and pass by a laser beam which emits the fluorescence.

Compensation is necessary due to the spillover of the fluorophores. Therefore, single color stainings are prepared on appropriate cells of each experiment and measured in the begin-

ning. The DIVA software (BD) calculates the spillover and substracts it from the measurements. Compensation matrices were always controlled and, if necessary, later adjusted in FlowJo.

The acquisition files were analyzed with the Flowjo 10 software. Figure 12 shows gating strategies of naïve and activated OT1 T cells as examples. By FSC-A and FSC-H parameters doublets can be excluded. The SSC-A and FSC-A plot allows to identify lymphocytes. The next gate excludes dead cells based on DAPI or FVD positivity, and then $CD8^+$ target populations are identified.

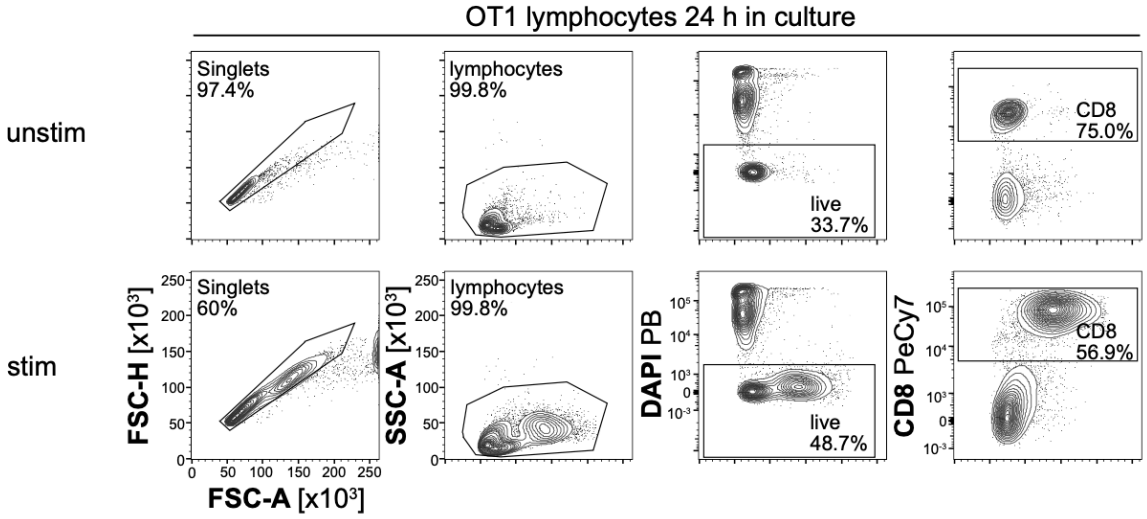

Figure 12: Gating strategy of naive and activated OT1 T cells.
Gating strategy is shown for unstimulated (upper panels) and stimulated $OT1^+$ T cells (lower panels). T cells are gated for Singlets, lymphocytes, live and $CD8^+$.

2.2.19 Imaging Flow Cytometry (Amnis)

$OT1^+$ T cells were stained for 47S rRNA, Hoechst33342 and appropriate surface markers and analyzed on an ImageStream^X MkII Imaging Flow cytometer (Merck). Therefore, the stained cells were resuspended in 50 µl PBS and transferred into 1.5 ml Eppendorf tubes, which could be entered into the Amnis reader. Compensation was done by recording single cell stainings and automatic calculations by the IDEAS software.

$CD8^+$ T cells were gated in the IDEAS Software and a Spot Count mask was applied to count 47S rRNA spots per cell. Additionally, nucleolus area, cellular and nuclear volume were defined using features of the IDEAS software by the following features and formulas:

Table 6: Features and formulas for Amnis analysis

Marker	Feature
Area cell (μm^2)	Mask AdaptiveErode(M01,BF1,95)
Area nucleus (μm^2)	Mask AdaptiveErode(M07,DAPI,80)
Area nucleolus (μm^2)	Mask AdaptiveErode(Spot(M11,47S rRNA,Bright,100,1,2),47S rRNA,90)
Volume cell (μm^3)	4/3 x π x (diameter_AdaptiveErode(M01,BF1,95/2)) x (diameter_AdaptiveErode (M01,BF1,95/2)) x (diameter_AdaptiveErode (M01,BF1,95/2))
Volume nucleus (μm^3)	4/3 x π x (diameter_AdaptiveErode(M07,DAPI,80/2)) x (diameter_AdaptiveErode (M07,DAPI,80/2)) x (diameter_AdaptiveErode(M07,DAPI,80/2))
Volume cytoplasm (μm^3)	volume cell – volume nucleus
Spot Count (n)	Dilate(Peak(M11,47S rRNA,Bright,15),1)

The data files were then exported as fcs files and further analyzed in FlowJo 10. An example for the gating strategy is shown in Figure 13.

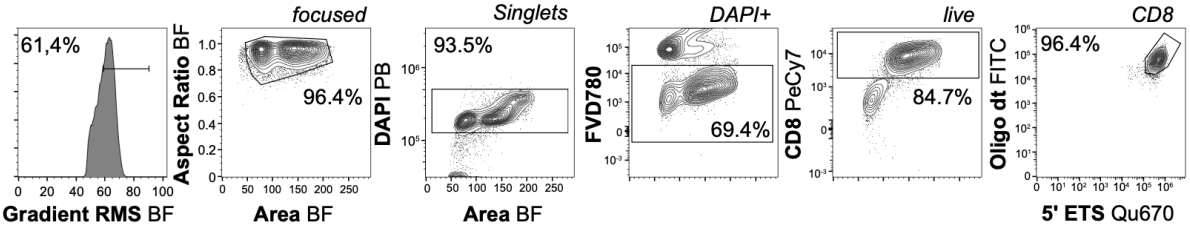

Figure 13: Gating strategy for Amnis data.
Gating strategy of acquired $CD8^+$ T cells in the IDEAS software is shown. T cells are gated for "focused", Singlets, $DAPI^+$, live and $CD8^+$.

2.2.20 Cell Sorting

Cell Sorting was carried out by Lisa Richter and Pardis Khosravani at the BMC Core Facility Flow Cytometry using Aria Fusion or FACS Aria III sorters (BD).

For volume measurements, the cells were stimulated 0-3 days and stained for DAPI, 1:1000 diluted in PBS to ensure only live cell acquisition. $DAPI^-$ cells were collected in 1.5 ml Eppendorf tubes, spun down and directly used for CASY measurement.

For sorting memory cells (refer to chapter 2.2.3), lymphocytes were isolated from spleens and pooled from 3-4 mice. The cells were stained for DAPI and CD44. $DAPI^-CD44^{hi}$ cells were sorted as "memory" T cells and $DAPI^-CD44^{low}$ cells as "naïve" in 14 ml snap cap tubes. The cells were then used in a restimulation assay.

The sorting purity was assessed directly post sorting by sample measurement as shown in Figure 14. Purities were between 95-100% for all experiments.

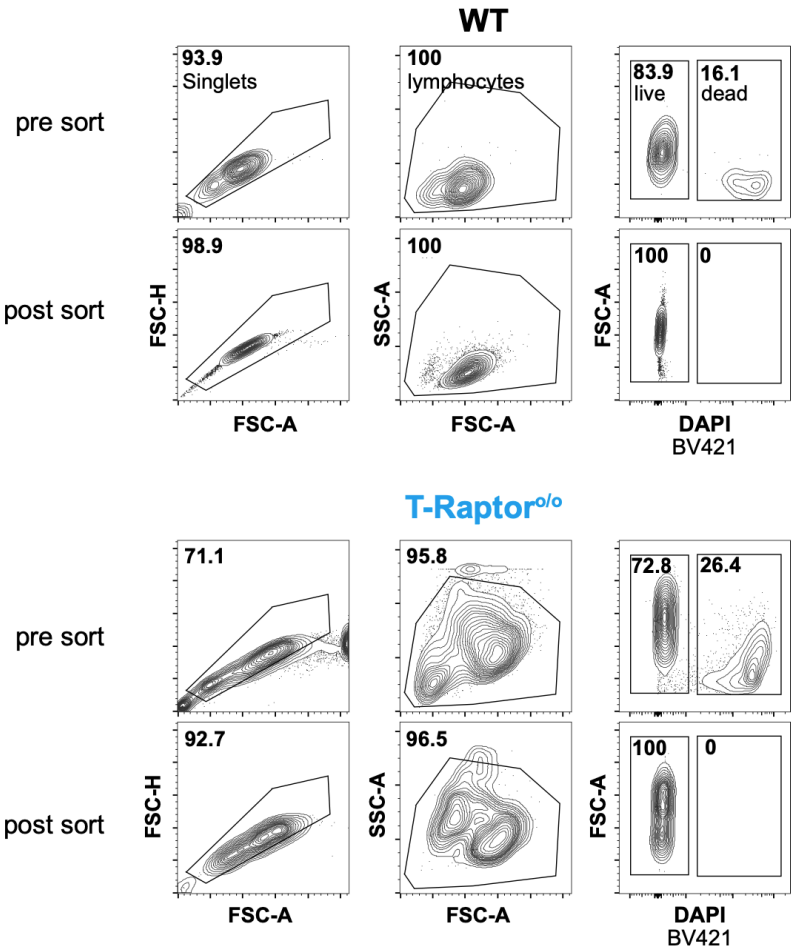

Figure 14: Post sort purity assessment of WT (top) and T-Rap$^{o/o}$ (bottom) T cells.
Upper panels show gating of pre- and post sorted T cells from WT mice, lower panels show T cells pre and post sort from T-Rap$^{o/o}$ mice. T cells were gated for Singlets, lymphocytes and live cells.

2.2.21 Protein lysis of T cells

MACS-enriched T-WT, T-Rap$^{o/o}$ and T-Ric$^{o/o}$ cells were stimulated with anti-CD3 and anti-CD28 mAbs for 1 or 2 days, harvested and washed twice with cold PBS. The cell pellet was resuspended in 25 µl lysis buffer (Copp et al., 2009) per 10x10^6 cells. Lysis buffer was prepared as decribed in the material section 2.1.7. Leupeptin, aprotinin and sodium orthovanadate were added freshly to the stock solution every time. Samples were incubated on ice for 20 minutes and centrifuged at 12000 rpm for 10 minutes at 4°C. The supernatant was transferred into a new tube and stored at -20°C until further processing, as Bradford assay and Western blotting.

2.2.22 Detection of protein concentration by Bradford Assay

The protein concentration of the samples was measured by Bradford assay according to the manufacturers protocol. Therefore 1 ml of Bradford solution was pipetted into a 1.5 ml tube and 10 µl of pre-diluted BSA standard or 1 µl of sample was added and mixed carefully. After a short incubation time of 5-10 minutes, samples were transferred into 1 ml micro cuvettes and measured at an Eppendorf BioSpectrometer. The BSA standard was prepared in lysis buffer as described in Table 7 (from manufacturers protocol). The generated standard curve is shown below in Figure 15.

Table 7: Preparation scheme of BSA standard for Bradford Assay

Vial	Volume of Diluent (µl)	Volume of BSA (µl)	Final BSA conc (µg/µl)
A	0	300 of stock	2000
B	125	375 of stock	1500
C	325	325 of stock	1000
D	175	175 of vial B	750
E	325	325 of vial C	500
F	325	335 of vial E	250
G	325	325 of vial F	125
H	400	100 of vial G	25
I	400	0	0 (Blank)

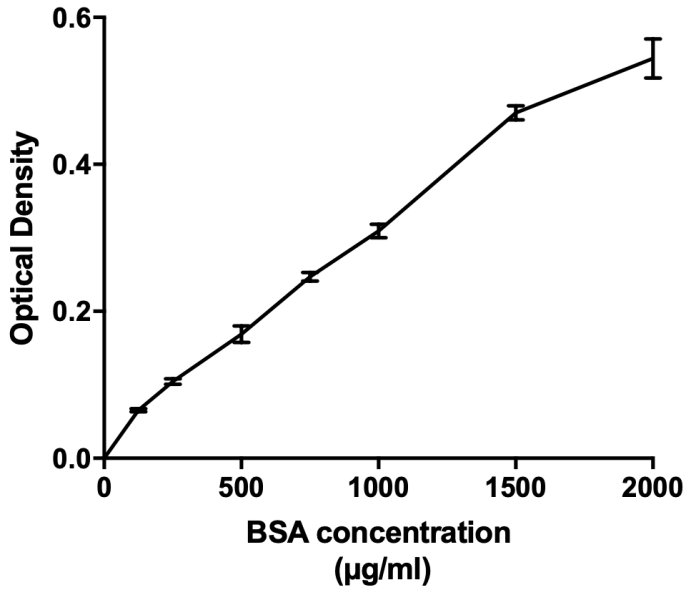

Figure 15: Standard curve for Bradford protein assay.
Different known concentrations of BSA were measured at a BioSpectrometer and corresponding OD values (Optical Density) plotted.

Concentration of samples could be calculated from the absorbance of unknown samples and the known standard concentrations and were automatically calculated by the spectrometer.

2.2.23 Western Blot

2.2.23.1 Sample preparation

Sample volume was adjusted by addition of lysis buffer according to the protein concentration. Then, 4x Laemmli buffer with freshly added ß-Mercaptoethanol was added 1 in 3. Samples were incubated at 95°C for 5 min to denature the protein before loading.

2.2.23.2 Gel separation

A 1.5 ml thick 8% separation gel was prepared according to Table 8, poured quickly into the chamber and overlaid with isopropanol. The separation gel needed around 15 minutes to solidify. The isopropanol was then poured off and the gel rinsed with VE water and dried with a filter paper. All reagents and buffers for the collection gel were combined (see Table 8) and poured on top of the separation gel with a comb with 8 lanes inserted into the gel. After 20 minutes the gel was put into the electrophoresis chamber, filled with 1x SDS Running Buffer. 7 µl of High range protein ladder and desired amount of protein samples (10-30 µg) were loaded onto the gel. The gel was run at 80V for 15 minutes until samples entered the separation gel and then at 120V for 1-2 hours, dependent on protein size.

Table 8: Reaction mix for separation and collection gel

Ingredient	8% separation gel (10 ml)	Collection gel (5 ml)
H_2O	4.6 ml	3.4 ml
Acrylamide	2.7 ml	830 µl
1.5M Tris/HCl, pH 8.8	2.5 ml	-
1M Tris/HCl, pH 6.8	-	630 µl
10% SDS	100 µl	50 µl
TEMED	10 µl	5 µl
10% APS	100 µl	50 µl

2.2.23.3 Blotting

The gel was removed from the chamber and transferred onto 2 Whatman Filters (6.5 cm x 9 cm) inside the gel-holder cassette. A PVDF membrane was cut to the same size, activated in Methanol and then laid on top of the gel. Two more Whatman Filters were laid on top of the

membrane and air bubbles removed. The gel holder cassette was closed and fixed into the chamber which was filled with Blotting buffer. Blotting ran at 4°C and 40V overnight on a magnetic stirrer.

2.2.23.4 Blocking and Primary antibody incubation

On the next day, the membrane was carefully transferred to a container and incubated in 5% BSA/ TBS-T for 1-2 hours on a shaking plate for blocking. Primary antibodies used were specific for mTOR, Raptor, Rictor and pS6 (all from Cell Signaling, rabbit IgG) and were diluted 1:1000 in 10 ml 5% BSA/TBS-T. Sodium azide was added 1:1000 to prevent bacterial growth. Primary antibodies were added onto the membrane in a closed container and incubated at 4°C on a slow shaker overnight. Primary antibodies were reused and stored at 4°C after each incubation. Alpha-tubulin (Cell Signaling, species rabbit) was used as control antibody and diluted 1:2000 in 5% BSA/TBS-T.

2.2.23.5 Secondary antibody incubation and detection

After overnight incubation, the membrane was washed three times for 5 minutes with TBS-T. Then a secondary goat anti-rabbit HRP-linked antibody was added (1:1000 in 5% BSA/TBS-T) and incubated for 1 hour. The membrane was washed three times with TBS-T and transferred into a new container. 3 µl of ECL solution 2 was mixed with 1 ml of ECL solution 1 (self-made) and pipetted over the membrane for around one minute. The membrane was transferred into a hypercassette and developed in the Developer in a dark room. Films were exposed between 2 seconds for alpha-tubulin and 1:30 minutes for the other proteins tested.

2.2.24 Statistical analysis

Statistical analysis of FACS data was performed using GraphPad Prism 7c, 7e and 10. Geometric mean or percentages were exported from Flowjo10 and analyzed by unpaired Student's t-test if not indicated otherwise. P values <0.05 were considered statistically significant with * = $P < 0.05$, ** = $P < 0.01$, *** = $P < 0.001$, **** = $P < 0.0001$, ns = $P > 0.05$.

3. Results

3.1 Reciprocal regulation of mTORC1 and ribosomal biosynthesis determines cell cycle progression

3.1.1 Description and confirmation of T cell specific deletion of Raptor and Rictor subunits

To investigate the relation between mTOR signaling, proliferation and the ribosomal biosynthesis in T cells, conditional knockout mice carrying loxP-flanked alleles of either Raptor or Rictor genes or both were used in this thesis and referred to as T-Rap$^{o/o}$, T-Ric$^{o/o}$ and T-Rap/T-Ric$^{o/o}$, respectively. The CD4-cre transgene (Tg(CD4-cre)1Cwi) (Lee et al., 2001) is used to delete exon 6 of the Raptor gene or exon 11 of the Rictor gene in CD4^{+} and CD8^{+} T cells. The mutations cause frameshifts in the respective open reading frames and create null alleles. In a first step, the deletion of Raptor and Rictor protein was verified by Western Blotting (Figure 16A). Purified T cells were stimulated for one day with 10 µg/ml anti-CD3/anti-CD28 mAbs, lysed, separated by SDS-PAGE and blotted. Different protein concentrations were loaded as indicated in Figure 16A. We observed that the mTOR protein is equally expressed in all samples, while Rictor expression is missing in T-Ric$^{o/o}$, and Raptor in T-Rap$^{o/o}$ T cells as expected.

As a marker for mTORC1 activity, the phosphorylation of the S6 ribosomal protein can be measured as it is rapidly phosphorylated by S6K1 upon mTORC1 activation. Within 2 hours of stimulation in vitro, the phospho-S6 (pS6) S235/236 signal is very high, as shown in Figure 16B, upper panel. In contrast, T-Rap$^{o/o}$ and T-Rap/Ric$^{o/o}$ T cells show a reduction in pS6 expression, indicating mTORC1 activity is strongly reduced when Raptor is deleted. Rictor deletion alone does not lead to decreased pS6 levels and is ashigh as in the wildtype T cells (Figure 16B, lower panel).

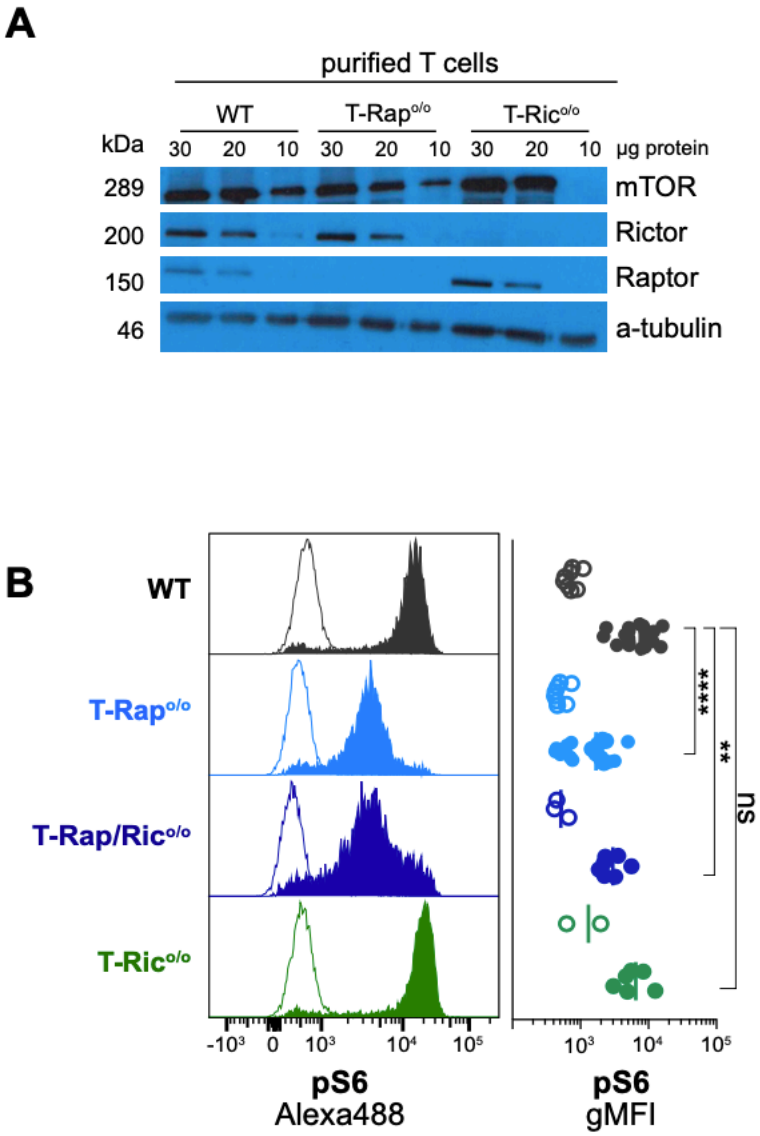

Figure 16: Identification of specific knockouts for mTORC1 and mTORC2.

(A) Western Blot of purified T cells, isolated from wildtype, T-Rap$^{o/o}$ and T-Ric$^{o/o}$ mice and stimulated for 24 hours with anti-CD3/CD28 mAbs. The expression of mTOR, Raptor and Rictor protein is shown. (B) Expression of mTORC1 downstream target phospho-S6 2 hours post stimulation of the indicated genotypes. Histograms are shown for all four genotypes and statistics plot shows the result of 6 individual experiments. Empty histograms represent unstimulated T cells, filled histograms stimulated T cells. Data are shown as mean gMFI. * = P < 0.05, ** = P < 0.01, *** = P < 0.001, **** = P < 0.0001, ns = P > 0.05; unpaired Student's t-test.

3.1.2 mTORC1 controls cell cycle progression and cell division in T cells

To investigate mTORC1 and mTORC2-dependent proliferation in vivo, we isolated T cells from lymph nodes of WT, T-Rap$^{o/o}$ and T-Ric$^{o/o}$ mice, labeled them with CTV and transferred the T cells into H2-A$^{b/bm12}$ (Figure 17A) or H2-K$^{b/bm1}$ recipients (Figure 17B) and control H2-A$^{b/b}$ and H2-K$^{b/b}$ mice. Mice were injected intraperitoneally (i.p.) one day before transfer with 20 µg anti-CD40 to activate dendritic cells for immunogenic antigen presentation (Obst et al., 2007).

The bm1 mutation of the H-2K^{b} gene carries 7 nucleotide differences leading to three amino acid substitutions (McKenzie et al., 1977), while the bm12 mutation differs from H-2A^{b} only by three nucleotides, resulting in three different amino acids (McKenzie et al., 1979). Therefore, cells of both mice containing these mutations present an altered repertoire of self-peptides and act as strong alloantigens (Rosenberg and Singer, 1992). Alloreactivity describes a response of 1-10% of T cells against variants of the MHC molecules (Suchin et al., 2001). One would expect that adoptively transferred CD4^{+} T cells with b/b background start proliferating in a graft-versus-host response to alloantigens in H2-A$^{b/bm12}$, and CD8^{+} T cells in H2-K$^{b/bm1}$ recipients. H2 heterozygous recipients were used as they are tolerant to H2^{b}. Previous data from our lab indicated that Raptor-deficient T cells proliferate less in this allogeneic system.

We reproduced these findings, in combination with T-Ric$^{o/o}$ T cells, as shown in Figure 17 C+D. CTV dilution was observed five days post transfer as shown in Figure 17C for transferred CD4^{+} T cells in b/b and b/bm12 recipients, and in Figure 17D for transferred CD8^{+} T cells into b/b and bm1 mice. We found that within 5 days WT and T-Ric$^{o/o}$ T cells have divided up to 6 times, while T-Rap$^{o/o}$ and T-Rap/Ric$^{o/o}$ only completed up to two divisions on average but were spread from 1-6 divisions. As expected, the T cells did not proliferate in the control mice (b/b), shown in the upper panels.

Altogether these data show that mTORC1 is essential in allogeneic T cell responses and is a rate-limiting factor for proliferation for each consecutive cell division.

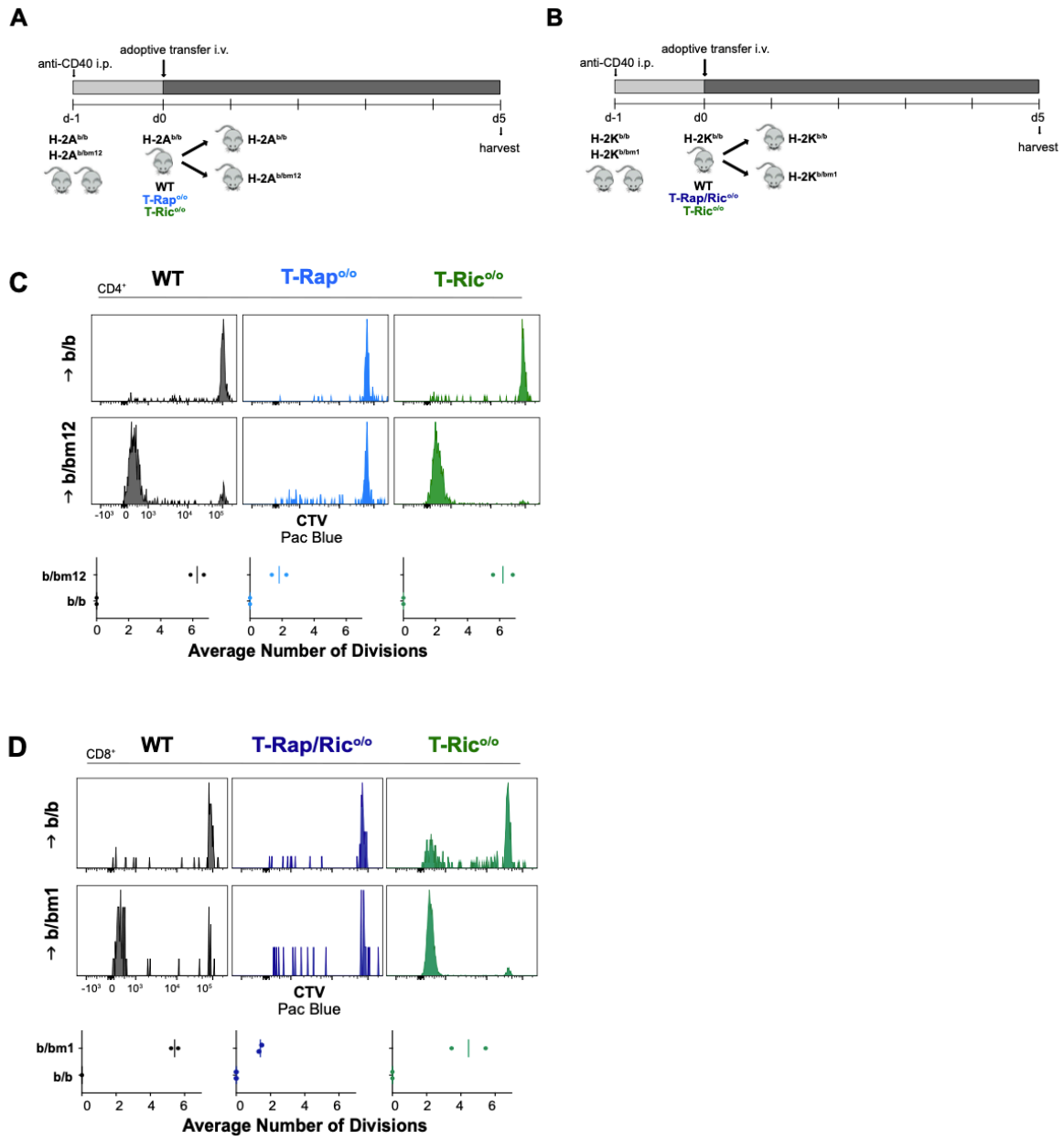

Figure 17: In vivo proliferation depends on mTORC1, but not C2.

(A) Experimental Scheme. Mice were injected i.p. with 20 µg anti-CD40 on day -1. CTV-labeled WT, T-Rap$^{o/o}$ and T-Ric$^{o/o}$ T cells, isolated from lymph nodes, were adoptively transferred into b/bm12 and control (b/b) mice on d0. Spleens were harvested and analyzed 5 days post transfer. (B) Experimental Scheme. Mice were injected i.p. with 20 µg anti-CD40 on day -1. CTV-labeled WT, T-Rap$^{o/o}$ and T-Ric$^{o/o}$ T cells, isolated from lymph nodes, were adoptively transferred into b/bm1 and control (b/b) mice on d0. Spleens were harvested and analyzed 5 days post transfer. (C) CTV dilution of transferred CD45.1^{+} B6, Raptor$^{o/o}$ or Rictor$^{o/o}$ purified T cells into b/b and b/bm12 (C) and b/b and b/bm1 (D) mice 5 days post transfer. Data are representative of two independent experiments with n=1 per condition. (C-D) Data are shown as mean number of divisions. * = P < 0.05, ** = P < 0.01, ns = P > 0.05; unpaired Student's t-test.

As we found a reduced proliferative rate in vivo, we looked at in vitro proliferation at different time points to investigate whether T-Rap$^{o/o}$ T cells divide slower, have a delayed onset of proliferation, or possibly die earlier. OT1-WT and OT1-T-Rap$^{o/o}$ spleen cells were labeled with CTR and stimulated them with 10 ng/ml pOVA. We took samples at different time points as indicated in Figure 18A. After 48 hours all WT T cells had divided at least once (N_{mean}=2.3±0.986) while T-Rap$^{o/o}$ cells had divided just once or not at all (N_{mean}=0.75±0.096). Only after 72 hours, T-Rap$^{o/o}$ T cells had completely entered proliferation, but with fewer divisions compared to WT T cells (N_{mean}=2.1±0.1 vs. N_{mean}=4.9±1.4). These data confirm that T-Rap$^{o/o}$ T cells have a delayed cell cycle entry and divide slower than WT T cells. This finding was additionally corroborated in an in vivo proliferation experiment in our lab by using TCR-transgenic cells. In that experiment, AND^{+} CD4^{+} T cells and OT1^{+} CD8^{+} T cells were transferred into iMCC and iOVA-specific mice and harvested at different time points post transfer (Pennavaria, 2019). We saw that the proliferation of T-Rap$^{o/o}$ T cells was delayed at all time points and not just the first division as published by Yang et al. (2013). Additionally, we observed a decreased accumulation of cells in the spleen, which could not be explained by the reduced proliferative rate but by apoptosis.

To examine in which cell cycle phase T cell proliferation is slowed by the Raptor deletion, we investigated the passing of T cells through the cell cycle by incorporation of EdU as shown in Figure 18B. OT1 T cells of the indicated genotypes were stimulated with 10 ng/ml pOVA for 2 days, followed by a one-hour incubation with 1 µM EdU which is a thymidine analog and is incorporated into the DNA during the S-phase of the cell cycle. After one hour the cells were washed and recultured to follow EdU-labeled cells through the cell cycle stages. In Figure 18B around 80% of WT cells were actively in S-phase during the labeling period, but only 50% of the T-Rap$^{o/o}$ cells (upper gate). Gated in the lower left corner are cells in G1 phase and gated in lower right are cells in M phase. After 3 hours in culture, the EdU/DNA plot shows a new population in the upper left corner, which includes cells that were initially labeled with EdU, completed one cell cycle and are back in G1 phase. From the initially labeled WT population, around 20% of the cells have completed one cell division by then and are again in G1 phase. However, of the T-Rap$^{o/o}$ cells only 5% had finished one cell cycle at the end of the 3-hour chase. Altogether these data indicate that T-Rap$^{o/o}$ cells are cycling less and need more time to progress through the S/G2/M phases. T-Ric$^{o/o}$ cells, expectedly, showed a similar behavior as WT cells, and T-Rap/Ric$^{o/o}$ cells displayed a reduced proliferative rate and speed as T-Rap$^{o/o}$ cells did. Unfortunately, the experiments with cells of the latter genotypes could not be repeated due to the lack of animals.

As we found a reduced number of labeled and divided cells in Figure 18B, we asked whether mTORC1-deleted T cells might encounter additional cell cycle restrictions. Therefore, we stained T cells of the indicated genotypes on day 2 with Hoechst and an antibody for Phos-

pho-H3 (H3P), a histone which is highly phosphorylated in metaphase in eukaryotic cells and is a widely used marker for cells in mitosis (Hans and Dimitrov, 2001). We saw that T-Rap$^{o/o}$ cells expressed less H3P (1.6% vs. 2.9% in WT), indicating that T-Rap$^{o/o}$ cells have a delayed cell cycle completion (Figure 18C). Furthermore, the percentage of cells in the G2 phase was comparable between WT and T-Rap$^{o/o}$ cells (19.8% vs. 17.0%), however, the percentage of cells in M phase among all cells in the G2/M phases is also reduced in T-Rap$^{o/o}$ cells (Figure 18C). This indicates that the G2/M transition is delayed in T-Rap$^{o/o}$ cells, resulting in slower completion of each cell cycle and thus, a reduced proliferative capacity. T-Ric$^{o/o}$ cells had a similar percentage of cells in G2 and M phase as WT cells and are thus unaffected.

From these data we conclude that the onset of proliferation as well as the progression through the cell cycle is dependent on mTORC1, but not on mTORC2. Both the G1/S and the G2/M transition points are affected by the Raptor deletion leading to an overall reduced proliferative rate.

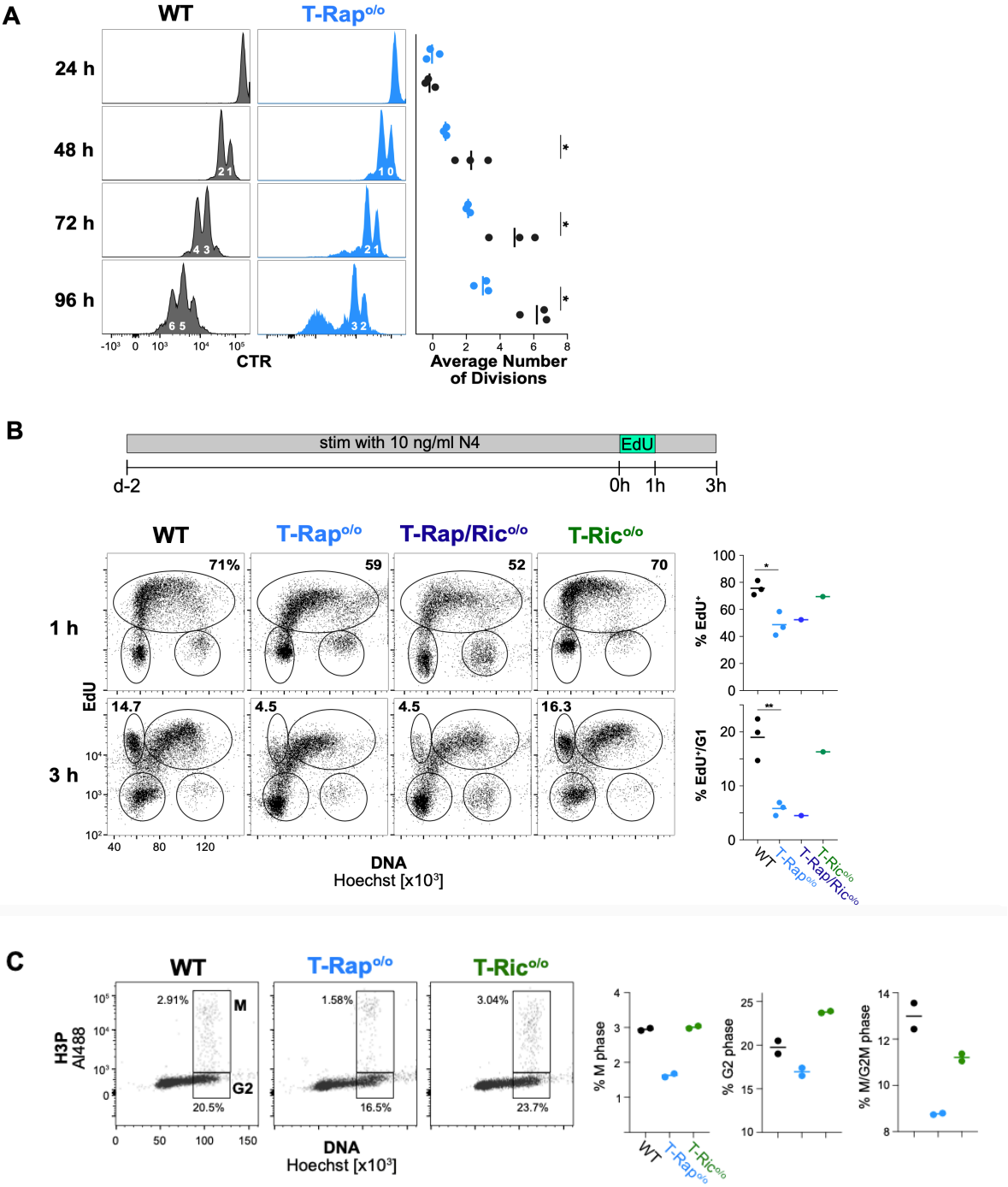

Figure 18: In vitro proliferation and cell cycle progression is regulated by mTORC1.
(A) CTR dilution of in vitro activated OT1 WT and T-Rap$^{o/o}$ CD8$^+$ T cells over time. T cells were stimulated with 10 ng/ml pOVA and samples taken to the indicated time points. Inset numbers indicate the corresponding division of each peak. Statistics panel shows result of three independent experiments. (B) OT1 T cells of indicated genotypes were stimulated with 10 ng/ml pOVA for 2 days, then pulsed with EdU for 1 hour and samples taken directly after the pulse and 3 hours later. Incorporation of EdU was analyzed by click chemistry and subsequent flow cytometry. Upper gate marks cells that incorporated EdU during S-phase, lower left G1 phase and lower right gate shows cells in M phase. Additional 3-hour gate in the upper left corner marks cells that were initially labeled with EdU and fully completed one cell cycle. Statistics panel shows result of three independent experiments for WT and Raptor$^{o/o}$. (C) Phospho-H3 expression of WT, T-Rap$^{o/o}$ and T-Ric$^{o/o}$ T cells on day 2 post stimulation with pOVA,

showing the percentage of cells in the M-phase of the cell cycle. Statistics panel shows two independent experiments. (A-C) Data are shown as mean. * = P < 0.05, ** = P < 0.01, ns = P > 0.05; unpaired Student's t-test.

3.1.3 TCR induces mTORC1 signaling

As indicated in Figure 16B, mTORC1 signaling is induced very quickly after TCR stimulation as shown by pS6 upregulation 2 hours after TCR stimulation. It was published before that mTORC1 is essential for the onset of proliferation, the "exit of quiescence", but not for later cell divisions (Yang et al., 2013). As we observed a delayed cell cycle progression of Raptor-deficient T cells in vivo and in vitro also on day 2 and 3, we asked whether mTOR signaling can be activated late following TCR signaling or IL-2-induced (Figure 19A). OT1 spleen cells were stimulated with 10 ng/ml pOVA for 48 hours leading to high pS6 expression in $CD8^+$ OT1 T cells after 4 hours and still after 48 hours, albeit slightly reduced (Figure 19B). At this timepoint, the cells have divided at least once (Figure 18A). Then, the cells were rested overnight without stimulation, which significantly reduced pS6 levels. At the same time CD25 expression increased over two days and remained at high levels even after TCR signaling stopped (Figure 19B). The cells were restimulated with 10 µg/ml anti-CD3 or 10 ng/ml IL-2 for 4 hours, as this timepoint is enough for initial upregulation of pS6. We observed that both anti-CD3 and IL-2 stimulation were able to re-induce mTORC1 signaling (Figure 19C).

Additionally, 1 µM Tofacitinib was added, which blocks IL-2R-associated Janus kinases (JAK) 1 and 3 signaling irreversibly (Preston et al., 2015). We found that stimulation with anti-CD3 was enough to induce mTORC1, irrespective of JAK1 and 3. However, IL-2 signaling alone was found to be strongly dependent on JAK1/3 and required its activity to induce mTORC1 signaling.

Altogether these data show that mTORC1 activity can independently be induced by late stimulation through CD3 and IL-2 signals in activated $CD25^+$ T cells.

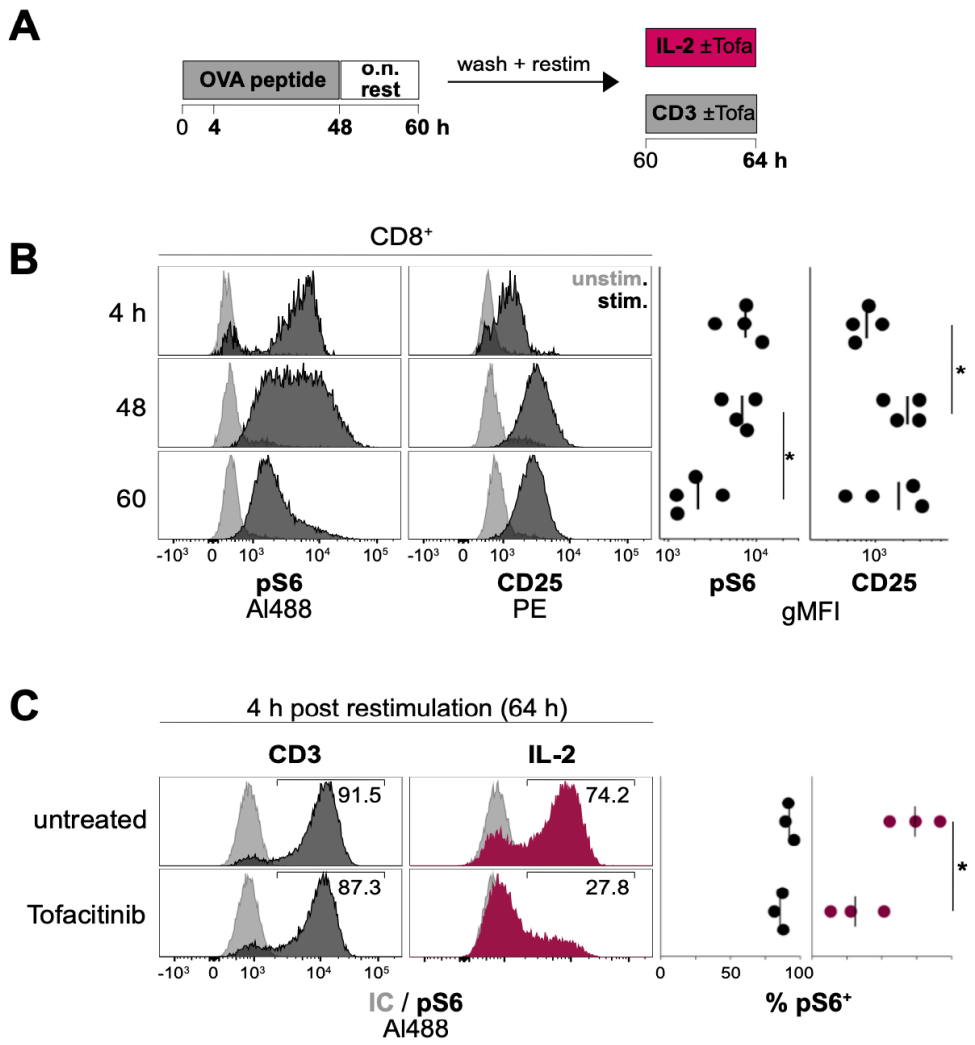

Figure 19: mTORC1 signaling can be induced by CD3 and IL-2, but only the latter depends on JAK/Stat signaling.

(A) Experimental Scheme. OT1 T cells were stimulated with 10 ng/ml pOVA for 48 h, then rested overnight and re-stimulated with anti-CD3 or IL-2 ± 1 µM Tofacitinib for 4 hours. (B) Histograms show phospho-S6 and CD25 expression to the indicated time points. (C) Panels show phospho-S6 expression 4 hours post restimulation, ± 1 µM Tofacitinib. Statistics panel shows result of four independent experiments. Data are shown as mean. * = P < 0.05, ** = P < 0.01, ns = P > 0.05; unpaired Student's t-test.

Upon peptide-MHC binding, T cell receptor signaling leads to the activation of several downstream effectors which prepare the T cells for cell division and effector cell differentiation. We generally used anti-CD3 and anti-CD28 mAbs at a high concentration to stimulate T cells in vitro. To see the stimulatory range and effect of CD28 co-stimulation, we performed titration experiments as shown in Figure 20A. Purified $CD8^+$ and $CD4^+$ (not shown) T cells were stimulated for 16 hours with immobilized anti-CD3, over the range of 10 µg/ml to 0.5 ng/ml. Dark filled circles show cells stimulated in the presence of additional immobilized 10 µg/ml anti-

CD28 mAb. Left panels show the expression of CD69, an early activation marker indicating conventional TCR stimulation. CD3 stimulation alone required high concentrations to induce CD69 surface expression (>1 µg/ml). CD28 stimulation lowered the stimulatory threshold for CD69 induction 100-fold (Figure 20A, left). A similar effect is seen with pS6 expression on the right, indicating that both conventional TCR signaling and mTORC1-dependent signaling are equally affected by CD28 costimulation. These data confirm Yang et al. 2013.

We then asked whether the classical TCR signaling pathways via Ca^{2+}/Calcineurin/NFAT, NF-κB and MAP kinases, must be fully active for CD69 expression. Cyclosporin A, a calcineurin inhibitor, GDC0973, a MEK inhibitor also known as Cobimetinib, and BAY117082, a NFkB inhibitor (IkB/IKK) were titrated and added to stimulated $OT1^+$ T cells for 16 hours. As shown in Figure 20B all three pathways are required for CD69 expression and thus all three have to be properly activated to ensure a proper consecutive T cell response.

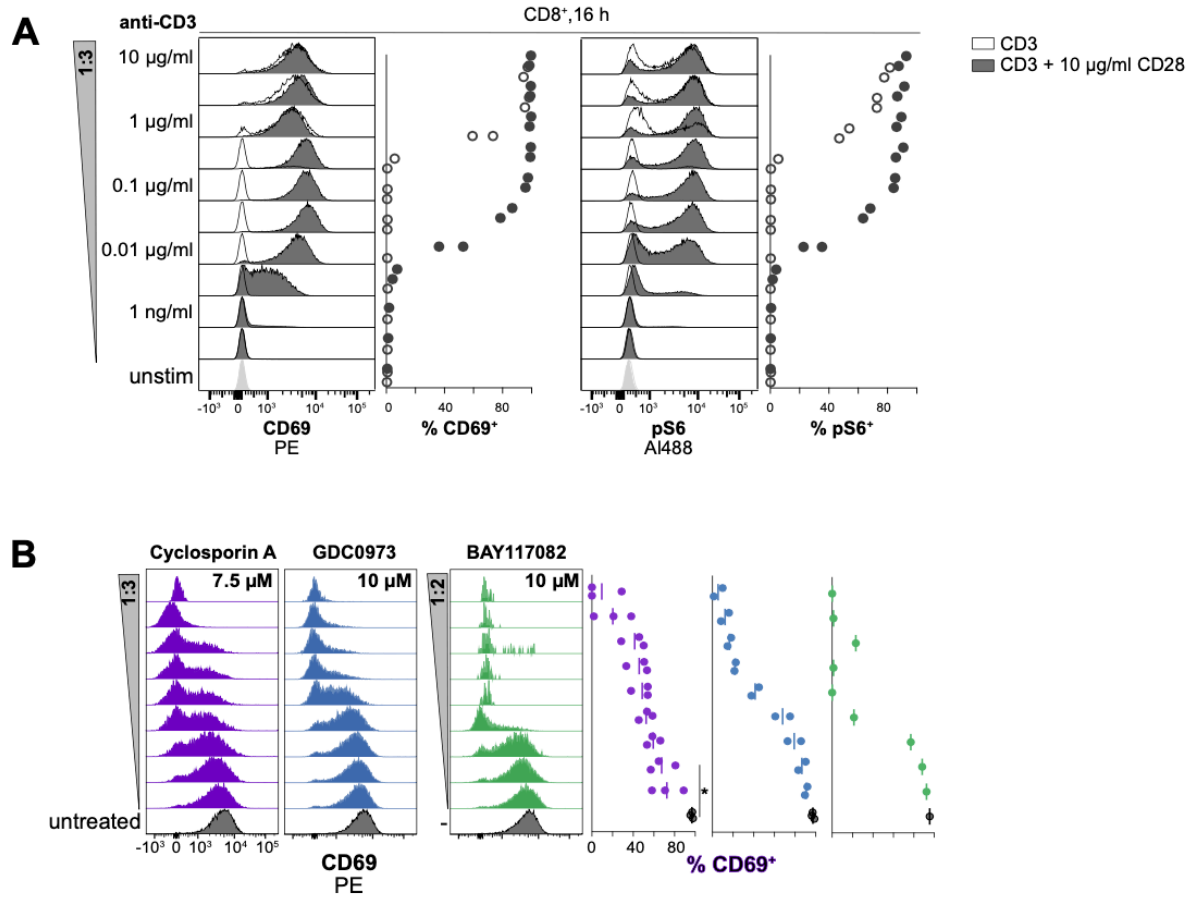

Figure 20: Crosstalk between conventional and mTORC1 signaling

(A) Surface CD69 and intracellular phospho-S6 expression in T cells stimulated with titrated CD3 ± 10 µg/ml CD28 immobilized on the culture plate. Titrated amounts of anti-CD3 mAb in the absence (open dots) or presence (filled dots) of 10 µg/ml immobilized anti-CD28 mAb. Statistics panel shows result of two independent experiments. (B) Titration of TCR signaling inhibitors Cyclosporin A, GDC0973 and BAY117082 on OT1 T cells, start concentrations are indicated in the upper panel. CD69 expression of each concentration is shown and quantified as percentage (%) $CD69^+$ cells. Data are representative of

three independent experiments for Cyclosporin A treatment, two experiments for GDC0973 and one for BAY117082. (A-B) Data are shown as mean. * = P < 0.05, ** = P < 0.01, ns = P > 0.05; unpaired Student's t-test.

3.1.4 Torin-1 blocks downstream signaling of mTORC1

The experiments on the classical TCR signaling through CD3 or peptide stimulation showed that phosphorylation of the mTORC1 target S6K occurs within 2 hours post stimulation (Figure 16), is sustained for 2 days and induced by late stimulation via the IL-2R (Figure 19); that costimulation with CD28 lowers the stimulatory threshold for CD69 and pS6 expression (Figure 20) and, that all three classical signaling pathways are required for complete induction of CD69 expression on T cells (Figure 20).

These three pathways involving Calcineurin/NFAT, PI3K/NF-κB and the Ras/Raf pathway are shown to be essential to induce gene transcription inside the nucleus in the first place. Besides these pathways, mTOR is activated via the PI3K signaling pathway by activation of Akt which negatively regulates TSC1/2. TSC1/2 is an upstream inhibitor of Rheb, which then activates mTORC1 and its targets S6K, 4EBP and many others. mTOR is known to be a key metabolic integrator and essential for the rapid activation and proliferation of T cells. Therefore, the direct actions of mTOR will be further investigated by specific inhibitors.

Torin-1 is a selective ATP competitive mTOR inhibitor, which inhibits both mTOR complexes. A titration over 2 µM to 7 nM showed that mTORC1 activity, marked by pS6 expression, was fully blocked at a concentration of 200 nM and above as shown in Figure 21A in the left panels. Classical TCR signaling, however, as indicated by CD69 and NR4a1 expression, measured by a Nur77-eGFP reporter, are regulated independently of mTOR activity.

We then asked whether mTORC1 affects the TCR signaling threshold and thus titrated pOVA from 10 ng/ml to 0.1 pg/ml. Indeed, we found that the presence of Torin-1 increased the threshold of CD69 (Figure 21B) and NR4a1 (Figure 21C) expression 3-fold, indicating that mTORC1 signaling tunes TCR sensitivity.

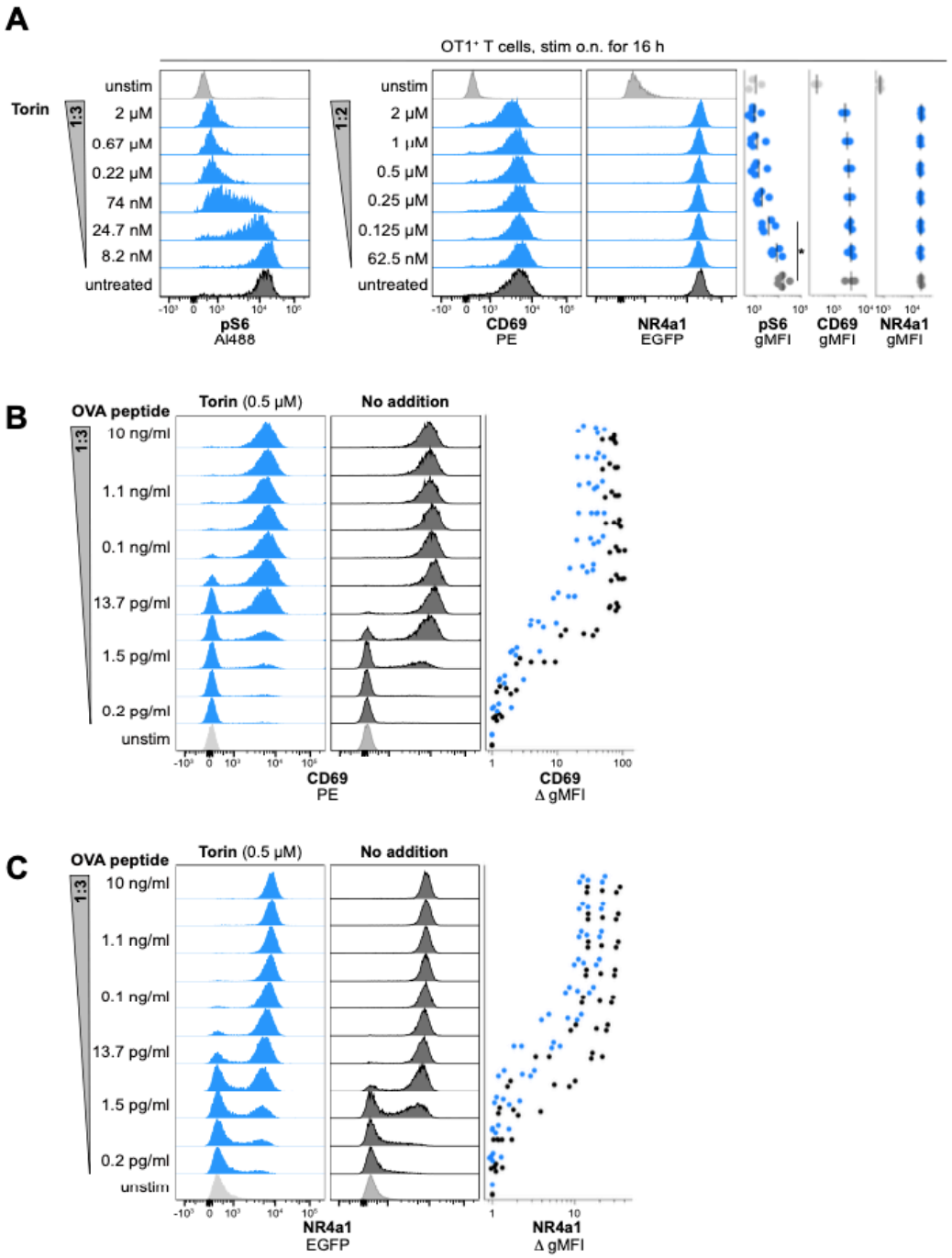

Figure 21: mTORC1 contributes to conventional TCR signaling.

(A) Histograms represent pS6, intracellular Nur77-GFP and surface CD69 expression of OT1 CD8⁺ T cells after overnight activation with titrated Torin-1 (ranging from 2 µM to 8 nM). Data are representative of at least three independent experiments. (B) Surface CD69 expression of T cells ± 500 nM Torin-1 after 24h with titrated OVA peptide (ranging from 10 ng/ml to 100 fg/ml). Data in all panels are representative of five independent experiments. (C) Intracellular Nur77 expression of T cells ± 500 nM Torin after 24h with titrated OVA peptide (ranging from 10 ng/ml to 100 fg/ml). Data in all panels are representative of five independent experiments. (A-C) Data are shown as mean. * = $P < 0.05$, ** = $P < 0.01$, ns = $P > 0.05$; unpaired Student's t-test.

3.1.5 RNA levels are reduced in Raptor-deficient T cells

Following stimulation, T cells increase their protein synthesis and undergo many metabolic changes towards an anabolic metabolism to fulfill their energy demands. Protein synthesis and translation require high ribosomal activity, which is known to be mTORC1-dependent. In the lab a staining protocol for RNA using the fluorescent dye Pyronin Y had been established (Pennavaria, 2019). In combination with DNA staining, it can be used to distinguish the G0 and G1 phases of the cell cycle, as well as the S phase entry (Shapiro, 1981).

We stimulated OT1 T cells with 10 ng/ml pOVA for 2 days and stained the cells' RNA and DNA as shown in Figure 22A. Unstimulated control cells on the left show low RNA levels and thus all cells in the G0 phase of the cell cycle. Upon stimulation, shown in the second panel from left, cells increase their RNA levels 9-fold, move from G0 to G1 and go through S phase with high RNA levels until they reach the G2 and M phases. However, T-Rap$^{o/o}$ cells increase their RNA levels only 5-fold and enter the S-phase without increasing RNA expression in G1. Additionally, only 27% of T-Rap$^{o/o}$ cells are actively cycling, as indicated on the upper histograms of DNA levels with a gate on the S-G2-M phases. In comparison, 54% of the WT cells are within this gate. Again, T-Ric$^{o/o}$ cells show no alteration of their RNA expression and resemble WT cells.

Figure 22B shows a kinetic of pS6 expression comparing WT and T-Rap$^{o/o}$ cells for which we stimulated OT1 T cells of both genotypes and harvested samples at different time points. Grey histograms in the background are FMO controls which visualize changes of autofluorescence due to the volume increase upon stimulation. We see that pS6 levels in WT cells are increased 3 hours post stimulation until 48 hours and afterwards decrease. However, in T-Rap$^{o/o}$ T cells no pS6 staining above FMO controls could be detected, indicating that S6 phosphorylation at Ser235/236 is an authentic indicator of mTORC1 activity. At the same time, RNA kinetic is depicted in Figure 22C and shows that WT T cells increase RNA from 18 hours post stimulation and further increase their levels until 48 hours. However, T-Rap$^{o/o}$ T cells very slowly induce their RNA levels after 24 hours post stimulation and even after 48 hours or 72 hours (not shown) do only reach around 50% of WT levels.

Altogether these data indicate that mTORC1 is required for the boost of RNA transcription in T cell activation.

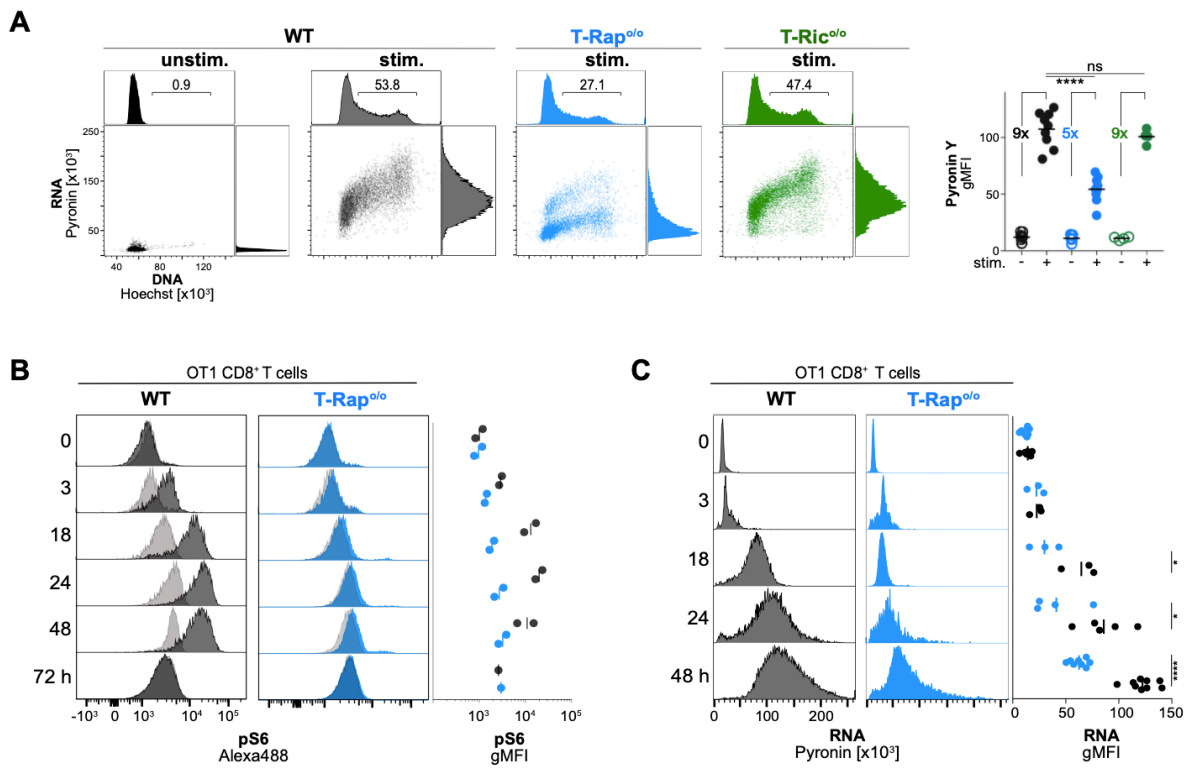

Figure 22: Induction of RNA synthesis is regulated by mTORC1.

(A) DNA and RNA levels of OT1 T cells of the indicated genotypes after 2 days in culture with 10 ng/ml pOVA. Percentages in upper DNA plots show cells in S, G2 and M phases of the cell cycle. Numbers in statistics panel indicate fold change of total RNA from unstimulated to stimulated for each genotype. Statistic panel shows the result of five independent experiments. (B) PS6 time course of in vitro activated WT and Raptor$^{o/o}$ T cells. Light grey histograms represent FMO control. Data are representative of two independent experiments. (C) Time course of RNA expression of in vitro activated WT and Raptor$^{o/o}$ T cells. Data are representative of three independent experiments. (A-C) Data are shown as mean. * = P < 0.05, ** = P < 0.01, *** = P < 0.001, **** = P < 0.0001, ns = P > 0.05; unpaired Student's t-test.

3.1.6 Rictor deletion does not lead to increased Raptor function

We observed from time to time a higher expression of pS6 and RNA, as well as a tendency towards an increased proliferation rate in the T-Ric$^{o/o}$ T cells, though never significant. We thus asked whether Rictor deletion leads to increased mTORC1 activity as more mTOR components are available due to the loss of Rictor. Therefore, we titrated immobilized anti-CD3 mAb over a large range of concentrations in the absence or presence of anti-CD28 mAb and tested for pS6 and CD69 expression levels. Figure 23A shows the CD69 expression of purified WT and T-Ric$^{o/o}$ T cells. We observed no significant differences at any of the concentrations tested. pS6 levels were also comparable to WT T cells (Figure 23B). The addition of anti-CD28 to the stimulation decreased the activation threshold of the cells 100-fold without any difference between the two genotypes (Figure 23C+D).

In conclusion, these data show that the activation of T cells through CD3 ± CD28 is independent of mTORC2 and especially, not improved by its absence.

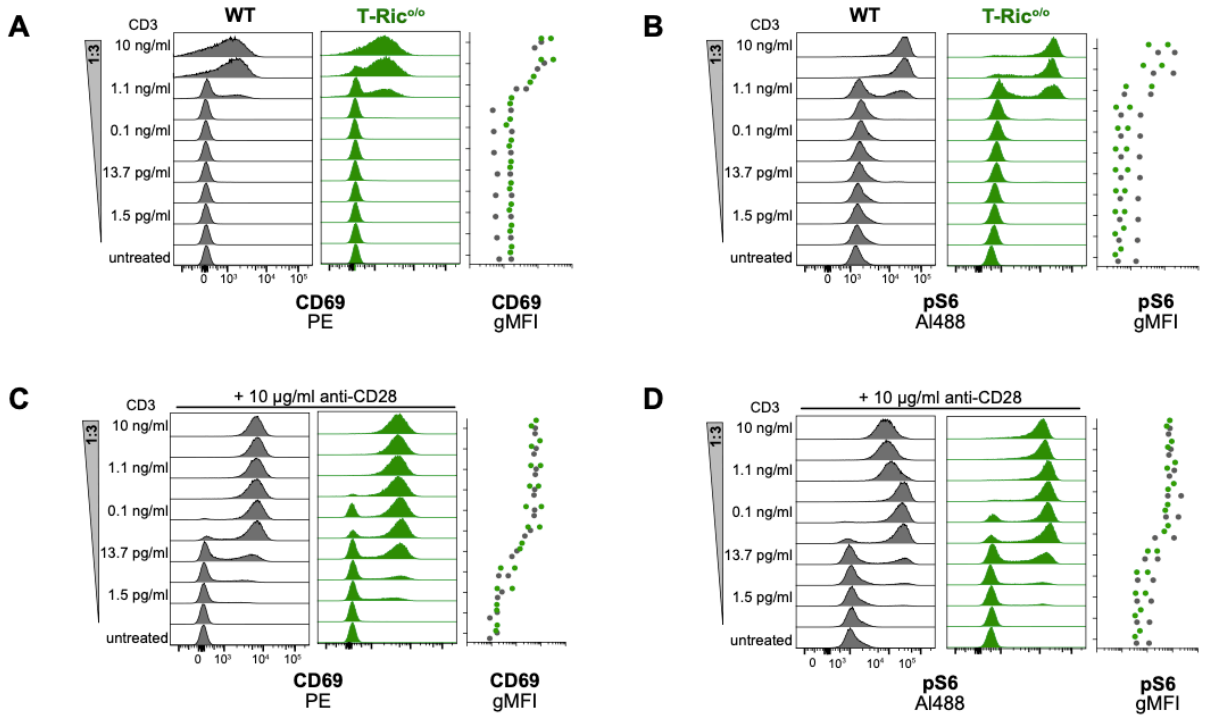

Figure 23. Rictor-deficient T cells are activated similarly by TCR signaling as WT T cells.
(A) Anti-CD3 was titrated with a start concentration of 10 µg/ml. Histograms show the surface CD69 expression of purified WT and Ric$^{o/o}$ T cells for each concentration. (B) Same titration as in (A). Histograms show intracellular pS6 expression levels for each concentration. (C) Anti-CD3 titration as in (A) and (B) with constant 10 µg/ml anti-CD28. CD69 expression of WT and Ric$^{o/o}$ T cells is shown. (D) Anti-CD3 titration as in (A) and (B) with constant 10 µg/ml anti-CD28. Histograms show pS6 expression. (A-D) Data are representative of two independent experiments.

3.1.7 Late TCR signaling is essential for complete RNA induction and proliferation of T cells

We next asked whether “late” TCR signaling, meaning later than the initial 18 hours of TCR engagement, is essential for proliferation and RNA synthesis and if all conventional TCR and mTORC1 signaling pathways equally contribute to this effect. Hence, graded amounts of Cyclosporin A (5 µM – 0.02 µM) and GDC0973 (20 µM – 0.08 µM) were added on day 1 to OT1 T cell cultures which were stimulated with 10 ng/ml pOVA. The cells were analyzed one day later. We found that proliferation is blocked by inhibition of calcineurin by high concentrations of Cyclosporin A and by MEK inhibition by GDC0973 (Figure 24A). At the same time RNA levels were reduced as well (Figure 24B).

GDC0941 is a PI3 kinase inhibitor which was added at concentrations from 20 µM to 0 µM to the OT1 cells, similar to Figure 24A+B. On day 2 DNA and RNA expression levels were analyzed as shown in Figure 24C. We saw that blocking PI3K has the same effects as direct blocking of mTOR with Torin, with a reduction in DNA and RNA synthesis in a dose-dependent manner.

Altogether these data show that late signaling of Calcineurin and MEK is still essential and contributes to full proliferative capacity and RNA synthesis in T cells. Blocking PI3K results in a dose-dependent downregulation of RNA synthesis and cell cycle induction similar to direct mTOR inhibition by Torin-1.

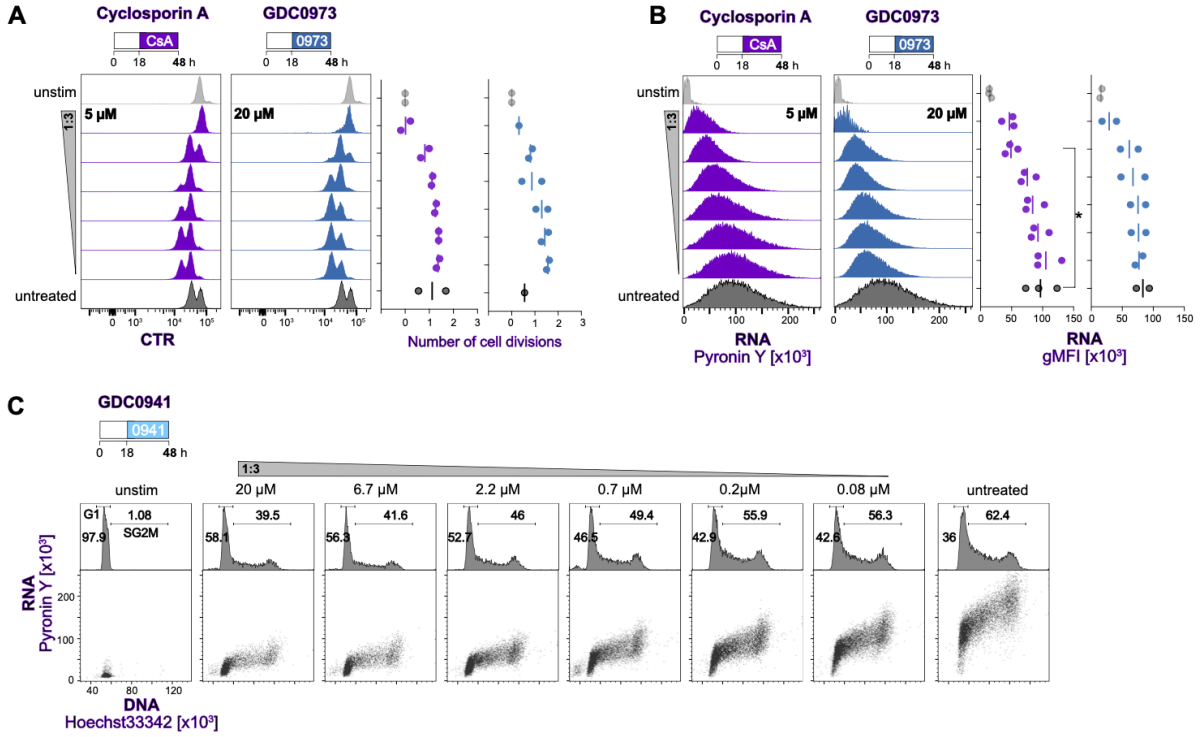

Figure 24. Late TCR signaling affects PY and CTV.
OT1 T cells were stimulated with 10 ng/ml pOVA for 48 hours. As indicated, titrated inhibitors were added after 18 hours of stimulation to the culture. (A) CTR dilution of Cyclosporin A (left) and GDC0973 (right) treated T cells. (B) RNA expression levels of T cells treated with Cyclosporin A (left) and GDC0973 (right). (C) DNA and RNA levels of T cells with titrated GDC0941, PI3K inhibitor. (A-C) Data are representative of at least two independent experiments.

Besides TCR signaling, Tan et al. (2017) showed that Raptor-deficient T cells had decreased mitochondrial biogenesis as well as reduced expression of several mitochondrial ribosomal proteins. Tigecyclin, an inhibitor of mitochondrial translation (Skrtic et al., 2011), affected T cell proliferation due to a defect in S phase entry, while survival and CD25 expression was

not affected (Tan et al., 2017). As mitochondrial ribosomal RNA is also a direct target of mTORC1, we asked whether its inhibition affects total RNA induction. Thus, we stimulated OT1 T cells with titrated amounts of Tigecyclin for 2 days. We found a dose-dependent effect as well on proliferation (Figure 25, left panel) and RNA levels (Figure 25, middle). At the same time, FSC-A was reduced accordingly (Figure 25, right).

These data show that mitochondrial translation is not only affected by mTORC1 deletion (Tan et al., 2017), but also affects T cell proliferation and RNA induction in a similar manner as mTORC1 and contributes to full T cell activation and cell cycle progression.

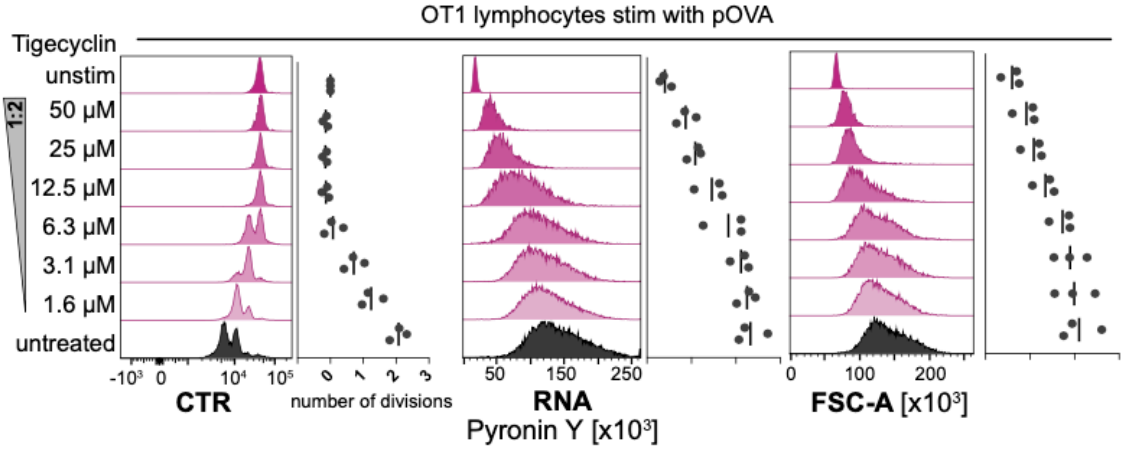

Figure 25: Mitochondrial protein translation contributes to T cell expansion.
OT1 T cells were cultured ± titrated Tigecyclin, ranging from 50 µM to 0 µM. CTR dilution, RNA expression and FSC-A are shown in the histograms for each concentration step. Data are representative of three individual experiments. Data are shown as mean.

3.1.8 Visualization of rRNA transcription with 5'ETS rRNA FISH probes

We observed before that total RNA levels, measured by Pyronin Y, are reduced in T-Rap$^{o/o}$ T cells. 85% of RNA in naïve and activated T cells is ribosomal RNA (Pennavaria, 2019). However, it is unclear if this increase is due to increased transcription or processing or decreased decay. Therefore, we established a way to detect the 47S rRNA precursor which is the initial substrate of RNA processing before being cleaved into 18S, 28S and 5.8S rRNA in ribosome biogenesis (Jorgensen and Tyers, 2004; Mayer and Grummt, 2006). Ribosomal RNA is transcribed by RNA Polymerase I which was shown before to be regulated by mTOR in yeast and cancer cell lines (Iadevaia et al., 2012; Li et al., 2006; Mahajan, 1994; Tsang et al., 2010). We designed Oligo probes for the 5'ETS site of the 47S pre-rRNA for use in a cell-

based RNA hybridization assay. Therefore, we stimulated OT1 T cells with 10 ng/ml pOVA for 2 days and harvested the cells as before. After surface staining, fixation and permeabilization, the cells were incubated in a Hybridization buffer containing the 5'ETS oligo probes for 16 hours at 37°C. We observed that WT and T-Ric$^{o/o}$ T cells on day 2 post stimulation have a 10- and 11-fold increase in 47S rRNA, respectively (Figure 26A). In contrast, T-Rap$^{o/o}$ T cells only increased their 47S ribosomal synthesis 5-fold. We also measured mRNA levels by RNA hybridization with an Oligo dT probe, binding to the polyA tail of mRNA. mRNA levels were as well slightly reduced in T-Rap$^{o/o}$ cells but the effect of the mTORC1 deletion was limited, contrasting with the results on rRNA (Figure 26A, right panels). This indicates that the transcription of 47S pre-rRNA is dependent on mTORC1 while processing seems unaffected.

To visualize the nucleolar sites of rRNA transcription, we acquired data of hybridized cells on an Imaging Flow Cytometer. We observed the expression of 47S rRNA over time, with samples stimulated for 1, 2 or 3 days and naïve cells as controls. As shown in the images in Figure 26B on the right, 5'ETS rRNA appears as 1-4 small dots per cell inside the nucleus, probably marking the fibrillar centers of nucleoli of the cell where RNA Pol I transcription takes place (Frottin et al., 2019).

These spots were quantified with the IDEAS software and shown in relation with their area in μm^2. We observed that WT, T-Rap$^{o/o}$ and T-Ric$^{o/o}$ T cells all increased the number of 5'ETS$^+$ sites 24 hours post stimulation (Figure 26B). However, only in WT and T-Ric$^{o/o}$ T cells these nucleoli also increase in size, from naïve 17.5 ± 1.3 μm^2 to 50.2 ± 4.4 μm^2 on day 1 in WT. Two days after stimulation the T-Rap$^{o/o}$ T cells further increased their number of nucleoli to 2.5 ± 0.2 nucleoli/cell while WT and T-Ric$^{o/o}$ nucleoli were slightly reduced (1.8 nucleoli/WT cell). Also, the area of the T-Rap$^{o/o}$ nucleoli further increased but were still smaller than those from WT and T-Ric$^{o/o}$ cells. On day three the size of T-Rap$^{o/o}$ nucleoli were higher compared to WT and T-Ric$^{o/o}$ T cells (41.8 ± 2.6 versus 27.5 ± 4 μm^2), but still did not reach the tallest size of WT and T-Ric$^{o/o}$ nucleoli on day 1 (50.15 ± 1.3 μm^2 in WT).

These data indicate that mTORC1 is essential for the rapid increase of rRNA, marked by a rapid increase in size of 5'ETS sites indicating high levels of 47S pre-rRNA transcription. Raptor-deficiency induces a deregulation of nucleoli with a delayed response and decreased pre-rRNA synthesis during the first days of T cell activation. These findings are in agreement with the RNA quantification with Pyronin shown in Figure 22A.

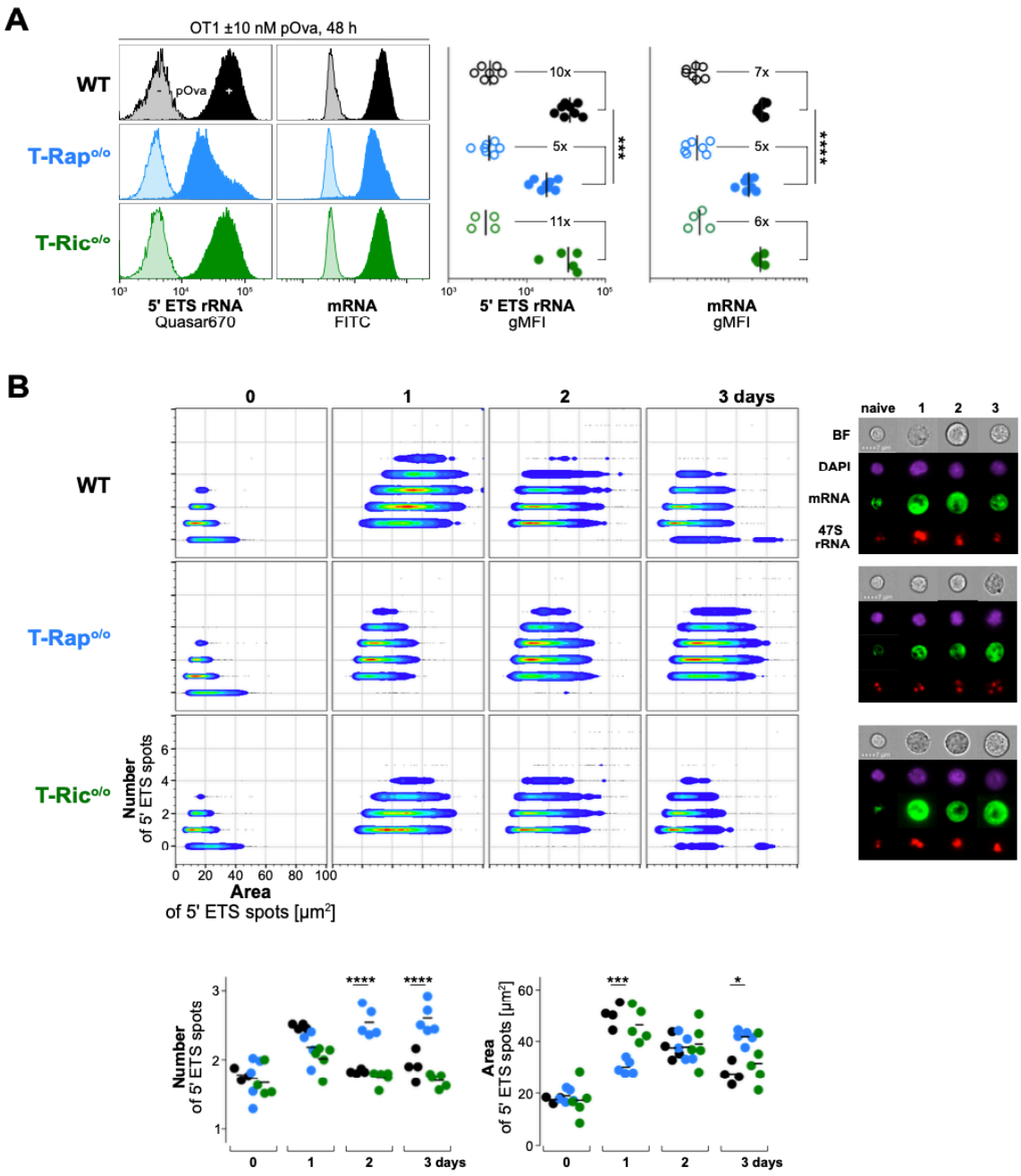

Figure 26: Nascent 47S ribosomal RNA is reduced in Raptor$^{o/o}$ T cells.

(A) 5'ETS and mRNA expression levels of OT1^{+} WT, Raptor$^{o/o}$ and Rictor$^{o/o}$ T cells two days post stimulation in vitro. Statistics panel shows result of five independent experiments. Numbers indicate the fold change from unstimulated to stimulated for each genotype. (B) Imagestream analysis of 5'ETS size and numbers over time in WT, Raptor$^{o/o}$ and Rictor$^{o/o}$ T cells. Analysis and calculation of spots was performed in IDEAS software. Pictures on the right were taken from the IDEAS Software and show Brightfield, DAPI, mRNA and 5'ETS staining of representative CD8^{+} T cells. Data are representative of four independent experiments. (A-B) Data are shown as mean. * = P < 0.05, ** = P < 0.01, *** = P < 0.001, **** = P < 0.0001, ns = P > 0.05; unpaired Student's t-test.

The Imaging data allowed us to quantify the size and volume increase of the nucleus, cytoplasm and cell as shown in Figure 27. The nuclear volume of WT T cells increased within one day from 100.7 ± 13.3 to 315.5 ± 109 µm^3, and then decreased by day two (215.3 ± 41.1 µm^3) and three (182 ± 25.6 µm^3). We found the same dynamic for cytoplasmic volume (Figure 27, middle panel) with the highest volume of 453.75 ± 26.4 µm^3 on day 2 with subsequent decrease the following day. In agreement with these findings, the total cellular volume was at its peak on day 1 with 672.75 ± 55.4 µm^3 and then decreased. In contrast, T-Rap$^{o/o}$ T cells showed a delayed response at the nuclear, cytoplasmic and cellular volumes which slowly increased over time with the highest volumes reached on day three post stimulation (655.6 ± 43.9 µm^3).

These results underline the finding that mTORC1 is an essential coordinator of the rapid increase of compartmental volumes of an activated T cell.

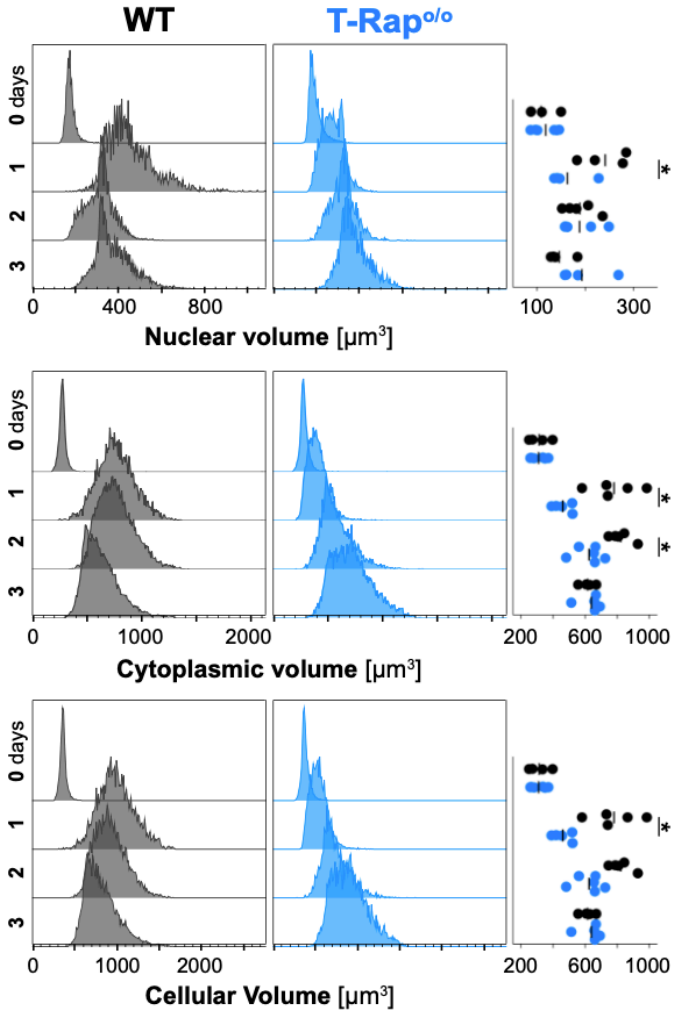

Figure 27: The increase of nuclear, cytoplasmic and cellular volumes is delayed in T-Rap$^{o/o}$ T cells.

Volume measurements of nucleus, cytoplasm and cell by Imagestream Analysis, arranged by genotype. Volume of nucleus, cytoplasm and cell were calculated in the IDEAS software. Statistics panel

shows result of four independent experiments. Data are shown as mean. * = P < 0.05, ** = P < 0.01, ns = P > 0.05; unpaired Student's t-test.

3.1.9 T cell volume increase is mTORC1-dependent

In order to obtain exact cell volume measurements of live cells, we used volume impedance measurements suggested as a "gold standard" of cell size measurement (Tzur et al., 2011). We purified T cells from WT and T-Rap$^{o/o}$ mice and stimulated them with anti-CD3/CD-28 for 1, 2 or 3 days and compared it with naïve, freshly isolated T cells as shown in Figure 28A. The cells were stained with DAPI and live cells sorted with a BD AriaFusion sorter to ensure live cells were used for volume measurements by the CASY counter, where no further gating is possible. Histograms of live cell volume were acquired, and the mean diameter and volume of the cells determined. We found that WT T cells increase their total volume from 120 fl to 615 fl ± 15 within two days (Figure 28B), which accounts for a 5-fold increase from naïve to activated cells. This massive increase is in agreement with electron microscopy data in human T cells (Wolf et al., 2020). On day 3, the volume of WT T cells slightly decreased but was still high with 588 fl ± 20. However, T-Rap$^{o/o}$ T cells increased their volume slower and reached a maximum of 538 fl ± 9 on day 3, which is still smaller compared to WT levels (Figure 28B). There were no quantitative differences between naïve WT and T-Rap$^{o/o}$ T cells.

The sorted live T cells were also analyzed by FACS for FSC-A, as shown in Figure 28C. By FSC-A measurements, we found only a 2-fold increase in both WT and T-Rap$^{o/o}$ T cells with almost no difference on day two and three. Only on day one, the difference of WT and T-Rap$^{o/o}$ T cell size was visible, albeit not significant.

In summary, we show that mTORC1 regulates the T cell volume in response to TCR stimulation which is underestimated by FSC-A data. In comparison to the Imaging data (Figure 27), the electronic volume measurements by the Coulter principle have the advantage that live cells are measured more accurately (5-fold increase vs. 3-fold increase). However, Imaging data include information on substructures as the nucleolus, nucleus and cytoplasm, revealing important insights in cellular changes and adaptations during T cell activation.

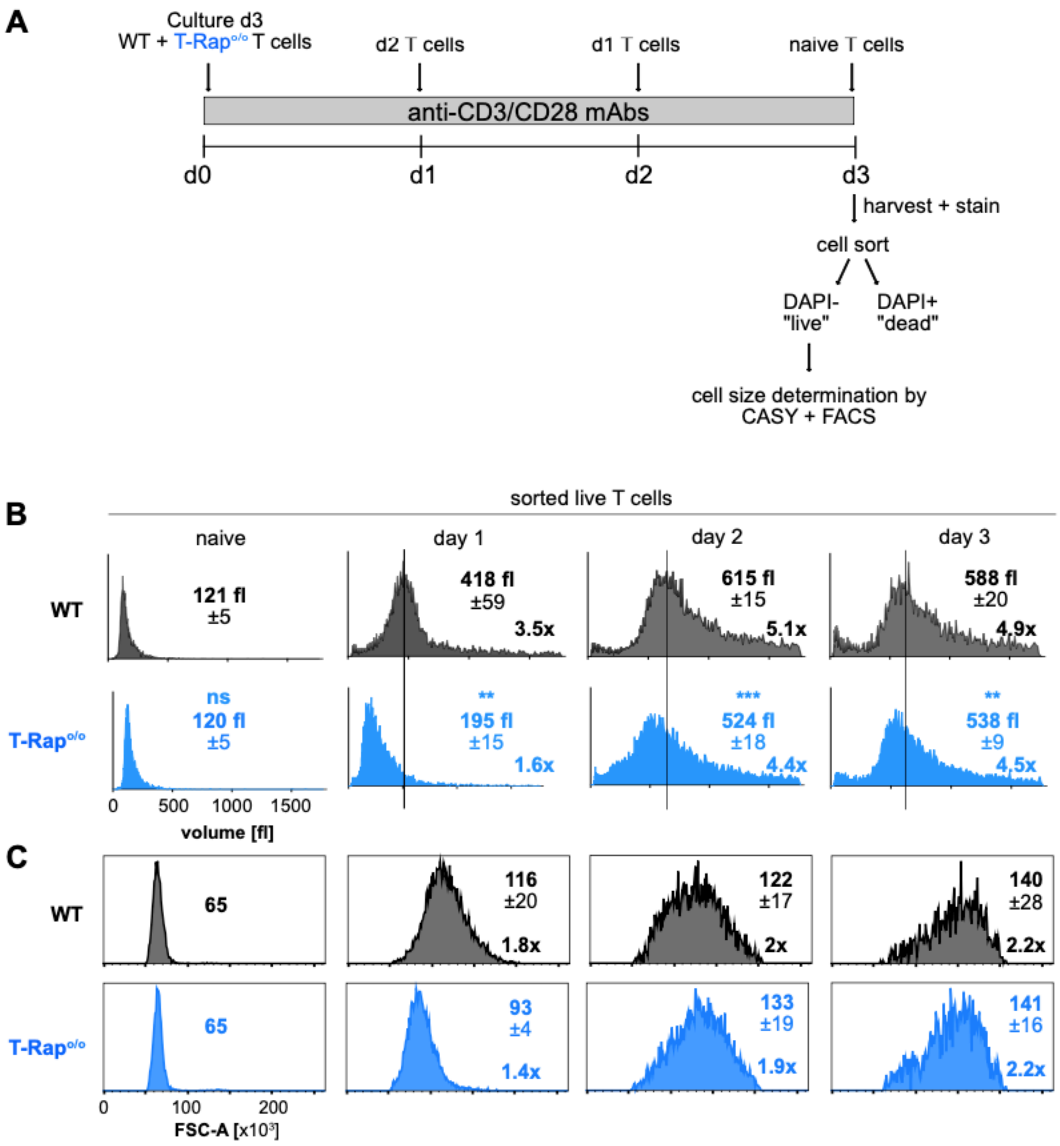

Figure 28: Volume increase is diminished in mTORC1-deficient cells.

(A) Experimental Scheme. Purified T cells were cultured with immobilized anti-CD3/CD28 mAbs for the indicated time points (0-3 days). T cells were then sorted for DAPI- cells to assure live cell measurement. Cell suspensions were then measured at the CASY Counter and at the Canto for comparison. (B) Volume in [fl] of WT and Raptor$^{o/o}$ T cells to the indicated time points. Inserted numbers show mean ± SD and fold change to naïve cells. Vertical lines demonstrate median of WT cells to visualize differences to Raptor$^{o/o}$ volumes below. (C) FSC-A levels of WT and Raptor$^{o/o}$ T cells to the indicated time points. Numbers indicate the mean gMFI ± SD, as well as fold changes to naïve levels. (B-C) Data are representative of three independent experiments with n=1-2. Data are shown as mean ± SD. * = P < 0.05, ** = P < 0.01, ns = P > 0.05; unpaired Student's t-test.

3.1.10 mTORC1 is essential for cell division and RNA biosynthesis throughout the expansion phase

Data depicted in Figure 18 suggest that mTORC1 is essential for each cell division so that proliferation is significantly delayed in T-Rap$^{o/o}$ T cells. To further investigate this issue, we added Torin-1 to stimulation cultures on day 1, day 2 or day 3 to block mTORC1/2 and the cells were analyzed 24 hours later. We had observed before that 47S rRNA expression is decreased in stimulated T-Rap$^{o/o}$ T cells (Figure 26A) and thus analyzed 5'ETS rRNA expression in this context now. Inhibition of mTORC1/2 in the first 24 hours blocked expression of 5'ETS completely and thus confirmed our finding with T-Rap$^{o/o}$ T cells (Figure 29A, left panel). In untreated cells, nascent pre-rRNA is highly expressed after 24 hours. When Torin-1 was added after 24 hours of stimulation, i.e. when 5'ETS is highly expressed, we observed a significant decrease of 5'ETS rRNA levels on day 2 compared to WT levels, showing that mTORC1/2 maintains the high levels throughout the first 2 days after stimulation (Figure 29A, middle panel). However, inhibition after day 2 does not change the expression of 47S rRNA (Figure 29A, right panel), suggesting that pre-ribosomal RNA can be stored in the nucleolus upon Pol I inhibition as it was described in tumor cells (Szaflarski et al., 2022).

In agreement with decreased 47S rRNA levels on day 2, the proliferation was also significantly slowed down as shown in Figure 29B (left panel). Proliferation was also affected by mTOR inhibition between days 2 and 3 (Figure 29B, right panel), although 5'ETS rRNA was detectable as in untreated cells. One explanation could be that, as described above, pre-rRNA is stored in the nucleolus but cannot re-enter ribosomal biogenesis and cannot be used by the cell.

Analyzing the cell cycle, we observed that Torin-1 treatment from day 1 until day 2 reduced RNA levels by half, measured by Pyronin Y (Figure 29C). In addition, 38% of cells were actively in cell cycle in S-G2-M phase, while in untreated cells over 65% were in these cell cycle phases. We quantified the cell cycle stages shown in Figure 29C (bar chart on the right) by Hoechst and Pyronin Y levels. These findings are in agreement with in vitro stimulated T-Rap$^{o/o}$ T cells that divide slower as WT T cells (Figure 18A).

Late inhibition (24 + 48 hours post stimulation) of mTORC1/2 also reduced the levels of phosphorylated H3 (H3P) as shown in Figure 29D, similar to T-Rap$^{o/o}$ cells (Figure 18C). The percentage of cells in M phase is significantly higher in WT T cells compared to T-Rap$^{o/o}$ (2.7% vs. 1.4%). However, there are fewer T-Rap$^{o/o}$ cells actively cycling due to the block in G1/S transition. Therefore, we looked at the percentage of cells in M phase of all cells in G2/M and found a significant reduction in T-Rap$^{o/o}$ cells as well (13% vs. 9%). We conclude

that the cells are not only blocked at the G1/S transition point by mTOR inhibition, but also at the G2/M transition leading to an additional delay in cell cycle progression.

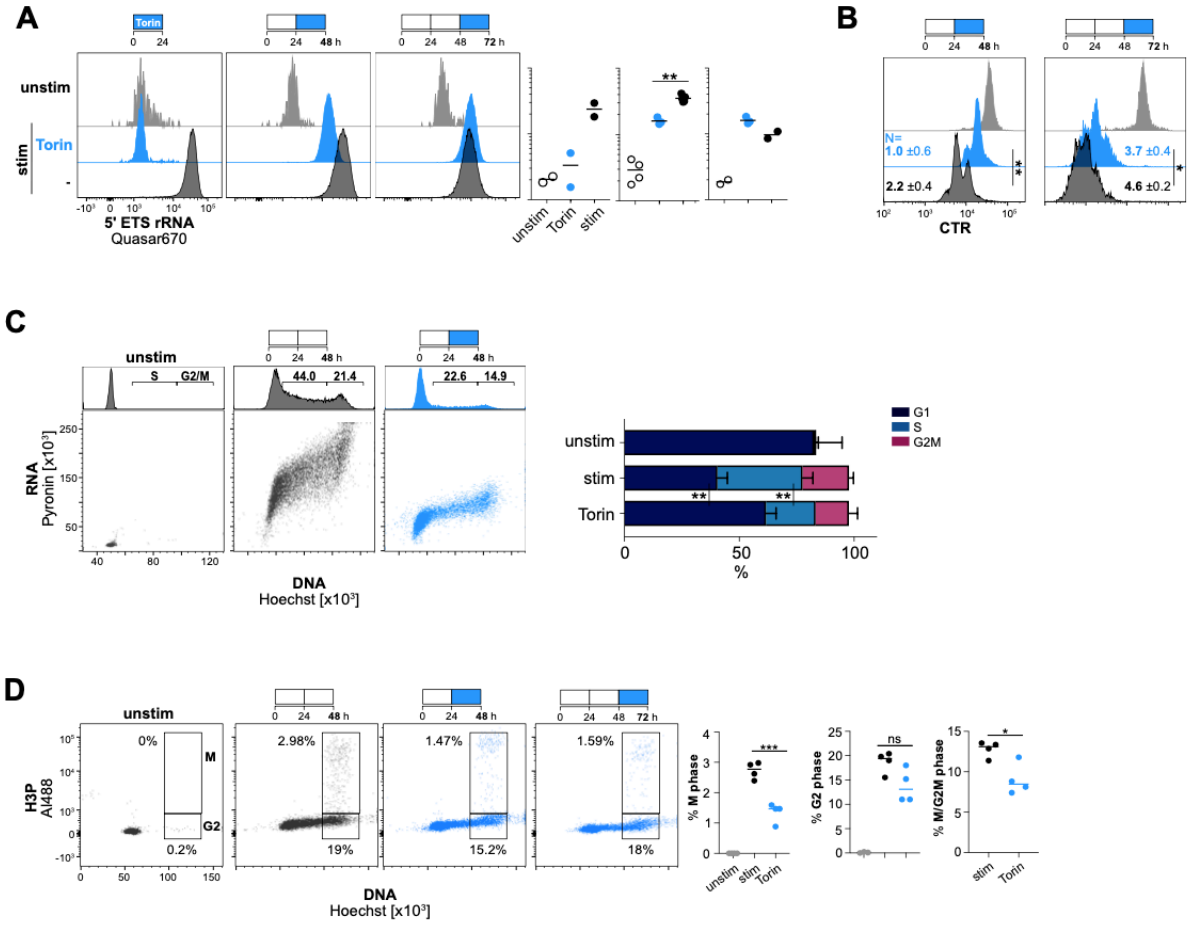

Figure 29: mTORC1 regulates RNA synthesis and cell cycle progression, but the effect decreases over time.

OT1 T cells were stimulated with 10 ng/ml pOVA and treated with Torin-1 to the above indicated timepoints. (A) 5' ETS expression of untreated vs. 24 h Torin-treated cells at different time points. Data are representative of at least two independent experiments. (B) CTR dilution of Torin vs. untreated OT1 T cells on day 2 and day 3. Inserted numbers indicate mean number of divisions ± SD. Data are representative of at least three independent experiments. (C) DNA and RNA expression of untreated vs. Torin-treated T cells. On the right, G1, S and G2M distribution of untreated and Torin treated cells are quantified. Data are representative of at least three independent experiments. (D) H3P expression of untreated and Torin-treated cells. Numbers indicate percentage of $H3P^+$ cells. Data are representative of five independent experiments. (A-D) Data are shown as mean. * = $P < 0.05$, ** = $P < 0.01$, ns = $P > 0.05$; unpaired Student's t-test.

As early and late inhibition of mTORC1/2 were shown to have strong effects on the expression levels of 5'ETS (Figure 29), we further assessed the dynamics of Torin-1 inhibition regarding proliferation and RNA induction and furthermore asked, to which extent Torin inhibition is reversible. As indicated in Figure 30A, OT1 T cells were stimulated for 2 days with 10 ng/ml pOVA and then treated with 1 µM Torin on day 3 and 4. The cells are compared to

untreated cells. By Torin-1 addition on day 3 proliferation was slowed down, however not significantly different from untreated cells yet. Continued inhibition until day four reduced proliferation in Torin-1 treated cells significantly (Figure 30A). We analyzed DNA and RNA levels of these cells and found a significant reduction of RNA on day three, in accordance with previous findings of Pyronin Y and 47S levels (Figure 30B). On day 4, Torin-treated cells had very low RNA levels, however, untreated cells also had started to downregulate their RNA levels.

To explore the reversibility of Torin-1 activity, we treated cells with Torin-1 from the beginning of the culture and released some of the cells on day 2. Proliferation had not begun by day 2 in the presence of Torin inhibition and RNA levels remained very low. However, as soon as Torin was washed away the cells started proliferating within one day and completed already 1.2 cell divisions (mean divisions) in the first 24 hours (Figure 30C) and 3.3 divisions until day 2. This shows, first, that mTOR inhibition is reversible and, second, that upon Torin release on day 2 the cells were able to enter S phase immediately, indicating that the cells were prepared for cell cycle progression except for mTOR signaling. At the same time RNA levels increased very quickly after Torin release on day three and four (Figure 30D), albeit less extensively than untreated cells (Figure 30B).

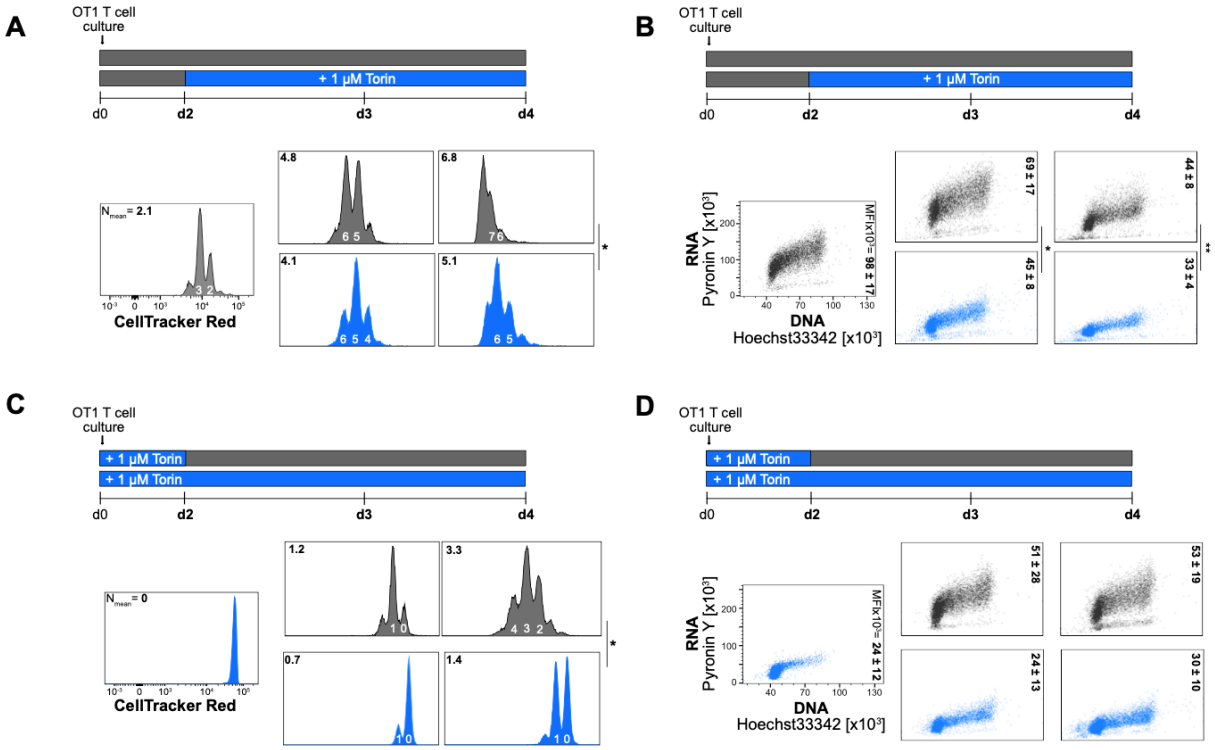

Figure 30: Effects of early and late mTORC1 inhibition.

(A) OT1 T cells were as indicated treated with 1 µM Torin from day 2 – day 4. CTR dilution is shown for T cells ± Torin on day 2, 3 and 4. Numbers in the upper left corner indicate mean number of divi-

sion and inserted numbers in white the number of peaks. (B) PY expression of the cells treated as in (A). (C) Torin is added to the culture from the beginning and in upper panels washed way on day 2. CTR dilution is shown of Torin-inhibited and -released cells. (D) RNA expression of cells treated as in (C). (A-D) Data are representative of at least three independent experiments. Data are shown as mean. * = P < 0.05, ** = P < 0.01, ns = P > 0.05; unpaired Student's t-test.

3.1.11 Nascent protein synthesis is regulated partially by mTORC1 in ongoing proliferation

Protein synthesis is one of the most important and best described effects of mTORC1 activation in T cells (Saxton and Sabatini, 2017). Protein synthesis is transmitted via mTORC1 downstream target 4EBP1. The translational machinery is a critical step during protein synthesis and was shown to be dynamically regulated by antigen stimulation and mTOR signals in activated T cells (Araki et al., 2017). Further studies showed a reduction of translation in cells treated with the mTOR inhibitors rapamycin or Torin-1 (Howden et al., 2019; Thoreen et al., 2012). We asked if differences of overall translation rates can be detected in cells that express only around 50% of RNA and ribosomes (Figure 22A and Figure 26A). We stimulated WT, T-Rap$^{o/o}$ and T-Ric$^{o/o}$ OT1 T cells with 10 ng/ml pOVA for two days, then harvested and washed the cells, and recultured the cells in methionine-free medium. L-Homopropargylglycine (HPG), a methionine analog, was added to the culture in a 1:1000 dilution according to the manufacturers protocol (Figure 31, top). HPG is incorporated into the protein sequence instead of methionine and can then be visualized by Click chemistry as described in section 2.2.15. We found that HPG levels were about 20% reduced in T-Rap$^{o/o}$ cells compared to WT T cells (Figure 31) albeit not significantly different, although we observed a reduction of RNA by 50% (Figure 26A). T-Ric$^{o/o}$ cells incorporated similar levels of HPG as WT T cells. However, latest experiments in the lab with T cells isolated from ANDxRap mice, where Raptor is deleted in CD4^{+} T cells, showed a 50% reduction in HPG signals on day 2 and 3 after stimulation with anti-CD3/28.

Altogether these data suggest that protein synthesis is slightly reduced in Raptor-deficient T cells but clear changes in overall translation are not detectable with this assay at that timepoint.

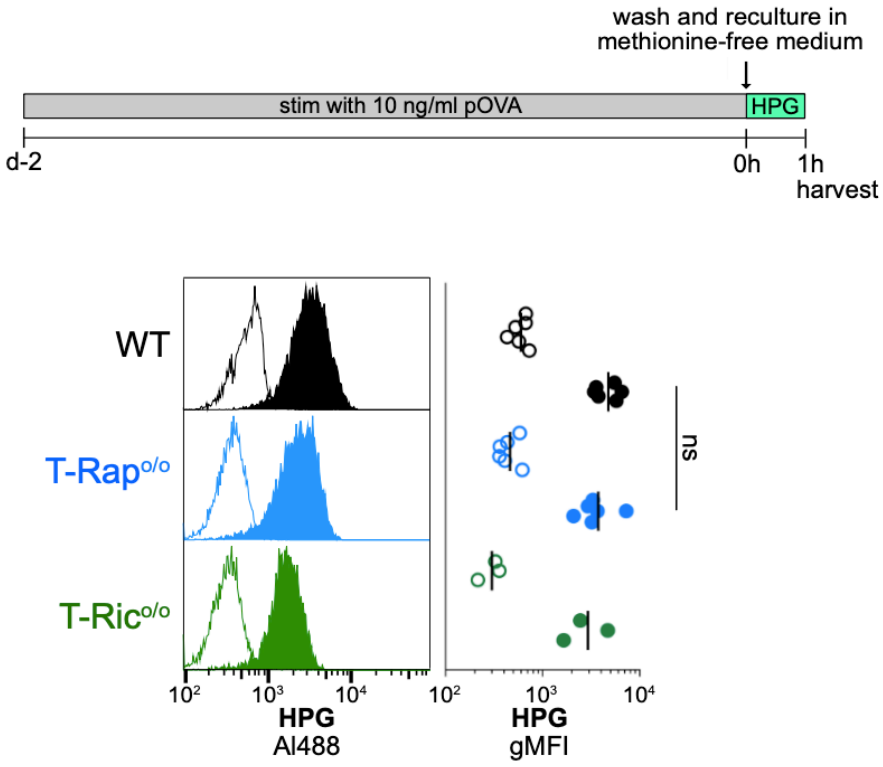

Figure 31: Protein synthesis on day 2 is slightly reduced in Raptor-deficient mice.
Experimental Scheme of L-Homopropargylglycine (HPG) assay. OT1 T cells were stimulated with 10 ng/ml pOVA for 2 days, then washed and re-cultured in methionine-free T cell culture medium ± HPG (1:1000 diluted) and incubated for 1 hour. HPG incorporation was detected by click chemistry and subsequent flow cytometry. Histograms show HPG incorporation of the indicated genotypes. Unfilled histograms represent unstimulated controls. Data are representative of at least three independent experiments. Data are shown as mean. * = P < 0.05, ** = P < 0.01, ns = P > 0.05; unpaired Student's t-test.

3.1.12 Inhibition of RNA Pol I affects cell cycle progression and RNA synthesis similar to mTORC1 inhibition

We further investigated the function of RNA Polymerase I and the nucleolus, as we observed not only functional, but also structural differences (Figure 26). To block RNA Pol I function, we used the two chemical inhibitors Quarfloxin (CX-3543) and BMH-21. To verify the mode of action of Quarfloxin, we stimulated OT1 T cells for one, two or three days and applied Quarfloxin for the last 24 hours. On day 1, 47S rRNA is entirely undetectable, showing that RNA Pol I activity is inhibited (Figure 32A, left panel). On day 2, the 47S rRNA signal is still significantly reduced (Figure 32A, middle panel). However, on day 3 post stimulation we observed a slightly reduced, but insignificant difference of 47S rRNA expression (Figure 32, right panel). This indicates the accumulation of unprocessed 47S rRNA intermediates as it

was observed in tumor cells and yeast before, once the rRNA transcription is blocked (Schneider et al., 2007; Szaflarski et al., 2022).

We also found that proliferation was affected by RNA Pol I inhibition as shown in Figure 32B. On day 2 as well as on day 3 post stimulation, proliferation was significantly reduced compared to untreated cells when RNA Pol I was inhibited 24 hours before. These findings indicate that T cell division is dependent on RNA Pol I regulated transcription.

We then analyzed the cell cycle by DNA and RNA staining and found that Quarfloxin inhibits the cell cycle at two checkpoints (Figure 32C). One is at the G1/S transition and the second one at the G2M/G1 transition. This effect was seen at both timepoints of addition. BMH21 treatment confirmed this finding, as shown in Figure 32D. We quantified the cell cycle stages according to the cells' DNA content and found a 3-fold increase in G2/M phase in Quarfloxin-treated T cells on day 2, and a 1.8-fold increase in G2/M even on day three. At the same time cells in S phase almost disappeared (Figure 32C, lower bar graphs). Likewise, in BMH-21 treated cells the percentage of cells in G2/M was increased (3.4-fold) and in accordance with that, almost no cells entered S-phase. It was shown in tumor cells, that Pol I transcription is highest during S and G2 phase (Iyer-Bierhoff and Grummt, 2019) and a similar regulation is indicated by these results in T cells. The G2/M block was also shown to be mTORC1 dependent (Figure 18B+C), suggesting a co-regulation by RNA Pol I and mTORC1.

We further assessed the phosphorylation of H3 on day three to identify cells in mitosis. Therefore, we stimulated OT1 T cells for 2 days and then treated them with or without 750 nM BMH-21. The H3P signal was clearly higher in untreated T cells than in BMH-21 treated cells (2.7% and 0.2%), indicating that ribosomal RNA transcription is required for the initiation of mitosis (Figure 32E). BMH-21 trapped the cells in the G2 phase (43.3% and 18.7% of WT T cells) indicating that ribosomal RNA transcription is essential for the G2/M transition.

Altogether these data on Quarfloxin and BMH-21 effects indicate that RNA Pol I is regulating cell division in T cells at two restriction points. T cells which were already in cell cycle progress through the S-phase and are then blocked at the G2/M while other cells are blocked at the G1/S transition. Both cell cycle checkpoints are thus regulated by RNA Pol I. RNA Pol I transcription was shown to be highly active during S and G2 phase in tumor cells (Iyer-Bierhoff and Grummt, 2019) and our findings suggest a similar regulation of the cell cycle in T cells.

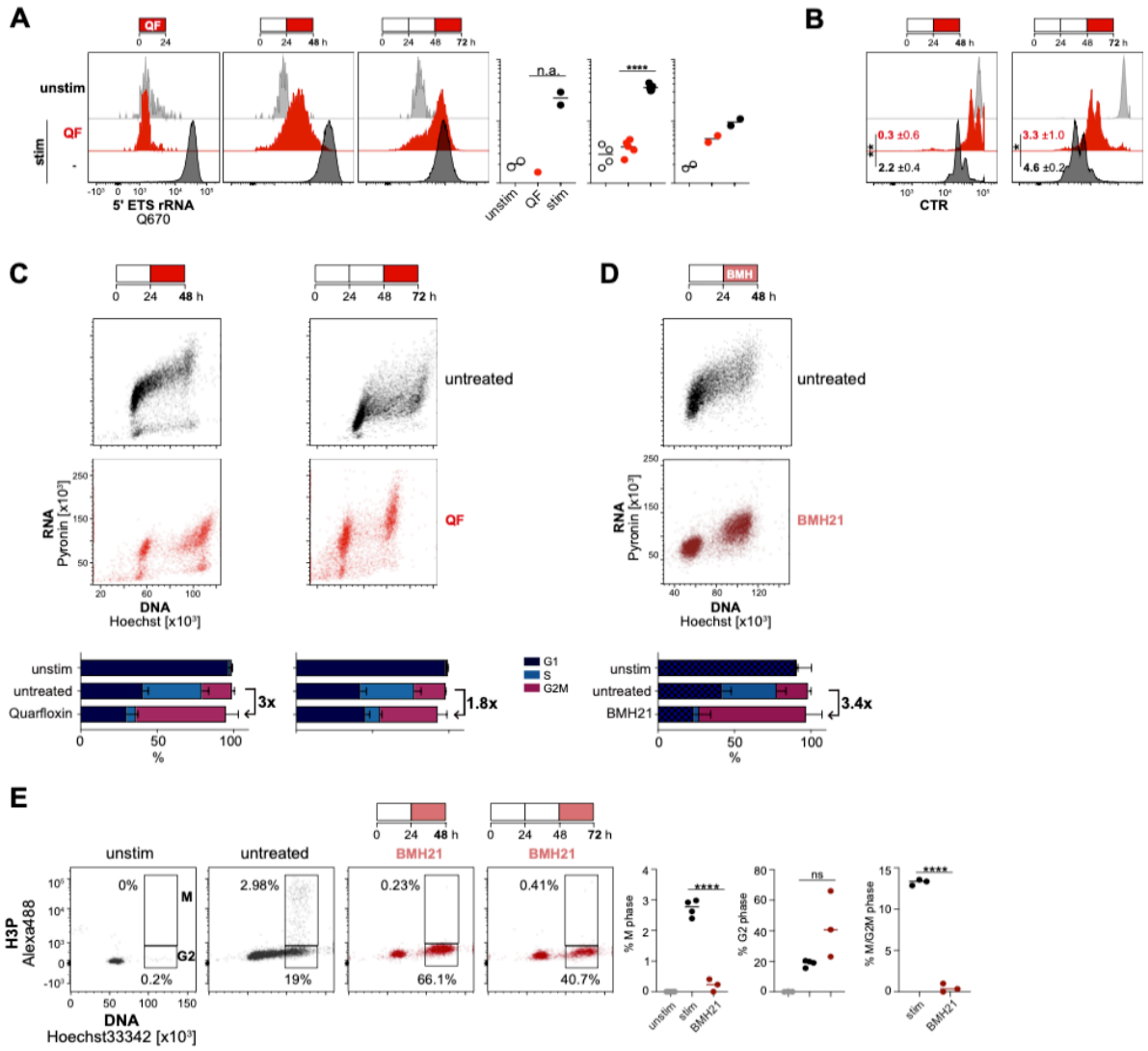

Figure 32: RNA Pol I controls cell cycle progression partially via mTOR.
OT1⁺ T cells were stimulated with 10 ng/ml pOVA and treated with inhibitors as indicated in each plot and harvested between d1-d3 post stimulation. QF is short for Quarfloxin (CX-3543) and BMH for BMH-21, another RNA Pol I inhibitor. (A) 5'ETS rRNA staining on d1, d2 and d3. Quarfloxin was added 24 hours before analysis. Data are representative of at least two independent experiments. (B) CTR dilution of untreated and Quarfloxin-treated cells on d2 and d3 post stimulation. 200 nM Quarfloxin were added to the culture 24 hours before. Data are representative of three independent experiments. (C) RNA and DNA levels, indicating the different cell cycle stages. (D) RNA and DNA levels of T cells treated with 750 nM BMH-21 for 24 hours as indicated. Cell cycle stages are quantified in percentage and shown below. (E) H3-phospho staining of BMH-21 and untreated cells on d3, indicating the amount of cells in mitosis. Data are representative of least five independent experiments. (A-E) Data are shown as mean. * = P < 0.05, ** = P < 0.01, *** = P < 0.001, **** = P < 0.0001, ns = P > 0.05; unpaired Student's t-test.

To assess further effects of Pol I inhibition, we investigated whether RNA Pol I has an impact on early targets of mTORC1 signaling such as phosphorylation of S6 protein and size increase. Thus, we titrated Quarfloxin, starting from 0.5 µM, and cultured OT1 T cells with and without the titrated inhibitor overnight. We found that Quarfloxin inhibited the size increase,

measured by FSC-A (Figure 33A, left) and also reduced S6 phosphorylation in a dose-dependent manner (Figure 33A, right), indicating that there is a feedback mechanism to mTOR signaling through RNA Pol I.

To assess how rRNA transcription and mTORC1 signaling are connected, we stimulated OT1 T cells for 21 hours, when 47S rRNA has reached maximal expression and mTORC1 showed maximal activity, and then added Quarfloxin to see a time-dependent effect. At 2 hours no difference was detected for both parameters. After 4 hours both pS6 and 47S rRNA decreased equally and were completely blocked after 6 hours (Figure 33B).

These data suggest that RNA Pol I activity and mTORC1 signaling are co-regulated and mutually dependent. Both are required to allow full T cell activation and rapid proliferation in response to antigen stimulation.

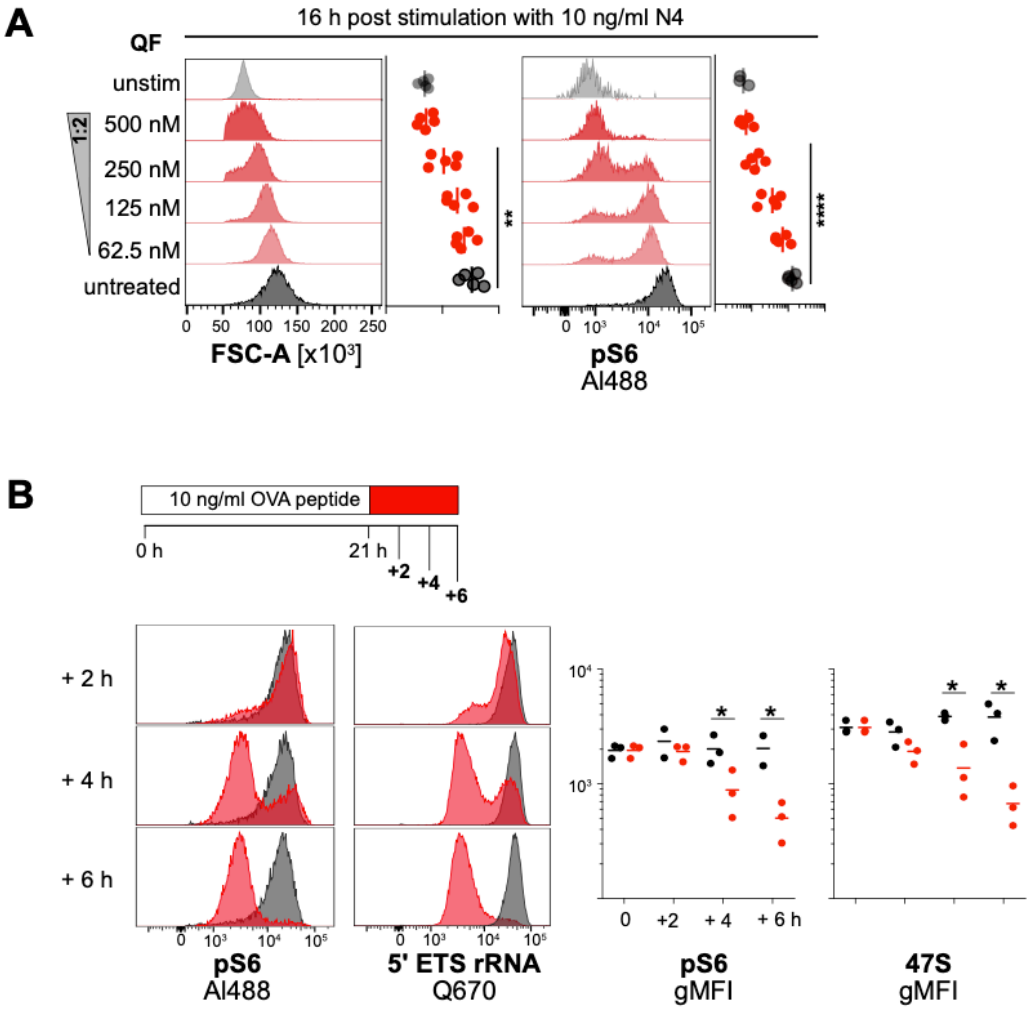

Figure 33: RNA Pol I and mTORC1 signaling are reciprocally regulated.

(A) FSC-A and pS6 expression of OT1 T cells treated with titrated Quarfloxin, ranging from 500 nM to 62.5 nM after overnight culture. Data are representative of three independent experiments. (B) pS6 and 5' ETS rRNA expression post QF addition on day 1. Data are representative of three independent

experiments. (A-B) Data are shown as mean. * = P < 0.05, ** = P < 0.01, *** = P < 0.001, **** = P < 0.0001, ns = P > 0.05; unpaired Student's t-test.

Our findings on FSC-A and pS6 expression were confirmed by using a second RNA Pol I inhibitor BMH-21 with a different mechanism of inhibition (Peltonen et al., 2010; Pitts and Laiho, 2022), as shown in Figure 34. Also here, we found a dose-dependent effect of RNA Pol I inhibition, underlining the importance of RNA Pol I for mTORC1 activity and T cell functionality.

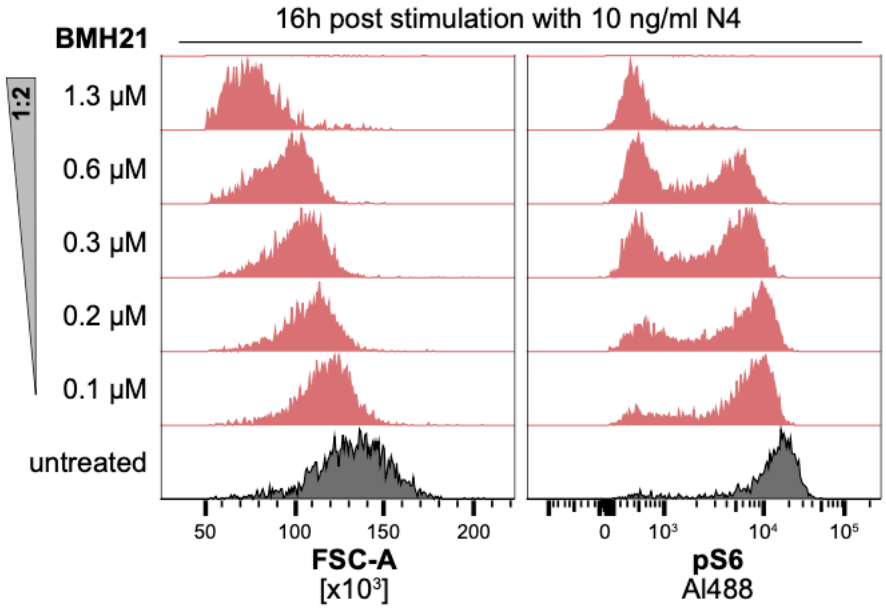

Figure 34: BMH21, another RNA Pol I inhibitor, confirms feedback signaling to mTORC1.
FSC-A and pS6 expression of OT1 T cells treated with titrated BMH-21, a RNA Pol I inhibitor, ranging from 5 µM to 0 µM after overnight culture. The first two concentrations were excluded due to cell death. N=1.

3.2 Re-challenge of memory T cells induces RNA levels to a similar level as naïve T cells

Following acute infection or vaccination, naïve $CD8^+$ T cells are activated and undergo clonal expansion to become T effector cells. During differentiation towards T_{eff} cells many transcriptional and metabolic changes occur and cytokines are produced (Powell et al., 2012). $CD8^+$ effector T cells directly kill infected target cells and thereby control the infection. After antigen clearance, most of the T cells die. Memory T cells are a small subset of cells that persist long time after an infection has been cleared as long-lived cells with stem cell-like features. They characteristically show a downregulated effector program and different metabolic capacities that is responsible for promoting persistence (O'Sullivan, 2019). As memory T cells are known to induce a strong and rapid immune response after a re-challenge (Barber et al., 2003; Lalvani et al., 1997), we wondered whether this is accompanied by an increased rate of RNA synthesis compared to naïve T cells.

We generated memory-like cells in vitro as described by T. Malek and colleagues (Carrio et al., 2004) (Figure 35A). OT1 T cells were stimulated with 10 ng/ml pOVA and 10 ng/ml IL-2 for three days, then washed and re-cultured either with 10 ng/ml IL-15 for memory-like T cells (T_{mem}) or 10 ng/ml IL-2 for effector T cells (T_{eff}) for four more days. On day 7, the cells were washed again and restimulated with 10 ng/ml pOVA and IL-2. We could show that on day 3 all cells were effector cells, with a $CD44^{high}$, $CD62L^{int}$ phenotype and high expression of CD25 and CD69 (Figure 35B). On day 7, T_{eff} cells showed only low levels of the memory cell marker Ly6C, whereas T_{mem} cells expressed high levels of Ly6C (Figure 35C). Upon restimulation, we found similar kinetics in RNA induction levels in such T_{mem} cells compared to freshly isolated naïve T cells (Figure 35D). Also, FSC-A levels increased simultaneously in both T_{mem} and naïve T cells.

Altogether these data indicate that memory T cells generated in vitro induce their RNA levels in a similar manner as naïve T cells do.

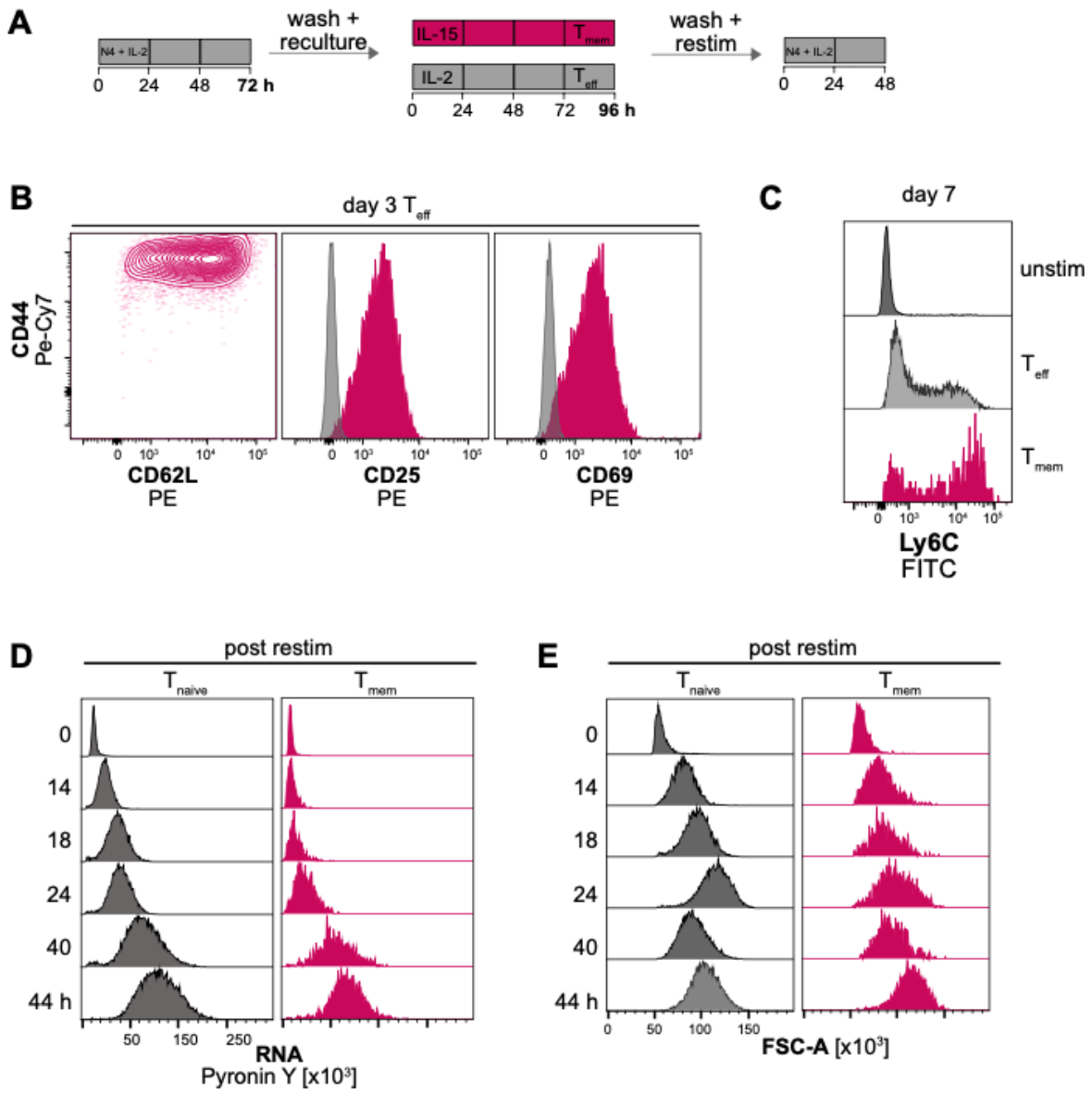

Figure 35: In vitro generated memory T cells upregulate RNA similar to naive cells.
(A) Experimental Scheme. OT1 T cells were stimulated with 10 ng/ml pOVA and 10 ng/ml IL-2 for 3 days. On day 3, cells were washed and re-cultured with either 10 ng/ml IL-2 ("effector T cells") or 10 ng/ml IL-15 ("memory T cells") for additional four days. Cells were then washed and restimulated with pOVA and IL-2 for 2 days. (B) Expression of activation markers CD62L, CD44, CD25 and CD69 in effector T cells three days post stimulation. (C) Ly6C expression of unstimulated, effector T cells and memory T cells on day 7 post stimulation. (D) Time course of RNA levels post restimulation, comparing memory T cells and freshly isolated naïve T cells. (E) Time course of FSC-A post restimulation, comparing memory and freshly isolated naïve T cells. Data are representative for at least one experiments for some time points.

As memory T cells generated in vitro are considered memory-like T cells and do not show all features compared to real memory cells, we further investigated this question with in vivo generated T cells. B10BR mice were twice immunized with B6 splenocytes by intraperitoneal injection (i.p.) as depicted in Figure 36A. 4 weeks later we harvested the spleens, purified T cells and stained them for CD44, which marks effector and memory T cells. The T cells were

then sorted by the flow cytometry into $CD44^{high}$ (T_{mem}) and $CD44^{low}$ ($T_{naïve}$) cells. After sorting, T_{mem} and T_{naive} cells were restimulated with anti-CD3/CD28, and samples taken at indicated time points.

Directly after the cell sort, T_{mem} cells expressed high levels of CD25, CD69, Ly6C and CD127 (Figure 36B, dark red histograms), which are all typical markers for the characterization of memory cells, while T_{naive} cells expressed very low levels of these markers (Figure 36B, dark grey histograms).

Upon restimulation, both $CD4^+$ and $CD8^+$ T_{mem} and T_{naive} cells displayed similar S6 phosphorylation levels, indicating high mTOR activity 18 hours after restimulation. We investigated RNA levels 22 hours post restimulation and found equal levels in T_{naive} and T_{mem} cells. The experiment was repeated at different time points (not shown). At all of them RNA levels were upregulated similarly.

In summary, these data show that in vitro as well as in vivo generated memory T cells have similar kinetics in RNA upregulation, size increase and mTOR activity. Thus, mTORC1 and ribosomal RNA synthesis regulate the activation of both naïve and memory T cells in a similar manner.

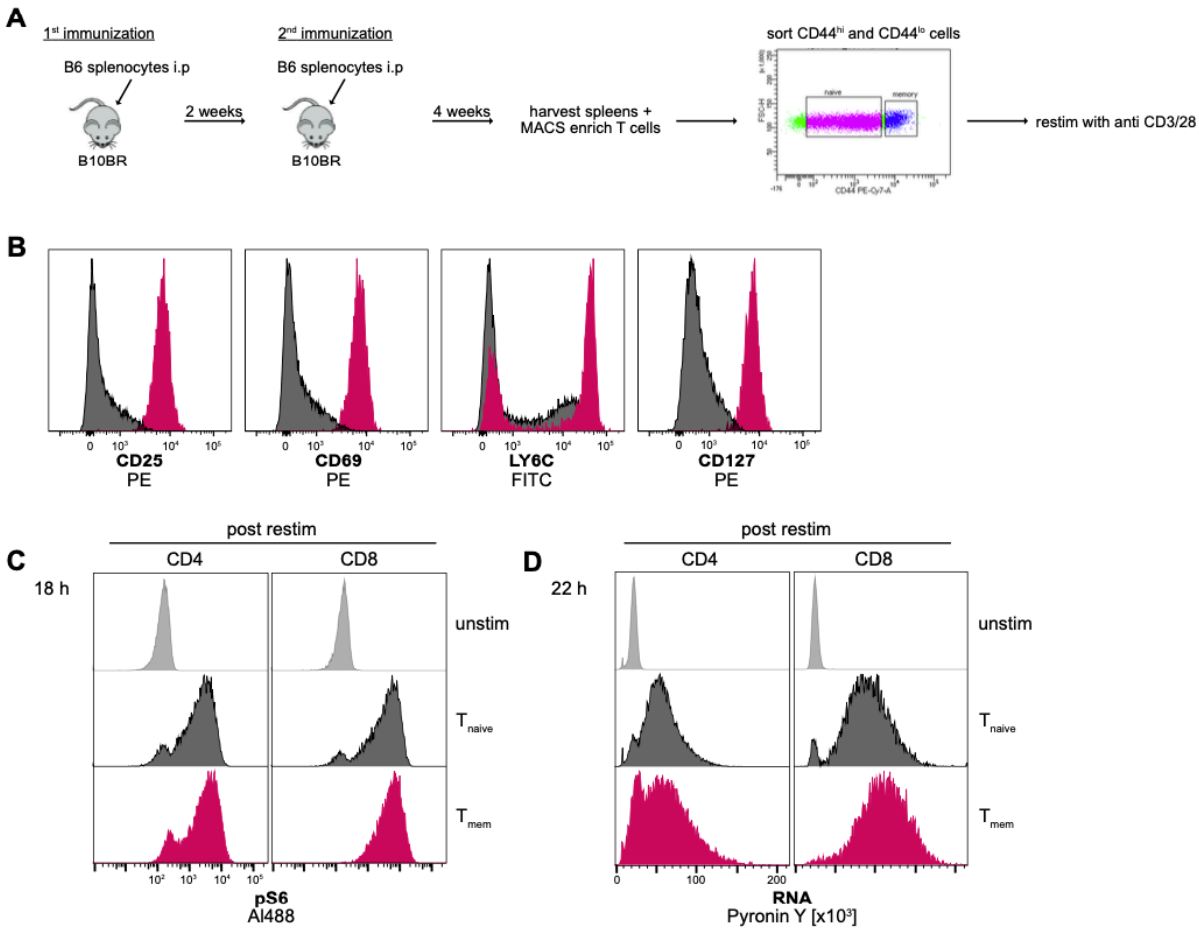

Figure 36: In vivo generated memory T cells have similar RNA and pS6 upregulation as naive T cells upon restimulation in vitro.

(A) Experimental Scheme. B10BR mice were immunized with splenocytes from a B6 mouse by intraperitoneal (i.p.) injection. 2 weeks later the same B10BR mice were immunized a second time with B6 splenocytes. After 4 weeks, mice were sacrificed, and T cells isolated from spleens. T cells were sorted regarding their expression of CD44 for $CD44^{high}$ (“memory”) and $CD44^{low}$ (“naïve”) population. The two populations were then restimulated with 10 µg/ml anti-CD3/CD28 and analyzed after one day. (B) Surface expression of CD25, CD69, Ly6C and CD127 in memory (dark red) versus naïve (dark grey) T cells post sorting. (C) pS6 expression levels of unstimulated, naïve and memory T cells 18 hours post restimulation. (D) RNA expression of unstimulated, naïve and memory T cells 22 hours post restimulation. Data are representative for at least one experiment.

4. Discussion

4.1 Downstream TCR signaling depends on mTORC1 activity

4.1.1 TCR signaling induced NR4 and CD69 expression

TCR signaling is induced within seconds after a peptide-MHC complex has bound to the T cell receptor. Among the three major signaling pathways downstream of TCR are the MAP kinase pathway, NF-kB signaling and the Ca^{2+}/NFAT pathway. Altogether these signaling cascades result in translocation of essential transcription factors, including NFAT, AP1 and NF-kB, into the nucleus, where they induce the transcription of genes important for T cell activation, differentiation and effector functions.

Besides p-MHC binding to the TCR, T cells can get activated indirectly by Interleukins or inflammatory mediators (Moran et al., 2011; Sun et al., 1998). To fully understand the mechanism and effects of T cell activation it is essential to distinguish between TCR-mediated activation and stimulation by other factors. Nur77, also known as NR4a1 transcriptional activator, is a specific reporter for TCR signaling (Moran et al., 2011; Zikherman et al., 2012), which is expressed very early, but does not respond to cytokine or interferon stimulation (Moran et al., 2011). It was shown to define antigen-activated lymphocytes more effectively compared to other activation markers like CD69 (Ashouri and Weiss, 2017). However, in this study we looked at both markers to evaluate the activation status of the cell.

We could show that Nur77 and CD69 expressions are induced very quickly after stimulation in vitro (Figure 21A). Downstream inhibition of mTOR signaling by Torin-1 did not affect the expression levels (Figure 21A). It was shown in another study by Ashouri et al., that rapamycin treatment did not affect Nur77 expression in $CD4^+$ T cells (Ashouri and Weiss, 2017). However, in response to limiting amounts of antigen, we observed that Torin-1 treated cells have reduced levels of Nur77 and CD69 compared to untreated WT T cells (Figure 21B+C). This shows that Torin-1 inhibition lowers the sensitivity of the OT1 TCR 3- to 9-fold when the amount of antigen is limited and thus increases the threshold for full activation of the T cell.

We could show that all major conventional TCR signaling cascades have to be fully active to allow full expression of CD69, as depicted in Figure 20B. The inhibition of each conventional signaling pathway, including the Ca^{2+}/Calcineurin/NFAT, MAP kinase/AP-1 and PI3K/Akt singnaling pathway, reduced the levels of CD69 in a dose-dependent manner.

Altogether, in our study CD69 turned out to be as effective as Nur77 as markers for T cell activation as we stimulated the T cells in vitro under controlled conditions with anti-CD3/CD28 antibodies or TCR transgenic T cells were stimulated with their specific antigen. Thus, the effect of other stimulatory molecules besides TCR could be minimized. Further-

more, our data underline that mTORC1 integrates signals initiated by the TCR and can affect its sensitivity.

4.1.2 mTORC1 signaling via downstream targets S6K1/2 and 4EBP1/2

mTORC1 signaling is activated via the PI3K/AKT pathway following TCR stimulation and functions through its downstream targets 4EBP1/2 and S6K1/2. S6K phosphorylates the ribosomal protein S6, which occurs quite fast following TCR stimulation (Fumagalli and Pende, 2022; Meyuhas, 2015). 2 hours post antigen stimulation, the signal is already high and increases further until 24 hours as shown in Figure 16B and Figure 22B. The S6 protein is also phosphorylated to a certain extent by RSK (p90RSK) following TCR stimulation (Salmond et al., 2009), and thus MEK inhibition reduced pS6 levels via RSK signaling, independent of mTORC1. However, it can be distinguished by different phosphorylation sites, and with our pS6 antibody we mainly investigated the mTORC1-dependent site at S235/S236. We could show that Torin-1 blocks the phosphorylation of S6 in a dose-dependent manner (Figure 21A). We had some indications from previous experiments that Rictor-deficiency leads to increased phosphorylation of rS6 or CD69 expression and suggested mTORC1 compensates the loss of Rictor by expressing more binding sites for Raptor. However, this was not the case when tested (Figure 23). Even in limiting amounts of antigen, WT and T-Ric$^{o/o}$ cells behaved likewise and the addition of anti-CD28 increased the stimulatory threshold 100-fold in both cell types.

We also found that co-stimulation with anti-CD28 increases the levels of pS6 100-fold in suboptimal CD3 stimulatory conditions for both CD69 and pS6 expression (Figure 20A), indicating that costimulation is regulated similarly in conventional and mTORC1-dependent TCR signaling.

Besides functioning via its classical downstream targets, mTORC1 induces the phosphorylation of around 3260 proteins following T cell activation, including NFAT, NfkB and MAPK components (Tan et al., 2017). Altogether, as mTORC1 was shown to affect TCR sensitivity and integrates cytokine signals, it is a key regulator of immune responses.

4.2 mTORC1 regulates proliferation, RNA levels and growth

4.2.1 Proliferation in T cells depends on mTORC1

It was shown in previous studies that mTOR regulates the exit of quiescence in T cells, but is not required for ongoing cell divisions (Howden et al., 2019; Terada et al., 1993a; Yang et al., 2013). Previous work in our lab with antigen-specific TCRs showed that the proliferation in vivo is delayed over time in Raptor-deficient T cells. We found as well that WT T cells prolif-

erate three times per day in vivo (Obst, 2015), whereas Raptor-deficient T cells only divide once per day. As shown in Figure 17, Raptor-deficient T cells were also unable to divide in H2-bm1 and bm12 mice, while Rictor-deficient T cells did not show any defects and behaved like WT cells. However, we observed a small percentage of Raptor-deficient T cells which divided as well but delayed. To further investigate these findings, in vitro assays measuring EdU incorporation were performed. These experiments revealed that first of all, less Raptor-deficient T cells are in S phase (59%) 42 hours post stimulation with OVA peptide and second, 3 hours later the cells still have not completed one cell cycle (Figure 18B). At the same time, 71% of WT T cells were in S-phase and 3 hours later we could find around 15% of these labeled cells back in G1, showing that cell cycle progression is much faster. Altogether, these data show that not only the first cell cycle but also all consecutive cell cycles are dependent on mTOR and that mTOR activation leads to three-fold faster responses.

In addition, late inhibition with mTOR inhibitor Torin-1 as well delayed cell cycle progression and led to a reduced proliferation rate (Figure 29B, Figure 30A), corroborating that mTOR signaling is required throughout the expansion phase for proper T cell function.

Other groups could not show the necessity of mTOR activity for ongoing proliferation, although similar experiments were performed (Yang et al., 2013). However, one difference is that only in vitro proliferation was investigated. We have shown before that transferred WT T cells into an antigen-inducible mouse model divided and accumulated in lymphoid organs with a rate of 3 divisions per day, while T-Rap$^{o/o}$ T cells divided less and died after day 5. We observed a delayed start of proliferation of transferred T-Rap$^{o/o}$ T cells and slowed down proliferation, but not a complete block of proliferation (Pennavaria, 2019). Another difference were the timepoints of the EdU experiments, which could not reveal differences in EdU incorporation in other studies. We found that especially the time frame how long a cell needs to progress through the cell cycle is different between WT and Raptor-deficient T cells and can only be observed by time course pulse chase experiments, which were not performed by other groups. As reason for a delayed exit of quiescence, Yang et al. showed a decreased expression of various cell cycle regulators such as cyclin D2, E and CDK2, 4 and 6 in Raptor-deficient T cells, but a delay in proliferation was not further investigated. Our data thus makes inhibition of mTORC1 a more reasonable therapeutic target in manifested autoimmune and inflammatory diseases.

4.2.2 Volume increase is mTORC1 dependent

Following TCR stimulation, the T cell has to adjust and prepare for rapid clonal expansion. One important characteristic is that the T cells massively increase their cellular volume for complete T cell functionality. That volume increase in T cells is known to be mTOR-dependent, however, exact sizes are not known. We activated sorted WT and T-Rap$^{o/o}$ T

cells with anti-CD3/28 for 1, 2 or 3 days and measured the size of the cells with a CASYCounter. With this method we found that naïve WT and T-Rap$^{o/o}$ T cells both have the same size of ~121 fl. Following stimulation both cell types increased their volume, whereas WT T cells reached a maximum on day 2 with 615 fl, while T-Rap$^{o/o}$ T cells reached their maximum volume of 538 fl only on day 3. However, the biggest differences we observed on day 1 post stimulation, when WT T cells had 418 fl and T-Rap$^{o/o}$ T cells only an increase to 195 fl, which makes a fold increase of 3.5 and only 1.6 in WT and T-Rap$^{o/o}$ T cells, respectively (Figure 28B). We saw this immense difference on day 1 as well with the FSC-A in common FACS data, with WT T cells showing 116 (x10^3), while T-Rap$^{o/o}$ T cells only reached 93 (x10^3) (Figure 28C). In contrast, in human T cells the size was shown to increase from 82.5 fl in naïve, to 670 fl in stimulated T cells, measured by electron microscopy (Wolf et al., 2020), which accounts for a 8-fold increase compared to the 5-fold increase in our murine cells but are in overall agreement with our measurements.

Looking further into cellular compartments by Imaging flow cytometry, we found that the reduced volume in Raptor-deficient T cells involves both nuclear volume and cytoplasm. The nuclear volume was reduced on day 1 only, but cytoplasm was reduced on day 1 and day 2. Total cell volume was reduced throughout all timepoints in Raptor-deficient T cells (Figure 27), while Rictor-deficient T cells did not show any defects in cellular adaptation.

Altogether these data provide exact numbers of the volume increase of activated murine T cells over time, showing Raptor has the most effect on volume increase already on day 1 of stimulation, however, Raptor-deficient T cells never reach the maximal values of WT T cells. Furthermore, mTORC1 regulates the rearrangement of cellular compartments upon stimulation to allow the cell to quickly adapt to the increased demands posed by rapid cell divison.

4.2.3 Total RNA and ribosomal RNA induction regulated by mTORC1

Pyronin Y was first described in 1981 by Shapiro as a fluorescent dye that stains dsRNA (Darzynkiewicz et al., 2004; Shapiro, 1981). In combination with a DNA dye such as DAPI or Hoechst33342 one can distinguish the different cell cycle stages. The transition from G0 to G1 is clearly marked by an increase in Pyronin Y levels, levels further increase throughout the S-phase and then reach G2-M phase at the 4n DNA stage. However, Pyronin Y was hardly used in lymphocytes in the recent years, for instance by the Victora lab on germinal center B cells (Ersching et al., 2017). In our study we stained Pyronin Y in combination with Hoechst33342 and found a 9-fold increase of total RNA levels in T cells two days post stimulation. Interestingly, Raptor-deficient T cells only increased their RNA levels 5-fold (Figure 22A). We looked at RNA upregulation over time and found that Raptor-deficient T cells had a delayed increase to all timepoints (Figure 22C). Although these cells increased RNA levels slowly until day 4, they never reached the maximum levels of WT T cells. At the same time,

we observed less cells actively in the S-G2-M phase of the cell cycle, in coordination with the reduced RNA levels and delayed cell proliferation as discussed before (Figure 18A+B). In accordance with that, Raptor-deficient T cells were shown to enter S-phase without having passed through a proper S1 phase with less RNA per cell. While mTORC1 is shown to have an immense impact, mTORC2 does not affect RNA induction.

We observed that the RNA levels are limited by mTORC1 activity. Even in late inhibition of T cells with Torin-1 on day 2 post stimulation, levels rapidly decrease within 24 hours (Figure 30B) and as well, Torin-1 release on day 2 post stimulation, results in an increase of RNA levels comparable to untreated levels (Figure 30D).

At the same time, total RNA levels are influenced by constant TCR signaling as shown in Figure 24B. Late inhibition of NFAT pathway by cyclosporin A or MAPK pathway by GDC0973 on day 2, leads to a drop in total RNA levels (Figure 24B). Similarly, late inhibition of PI3K, an upstream regulator of mTORC1, results in downregulation of RNA levels as well in a dose-dependent manner (Figure 24C).

We established a new method in our lab to investigate the expression of 47S pre-ribosomal RNA by RNA hybridization. Therefore, 48 oligonucleotide FISH probes binding to the 5'ETS site of the ribosomal RNA were coupled to a fluorescent dye and could be used to determine the generation of nascent ribosomal RNA (Antony et al., 2022; Claiborne et al., 2022). The 5'ETS is cleaved and destroyed within minutes after rRNA synthesis in tumor cells like Hela (Popov et al., 2013). We found a 10-fold increase of 47S rRNA in WT T cells upon activation by antigen compared to a 5-fold increase in Raptor-deficient T cells (Figure 26A).

Altogether these data show that mTORC1 regulates the increase of total RNA in T cells post stimulation as well as the nascent synthesis of ribosomal RNA. In dependence of mTORC1 activity, RNA levels can be quickly adjusted to prepare the cell for rapid cell division.

4.3 Nucleoli and 47S pre-rRNA generation as rate limiting step during mTOR-dependent activation of T cells

4.3.1 Structural changes of nucleoli and cellular compartments

Besides the reduction of 47S ribosomal RNA in Raptor-deficient T cells, we also observed structural changes and differences in T-Rap$^{o/o}$ T cells compared to WT T cells. By imaging flow cytometry, as depicted in Figure 26B, we showed that 47S sites, referred to as nucleoli where rRNA synthesis takes place, were increased in Rap$^{o/o}$ T cells following stimulation. In WT T cells we measured maximum 2.4 nucleoli/cell on day 1 post stimulation, while Rap$^{o/o}$ T

cells had 2.2 nucleoli/cell. However, T-Rap$^{o/o}$ T cells increased their nucleoli up to 2.6 nucleoli/cell on day 3 post stimulation, while WT T cells decreased their sites after day 1. At the same time, T-Rap$^{o/o}$ T cells had smaller nucleoli than WT T cells, with a maximum area of ~42 versus ~50 µm^2, respectively. The massive increase of nucleoli size in WT T cells could be an indication of hypertranscription, which was described already decades ago as the upregulation of transcriptome for transitional processes in cells; for instance during stem cell expansion, embryonic development, regeneration and cancer (Lin et al., 2012; Percharde et al., 2017). The concept of hypertranscription might provide an explanation for the rapid biomass production that is required for clonal T cell expansion. Furthermore, the massive and rapid change in nucleolar size and numbers might make the nucleolus and its substructures potential novel immunological biomarkers.

But not only the nucleoli showed differences, but also the volume increase of nucleus, cytoplasm and cell had different kinetics in dependence of mTORC1. The nuclear volume was significantly higher in WT T cells on day 1 with an increase from naïve ~101 to 316 µm^3. The cytoplasm increased as well significantly on day 1 and even further on day 2, as shown in Figure 27. Similar to the CASY Counter measurement of cell size, the gold standard of cell size measurements (Tzur et al., 2011) of unfixed cells, we also quantified the total cell volume from Imaging Flow data and observed that fixed WT cells reached a maximum on day 1 with ~673 µm^3, while Raptor-deficient T cells reached a maximum of ~656 µm^3 only on day 3.

While WT T cells increase their cellular volume 5-fold, the amount of RNA per cell, which is up to 85% ribosomal RNA, increases at least 9-fold. Early studies on dry biomass production showed a comparable increase in PHA-stimulated lymphocytes from 30 to 400 pg (Darzynkiewicz et al., 1967). The cytoplasmic concentration of ribosomes thus increases ~2-fold dependent on mTORC1, which is likely to change the biophysical properties of the cytoplasm. It was shown in tumor cells, that mTORC1 can adjust the ribosomal abundance and thereby the phase separation properties of the cytoplasm (Delarue et al., 2018). Our data suggest that ribosomal abundance is not a fixed but a flexible parameter during T cell activation.

These kinds of observations were not known in T cells before and indicate a tight connection of mTORC1 signaling and the nucleolus, where ribosomal RNA synthesis takes place, which in turn has further effects on cell growth and growth of various cellular compartments. Raptor-deficient T cells showed a slow and continuous increase in size and volume of all analyzed compartments over time, suggesting that mTORC1 signaling pushes the cell to a faster response within only one day instead of three or more.

4.3.2 RNA Pol I activity controls both cell cycle and mTORC1 activation

One of the major functions of mTORC1 is promoting translation initiation and subsequent protein synthesis, so we wondered whether a reduction in protein synthesis in our $Rap^{o/o}$ T cells is responsible for the cell cycle delay as well as the delayed size increase in cellular compartments. We measured the nascent protein synthesis on day 2 by incorporation of HPG into the cells and found no significant difference between WT and $Rap^{o/o}$ T cells as shown in Figure 31. Although initial protein synthesis is decreased by 50% in Raptor-deficient T cells as shown in various other studies (Howden et al., 2019; Hukelmann et al., 2016), we couldn't detect a difference in nascent total protein content after 48 h post stimulation, indicating that T cells do not require mTORC1 signaling for translational activity in expanding cells.

As the reduction in 47S rRNA in Raptor-deficient T cells was very striking as well as cellular growth differences, we further investigated how rRNA controls and regulated cell cycle progression. Quarfloxin (QF) and BMH-21 chemicals were used to block RNA Pol I activity in vitro, as depicted in Figure 32. Quarfloxin is a small molecule and functions through disrupting the interaction between G-quadruplexes rDNA and the nucleolin protein, which thus blocks the activity of RNA Pol I (Duquette et al., 2004). BMH-21 intercalates into the DNA and binds to GC rich regions, without inducing DNA damage. It inhbits RNA Pol I specifically by inducing proteasome-mediated degradation of one of its subunits, RPA1 (Peltonen et al., 2014). As a proof-of-concept we looked at 5'ETS signals on day 1, 2 and 3 with addition of inhibitor 24 hours before and showed that on day 1, the signal is completely missing and on day 2 it is decreased significantly (Figure 32A). On day 3 post stimulation, 5'ETS expression was rather independent of RNA Pol I inhibition, indicating the storage of unprocessed synthesized rRNA as it was described in yeast and tumor cells (Schneider et al., 2007; Szaflarski et al., 2022). Interestingly, similar to mTORC1 deletion (Figure 18) and mTOR inhibition by Torin-1 (Figure 29), we found a block in proliferation in QF-treated cells, as depicted in Figure 32B. Both on day 2 and day 3, QF-treated cells had completed less cell cycles. Surprisingly we found by RNA/DNA staining that QF-treated cells did not enter S-phase any longer and accumulated either in G1 or G2M phase of the cell cycle (Figure 32C). This finding was confirmed as well by BMH-21 treatment as shown Figure 32D. G1-S transition is known to be regulated by mTORC1 as well, however, G2M transition seems to be RNA Pol I dependent. H3-phospho staining confirmed that the T cells are blocked in G2-phase, as none of the cells express H3-P (Figure 32E), indicating that rRNA transcription is necessary for the initiation of mitosis. RNA Pol I was shown to be essential during S and G2 Phase in tumor cells (Iyer-Bierhoff and Grummt, 2019) and our data suggests a similar regulation in T cells.

These data indicate a strong connection between mTORC1 and RNA Pol I, as well as an essential role of RNA Pol I in regulating cell cycle progression in activated T cells. RNA Pol I is an essential regulator of the cell cycle at the G1/S and the G2/M transition.

4.3.3 Feedback signaling to mTORC1

We further investigated the role of QF and RNA Pol I inhibition on cell growth and signaling as shown in Figure 33A. We found that QF regulates the cell size increase after overnight stimulation (Figure 33A) in a dose-dependent manner. We observed that mTORC1 downstream signal phospho-S6 was as well regulated by the activity of RNA Pol I, as shown in Figure 33A. Complete inhibition of RNA Pol I function by QF led to a blockade in pS6 signaling. Interestingly, pS6 and 47S signals go down simultaneously after late RNA Pol I inhibition on day 2 (Figure 33B). 4 hours post QF addition both signals were half downregulated and completely gone after 6 hours.

Altogether these data show that there is a strong connection of mTORC1 signaling and the activity of ribosomal biosynthesis, which co-regulate each other and, that RNA Pol I gives negative feedback signals to mTORC1 in case it cannot perform properly (Figure 37). The nucleolus thus seems to be an essential caretaker of proper T cell activation and expansion by the reciprocal regulation of both mTORC1 and ribosomal biosynthesis.

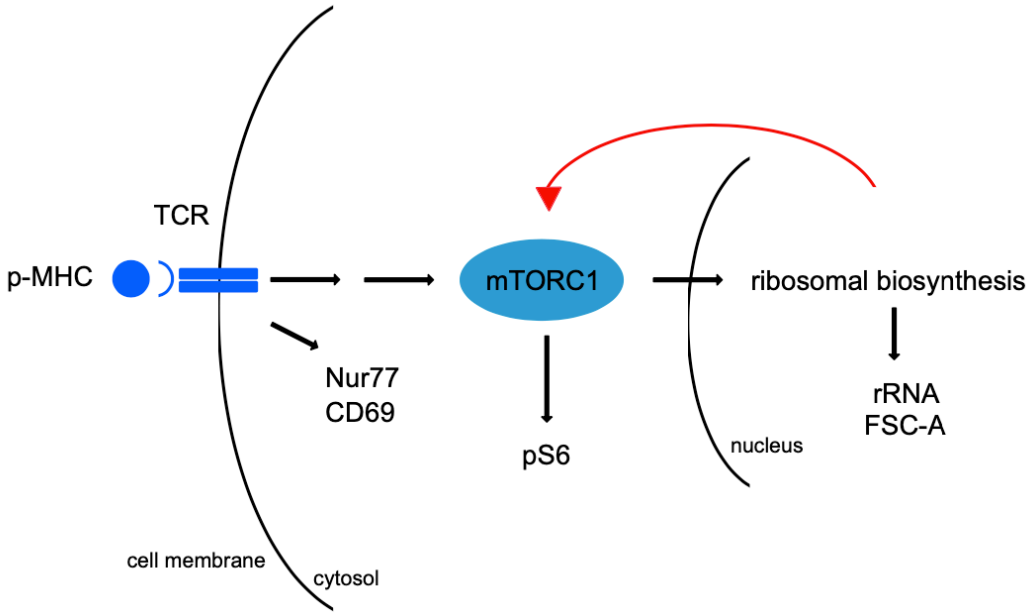

Figure 37: Summary of reciprocal regulation of mTORC1 and ribosomal biosynthesis.
mTORC1 signaling is induced directly by TCR signaling and in turn induces the phosphorylation of S6 ribosomal protein and activates ribosomal biosynthesis in the nucleolus, marked by an increase of ribosomal RNA and cell growth. Ribosomal biosynthesis gives feedback signals to mTORC1.

5. Outlook

This work shows that mTORC1 and RNA Pol I activities are co-regulated and mutually dependent to ensure proper activation, growth and proliferation throughout the expansion phase of T cells. However, there are still remaining questions to be addressed in the future.

One major question that remains is the mechanism how ribosomes regulate mTOR signaling. Therefore, Tif1a KO mice might give an idea. First experiments with Tif1a-deleted T cells appeared to die in the periphery and could not be detected by our common cell culture methods. As a solution, a Cre-retrovirus was tested to deplete Tif1a in an in vitro assay. Therefore Cre-negative Tif1a$^{fl/fl}$ T cells are stimulated in vitro and two days later infected with the virus, resulting in Tif-deletion in these cells within 6 hours. Proliferation rates and pS6 signaling can thus be analyzed the following day to show the feedback regulation of Tif1a to major cellular effectors as proliferation and signaling.

Besides this, cyclins and CDKs can be analyzed in the Tif1a KO T cells, as mTOR is known to downregulate some of these as described in chapter 1.5. Tif1a or RNA Pol I might have a direct impact on the expression levels of certain cyclins and CDKs and thus directly regulate cell cycle progression.

Another important factor during T cell activation as outlined in section 1.4.4 is the generation of nucleotides for rRNA synthesis. One has to consider that T-Rap$^{o/o}$ T cells might have a reduced proliferative capacity not due to a lack of nucleotide synthesis, but due to a downregulation of nucleotide transporters that transport the nucleotides inside the cell. By SLO experiments one could mimic the nucleotide transport into the cell and show whether lack of nutrients is responsible for the delayed cellular response.

Lastly, it remains still unknown how the downstream targets of mTORC1, S6K and 4EBP1, function and via which route the effects of mTORC1 signaling are transmitted. We started analyzing the role of S6K1 and 2 by different inhibitors and a mouse line with a complete S6K1/2 knockout. These experiments suggested that proliferation is not regulated by S6K. More experiments on the role of S6K1/2 have to be performed and can be done by combining knockout mice with specific inhibitors of S6K1 and 2.

Literature

Akondy, R.S., M. Fitch, S. Edupuganti, S. Yang, H.T. Kissick, K.W. Li, B.A. Youngblood, H.A. Abdelsamed, D.J. McGuire, K.W. Cohen, G. Alexe, S. Nagar, M.M. McCausland, S. Gupta, P. Tata, W.N. Haining, M.J. McElrath, D. Zhang, B. Hu, W.J. Greenleaf, J.J. Goronzy, M.J. Mulligan, M. Hellerstein, and R. Ahmed. 2017. Origin and differentiation of human memory CD8 T cells after vaccination. *Nature* 552:362-367.

Aleem, E., and R.J. Arceci. 2015. Targeting cell cycle regulators in hematologic malignancies. *Front Cell Dev Biol* 3:16.

Andersen, J.S., Y.W. Lam, A.K. Leung, S.E. Ong, C.E. Lyon, A.I. Lamond, and M. Mann. 2005. Nucleolar proteome dynamics. *Nature* 433:77-83.

Antony, C., S.S. George, J. Blum, P. Somers, C.L. Thorsheim, D.J. Wu-Corts, Y. Ai, L. Gao, K. Lv, M.G. Tremblay, T. Moss, K. Tan, J.E. Wilusz, A.R.D. Ganley, M. Pimkin, and V.R. Paralkar. 2022. Control of ribosomal RNA synthesis by hematopoietic transcription factors. *Mol Cell* 82:3826-3839 e3829.

Appleman, L.J., A. Berezovskaya, I. Grass, and V.A. Boussiotis. 2000. CD28 costimulation mediates T cell expansion via IL-2-independent and IL-2-dependent regulation of cell cycle progression. *J Immunol* 164:144-151.

Apsel, B., J.A. Blair, B. Gonzalez, T.M. Nazif, M.E. Feldman, B. Aizenstein, R. Hoffman, R.L. Williams, K.M. Shokat, and Z.A. Knight. 2008. Targeted polypharmacology: discovery of dual inhibitors of tyrosine and phosphoinositide kinases. *Nat Chem Biol* 4:691-699.

Araki, K., M. Morita, A.G. Bederman, B.T. Konieczny, H.T. Kissick, N. Sonenberg, and R. Ahmed. 2017. Translation is actively regulated during the differentiation of $CD8^+$ effector T cells. *Nat Immunol* 18:1046-1057.

Araki, K., A.P. Turner, V.O. Shaffer, S. Gangappa, S.A. Keller, M.F. Bachmann, C.P. Larsen, and R. Ahmed. 2009. mTOR regulates memory CD8 T-cell differentiation. *Nature* 460:108-112.

Ashouri, J.F., and A. Weiss. 2017. Endogenous Nur77 is a specific indicator of antigen receptor signaling in human T and B cells. *J Immunol* 198:657-668.

Austin, W.R., A.L. Armijo, D.O. Campbell, A.S. Singh, T. Hsieh, D. Nathanson, H.R. Herschman, M.E. Phelps, O.N. Witte, J. Czernin, and C.G. Radu. 2012. Nucleoside salvage pathway kinases regulate hematopoiesis by linking nucleotide metabolism with replication stress. *J Exp Med* 209:2215-2228.

Barber, D.L., E.J. Wherry, and R. Ahmed. 2003. Cutting edge: rapid in vivo killing by memory CD8 T cells. *J Immunol* 171:27-31.

Barlow, J.L., L.F. Drynan, D.R. Hewett, L.R. Holmes, S. Lorenzo-Abalde, A.L. Lane, H.E. Jolin, R. Pannell, A.J. Middleton, S.H. Wong, A.J. Warren, J.S. Wainscoat, J. Boultwood, and A.N. McKenzie. 2010. A p53-dependent mechanism underlies macrocytic anemia in a mouse model of human 5q- syndrome. *Nat Med* 16:59-66.

Battaglioni, S., D. Benjamin, M. Walchli, T. Maier, and M.N. Hall. 2022. mTOR substrate phosphorylation in growth control. *Cell* 185:1814-1836.

Beach, D., R. Gonen, Y. Bogin, I.G. Reischl, and D. Yablonski. 2007. Dual role of SLP-76 in mediating T cell receptor-induced activation of phospholipase C-gamma1. *J Biol Chem* 282:2937-2946.

Ben-Sahra, I., J.J. Howell, J.M. Asara, and B.D. Manning. 2013. Stimulation of de novo pyrimidine synthesis by growth signaling through mTOR and S6K1. *Science* 339:1323-1328.

Ben-Sahra, I., G. Hoxhaj, S.J.H. Ricoult, J.M. Asara, and B.D. Manning. 2016. mTORC1 induces purine synthesis through control of the mitochondrial tetrahydrofolate cycle. *Science* 351:728-733.

Ben-Sahra, I., and B.D. Manning. 2017. mTORC1 signaling and the metabolic control of cell growth. *Curr Opin Cell Biol* 45:72-82.

Benjamin, D., M. Colombi, C. Moroni, and M.N. Hall. 2011. Rapamycin passes the torch: a new generation of mTOR inhibitors. *Nat Rev Drug Discov* 10:868-880.

Bensaude, O. 2011. Inhibiting eukaryotic transcription: Which compound to choose? How to evaluate its activity? *Transcription* 2:103-108.

Berridge, M.J. 2009. Inositol trisphosphate and calcium signalling mechanisms. *Biochim Biophys Acta* 1793:933-940.

Bertin, S., B. Lozano-Ruiz, V. Bachiller, I. Garcia-Martinez, S. Herdman, P. Zapater, R. Frances, J. Such, J. Lee, E. Raz, and J.M. Gonzalez-Navajas. 2015. Dual-specificity phosphatase 6 regulates $CD4^+$ T-cell functions and restrains spontaneous colitis in IL-10-deficient mice. *Mucosal Immunol* 8:505-515.

Bodem, J., G. Dobreva, U. Hoffmann-Rohrer, S. Iben, H. Zentgraf, H. Delius, M. Vingron, and I. Grummt. 2000. TIF-IA, the factor mediating growth-dependent control of ribosomal RNA synthesis, is the mammalian homolog of yeast Rrn3p. *EMBO Rep* 1:171-175.

Boisvert, F.M., S. van Koningsbruggen, J. Navascues, and A.I. Lamond. 2007. The multifunctional nucleolus. *Nat Rev Mol Cell Biol* 8:574-585.

Bossaert, M., A. Pipier, J.F. Riou, C. Noirot, L.T. Nguyen, R.F. Serre, O. Bouchez, E. Defrancq, P. Calsou, S. Britton, and D. Gomez. 2021. Transcription-associated topoisomerase 2alpha (TOP2A) activity is a major effector of cytotoxicity induced by G-quadruplex ligands. *Elife* 10:

Boulon, S., B.J. Westman, S. Hutten, F.M. Boisvert, and A.I. Lamond. 2010. The nucleolus under stress. *Mol Cell* 40:216-227.

Boussiotis, V.A., G.J. Freeman, P.A. Taylor, A. Berezovskaya, I. Grass, B.R. Blazar, and L.M. Nadler. 2000. p27kip1 functions as an anergy factor inhibiting interleukin 2 transcription and clonal expansion of alloreactive human and mouse helper T lymphocytes. *Nat Med* 6:290-297.

Boyman, O., and J. Sprent. 2012. The role of interleukin-2 during homeostasis and activation of the immune system. *Nat Rev Immunol* 12:180-190.

Brown, E.J., M.W. Albers, T.B. Shin, K. Ichikawa, C.T. Keith, W.S. Lane, and S.L. Schreiber. 1994. A mammalian protein targeted by G1-arresting rapamycin-receptor complex. *Nature* 369:756-758.

Brugarolas, J.B., F. Vazquez, A. Reddy, W.R. Sellers, and W.G. Kaelin, Jr. 2003. TSC2 regulates VEGF through mTOR-dependent and -independent pathways. *Cancer Cell* 4:147-158.

Bruno, P.M., M. Lu, K.A. Dennis, H. Inam, C.J. Moore, J. Sheehe, S.J. Elledge, M.T. Hemann, and J.R. Pritchard. 2020. The primary mechanism of cytotoxicity of the chemotherapeutic agent CX-5461 is topoisomerase II poisoning. *Proc Natl Acad Sci U S A* 117:4053-4060.

Budde, A., and I. Grummt. 1999. p53 represses ribosomal gene transcription. *Oncogene* 18:1119-1124.

Burger, K., B. Muhl, T. Harasim, M. Rohrmoser, A. Malamoussi, M. Orban, M. Kellner, A. Gruber-Eber, E. Kremmer, M. Holzel, and D. Eick. 2010. Chemotherapeutic drugs inhibit ribosome biogenesis at various levels. *J Biol Chem* 285:12416-12425.

Cafferkey, R., P.R. Young, M.M. McLaughlin, D.J. Bergsma, Y. Koltin, G.M. Sathe, L. Faucette, W.K. Eng, R.K. Johnson, and G.P. Livi. 1993. Dominant missense mutations in a novel yeast protein related to mammalian phosphatidylinositol 3-kinase and VPS34 abrogate rapamycin cytotoxicity. *Mol Cell Biol* 13:6012-6023.

Cantrell, D.A. 2002. T-cell antigen receptor signal transduction. *Immunology* 105:369-374.

Carrio, R., O.F. Bathe, and T.R. Malek. 2004. Initial antigen encounter programs $CD8^+$ T cells competent to develop into memory cells that are activated in an antigen-free, IL-7- and IL-15-rich environment. *J Immunol* 172:7315-7323.

Chakraborty, A.K., and A. Weiss. 2014. Insights into the initiation of TCR signaling. *Nat Immunol* 15:798-807.

Chan, P.K., D.A. Bloom, and T.T. Hoang. 1999. The N-terminal half of NPM dissociates from nucleoli of HeLa cells after anticancer drug treatments. *Biochem Biophys Res Commun* 264:305-309.

Chaplin, D.D. 2010. Overview of the immune response. *J Allergy Clin Immunol* 125:S3-23.

Chapman, N.M., and H. Chi. 2018. Hallmarks of T-cell Exit from Quiescence. *Cancer Immunol Res* 6:502-508.

Chi, H. 2012. Regulation and function of mTOR signalling in T cell fate decisions. *Nat Rev Immunol* 12:325-338.

Choesmel, V., D. Bacqueville, J. Rouquette, J. Noaillac-Depeyre, S. Fribourg, A. Cretien, T. Leblanc, G. Tchernia, L. Da Costa, and P.E. Gleizes. 2007. Impaired ribosome biogenesis in Diamond-Blackfan anemia. *Blood* 109:1275-1283.

Choo, A.Y., S.O. Yoon, S.G. Kim, P.P. Roux, and J. Blenis. 2008. Rapamycin differentially inhibits S6Ks and 4E-BP1 to mediate cell-type-specific repression of mRNA translation. *Proc Natl Acad Sci U S A* 105:17414-17419.

Chunder, N., L. Wang, C. Chen, W.W. Hancock, and A.D. Wells. 2012. Cyclin-dependent kinase 2 controls peripheral immune tolerance. *J Immunol* 189:5659-5666.

Claiborne, M.D., S. Sengupta, L. Zhao, M.L. Arwood, I.M. Sun, J. Wen, E.A. Thompson, M. Mitchell-Flack, M. Laiho, and J.D. Powell. 2022. Persistent CAD activity in memory $CD8^+$ T cells supports rRNA synthesis and ribosomal biogenesis required at rechallenge. *Sci Immunol* 7:eabh4271.

Colis, L., K. Peltonen, P. Sirajuddin, H. Liu, S. Sanders, G. Ernst, J.C. Barrow, and M. Laiho. 2014. DNA intercalator BMH-21 inhibits RNA polymerase I independent of DNA damage response. *Oncotarget* 5:4361-4369.

Colombo, E., J.C. Marine, D. Danovi, B. Falini, and P.G. Pelicci. 2002. Nucleophosmin regulates the stability and transcriptional activity of p53. *Nat Cell Biol* 4:529-533.

Copp, J., G. Manning, and T. Hunter. 2009. TORC-specific phosphorylation of mammalian target of rapamycin (mTOR): phospho-Ser2481 is a marker for intact mTOR signaling complex 2. *Cancer Res* 69:1821-1827.

Dai, M.S., R. Sears, and H. Lu. 2007. Feedback regulation of c-Myc by ribosomal protein L11. *Cell Cycle* 6:2735-2741.

Damoiseaux, J. 2020. The IL-2 - IL-2 receptor pathway in health and disease: The role of the soluble IL-2 receptor. *Clin Immunol* 218:108515.

Danilova, N., and H.T. Gazda. 2015. Ribosomopathies: how a common root can cause a tree of pathologies. *Dis Model Mech* 8:1013-1026.

Danilova, N., K.M. Sakamoto, and S. Lin. 2008. Ribosomal protein S19 deficiency in zebrafish leads to developmental abnormalities and defective erythropoiesis through activation of p53 protein family. *Blood* 112:5228-5237.

Darzynkiewicz, Z., V.K. Dokov, and M. Pienkowski. 1967. Dry mass of lymphocytes during transformation after stimulation by phytohaemagglutinin. *Nature* 214:1265-1266.

Darzynkiewicz, Z., G. Juan, and E.F. Srour. 2004. Differential staining of DNA and RNA. *Curr Protoc Cytom* Chapter 7:Unit 7 3.

de la Fuente, M.A., M. Recher, N.L. Rider, K.A. Strauss, D.H. Morton, M. Adair, F.A. Bonilla, H.D. Ochs, E.W. Gelfand, I.M. Pessach, J.E. Walter, A. King, S. Giliani, S.Y. Pai, and L.D. Notarangelo. 2011. Reduced thymic output, cell cycle abnormalities, and increased apoptosis of T lymphocytes in patients with cartilage-hair hypoplasia. *J Allergy Clin Immunol* 128:139-146.

Delarue, M., G.P. Brittingham, S. Pfeffer, I.V. Surovtsev, S. Pinglay, K.J. Kennedy, M. Schaffer, J.I. Gutierrez, D. Sang, G. Poterewicz, J.K. Chung, J.M. Plitzko, J.T. Groves, C. Jacobs-Wagner, B.D. Engel, and L.J. Holt. 2018. mTORC1 Controls Phase Separation and the Biophysical Properties of the Cytoplasm by Tuning Crowding. *Cell* 174:338-349 e320.

Delgoffe, G.M., T.P. Kole, Y. Zheng, P.E. Zarek, K.L. Matthews, B. Xiao, P.F. Worley, S.C. Kozma, and J.D. Powell. 2009. The mTOR kinase differentially regulates effector and regulatory T cell lineage commitment. *Immunity* 30:832-844.

Delgoffe, G.M., K.N. Pollizzi, A.T. Waickman, E. Heikamp, D.J. Meyers, M.R. Horton, B. Xiao, P.F. Worley, and J.D. Powell. 2011. The kinase mTOR regulates the differentiation of helper T cells through the selective activation of signaling by mTORC1 and mTORC2. *Nat Immunol* 12:295-303.

Derenzini, M., L. Montanaro, and D. Trere. 2009. What the nucleolus says to a tumour pathologist. *Histopathology* 54:753-762.

Drygin, D., W.G. Rice, and I. Grummt. 2010. The RNA polymerase I transcription machinery: an emerging target for the treatment of cancer. *Annu Rev Pharmacol Toxicol* 50:131-156.

Drygin, D., A. Siddiqui-Jain, S. O'Brien, M. Schwaebe, A. Lin, J. Bliesath, C.B. Ho, C. Proffitt, K. Trent, J.P. Whitten, J.K. Lim, D. Von Hoff, K. Anderes, and W.G. Rice. 2009. Anticancer activity of CX-3543: a direct inhibitor of rRNA biogenesis. *Cancer Res* 69:7653-7661.

Duquette, M.L., P. Handa, J.A. Vincent, A.F. Taylor, and N. Maizels. 2004. Intracellular transcription of G-rich DNAs induces formation of G-loops, novel structures containing G4 DNA. *Genes Dev* 18:1618-1629.

Duvel, K., J.L. Yecies, S. Menon, P. Raman, A.I. Lipovsky, A.L. Souza, E. Triantafellow, Q. Ma, R. Gorski, S. Cleaver, M.G. Vander Heiden, J.P. MacKeigan, P.M. Finan, C.B. Clish, L.O. Murphy, and B.D. Manning. 2010. Activation of a metabolic gene regulatory network downstream of mTOR complex 1. *Mol Cell* 39:171-183.

Ebinu, J.O., D.A. Bottorff, E.Y. Chan, S.L. Stang, R.J. Dunn, and J.C. Stone. 1998. RasGRP, a Ras guanyl nucleotide-releasing protein with calcium- and diacylglycerol-binding motifs. *Science* 280:1082-1086.

el-Deiry, W.S., J.W. Harper, P.M. O'Connor, V.E. Velculescu, C.E. Canman, J. Jackman, J.A. Pietenpol, M. Burrell, D.E. Hill, Y. Wang, and et al. 1994. WAF1/CIP1 is induced in p53-mediated G1 arrest and apoptosis. *Cancer Res* 54:1169-1174.

ElTanbouly, M.A., and R.J. Noelle. 2021. Rethinking peripheral T cell tolerance: checkpoints across a T cell's journey. *Nat Rev Immunol* 21:257-267.

Ersching, J., A. Efeyan, L. Mesin, J.T. Jacobsen, G. Pasqual, B.C. Grabiner, D. Dominguez-Sola, D.M. Sabatini, and G.D. Victora. 2017. Germinal center selection and affinity maturation require dynamic regulation of mTORC1 kinase. *Immunity* 46:1045-1058 e1046.

Farley, K.I., Y. Surovtseva, J. Merkel, and S.J. Baserga. 2015. Determinants of mammalian nucleolar architecture. *Chromosoma* 124:323-331.

Feldman, M.E., B. Apsel, A. Uotila, R. Loewith, Z.A. Knight, D. Ruggero, and K.M. Shokat. 2009. Active-site inhibitors of mTOR target rapamycin-resistant outputs of mTORC1 and mTORC2. *PLoS Biol* 7:e38.

Ferrer, I.R., M.E. Wagener, J.M. Robertson, A.P. Turner, K. Araki, R. Ahmed, A.D. Kirk, C.P. Larsen, and M.L. Ford. 2010. Cutting edge: Rapamycin augments pathogen-specific but not graft-reactive $CD8^+$ T cell responses. *J Immunol* 185:2004-2008.

Fields, P.E., T.F. Gajewski, and F.W. Fitch. 1996. Blocked Ras activation in anergic $CD4^+$ T cells. *Science* 271:1276-1278.

Finlay, B.B., and G. McFadden. 2006. Anti-immunology: evasion of the host immune system by bacterial and viral pathogens. *Cell* 124:767-782.

Flanagan, M.E., T.A. Blumenkopf, W.H. Brissette, M.F. Brown, J.M. Casavant, C. Shang-Poa, J.L. Doty, E.A. Elliott, M.B. Fisher, M. Hines, C. Kent, E.M. Kudlacz, B.M. Lillie, K.S. Magnuson, S.P. McCurdy, M.J. Munchhof, B.D. Perry, P.S. Sawyer, T.J. Strelevitz, C. Subramanyam, J. Sun, D.A. Whipple, and P.S. Changelian. 2010. Discovery of CP-690,550: a potent and selective Janus kinase (JAK) inhibitor for the treatment of autoimmune diseases and organ transplant rejection. *J Med Chem* 53:8468-8484.

Flanagan, W.M., B. Corthesy, R.J. Bram, and G.R. Crabtree. 1991. Nuclear association of a T-cell transcription factor blocked by FK-506 and cyclosporin A. *Nature* 352:803-807.

Folkes, A.J., K. Ahmadi, W.K. Alderton, S. Alix, S.J. Baker, G. Box, I.S. Chuckowree, P.A. Clarke, P. Depledge, S.A. Eccles, L.S. Friedman, A. Hayes, T.C. Hancox, A. Kugendradas, L. Lensun, P. Moore, A.G. Olivero, J. Pang, S. Patel, G.H. Pergl-Wilson, F.I. Raynaud, A. Robson, N. Saghir, L. Salphati, S. Sohal, M.H. Ultsch, M. Valenti, H.J. Wallweber, N.C. Wan, C. Wiesmann, P. Workman, A. Zhyvoloup, M.J. Zvelebil, and S.J. Shuttleworth. 2008. The identification of 2-(1H-indazol-4-yl)-6-(4-methanesulfonyl-piperazin-1-ylmethyl)-4-morpholin-4-yl-thieno[3,2-d]pyrimidine (GDC-0941) as a potent, selective, orally bioavailable inhibitor of class I PI3 kinase for the treatment of cancer. *J Med Chem* 51:5522-5532.

French, S.L., Y.N. Osheim, F. Cioci, M. Nomura, and A.L. Beyer. 2003. In exponentially growing Saccharomyces cerevisiae cells, rRNA synthesis is determined by the summed RNA polymerase I loading rate rather than by the number of active genes. *Mol Cell Biol* 23:1558-1568.

Frias, M.A., C.C. Thoreen, J.D. Jaffe, W. Schroder, T. Sculley, S.A. Carr, and D.M. Sabatini. 2006. mSin1 is necessary for Akt/PKB phosphorylation, and its isoforms define three distinct mTORC2s. *Curr Biol* 16:1865-1870.

Frottin, F., F. Schueder, S. Tiwary, R. Gupta, R. Korner, T. Schlichthaerle, J. Cox, R. Jungmann, F.U. Hartl, and M.S. Hipp. 2019. The nucleolus functions as a phase-separated protein quality control compartment. *Science* 365:342-347.

Fumagalli, S., and M. Pende. 2022. S6 kinase 1 at the central node of cell size and ageing. *Front Cell Dev Biol* 10:949196.

Fumagalli, S., and G. Thomas. 2011. The role of p53 in ribosomopathies. *Semin Hematol* 48:97-105.

Furumoto, Y., and M. Gadina. 2013. The arrival of JAK inhibitors: advancing the treatment of immune and hematologic disorders. *BioDrugs* 27:431-438.

Garcia-Martinez, J.M., and D.R. Alessi. 2008. mTOR complex 2 (mTORC2) controls hydrophobic motif phosphorylation and activation of serum- and glucocorticoid-induced protein kinase 1 (SGK1). *Biochem J* 416:375-385.

Gorentla, B.K., and X.P. Zhong. 2012. T cell receptor signal transduction in T lymphocytes. *J Clin Cell Immunol* 2012:5.

Gowans, J.L., G.D. Mc, and D.M. Cowen. 1962. Initiation of immune responses by small lymphocytes. *Nature* 196:651-655.

Grummt, I. 2003. Life on a planet of its own: regulation of RNA polymerase I transcription in the nucleolus. *Genes Dev* 17:1691-1702.

Grummt, I. 2013. The nucleolus-guardian of cellular homeostasis and genome integrity. *Chromosoma* 122:487-497.

Grummt, I., and G. Langst. 2013. Epigenetic control of RNA polymerase I transcription in mammalian cells. *Biochim Biophys Acta* 1829:393-404.

Gubser, P.M., G.R. Bantug, L. Razik, M. Fischer, S. Dimeloe, G. Hoenger, B. Durovic, A. Jauch, and C. Hess. 2013. Rapid effector function of memory $CD8^+$ T cells requires an immediate-early glycolytic switch. *Nat Immunol* 14:1064-1072.

Guo, W., S. Schubbert, J.Y. Chen, B. Valamehr, S. Mosessian, H. Shi, N.H. Dang, C. Garcia, M.F. Theodoro, M. Varella-Garcia, and H. Wu. 2011. Suppression of leukemia development caused by PTEN loss. *Proc Natl Acad Sci U S A* 108:1409-1414.

Halperin, D.S., and M.H. Freedman. 1989. Diamond-blackfan anemia: etiology, pathophysiology, and treatment. *Am J Pediatr Hematol Oncol* 11:380-394.

Hamperl, S., M. Wittner, V. Babl, J. Perez-Fernandez, H. Tschochner, and J. Griesenbeck. 2013. Chromatin states at ribosomal DNA loci. *Biochim Biophys Acta* 1829:405-417.

Hans, F., and S. Dimitrov. 2001. Histone H3 phosphorylation and cell division. *Oncogene* 20:3021-3027.

Hara, K., Y. Maruki, X. Long, K. Yoshino, N. Oshiro, S. Hidayat, C. Tokunaga, J. Avruch, and K. Yonezawa. 2002. Raptor, a binding partner of target of rapamycin (TOR), mediates TOR action. *Cell* 110:177-189.

Hayden, M.S., A.P. West, and S. Ghosh. 2006. NF-kappaB and the immune response. *Oncogene* 25:6758-6780.

Hein, N., K.M. Hannan, A.J. George, E. Sanij, and R.D. Hannan. 2013. The nucleolus: an emerging target for cancer therapy. *Trends Mol Med* 19:643-654.

Henras, A.K., C. Plisson-Chastang, M.F. O'Donohue, A. Chakraborty, and P.E. Gleizes. 2015. An overview of pre-ribosomal RNA processing in eukaryotes. *Wiley Interdiscip Rev RNA* 6:225-242.

Hernandez, R., J. Poder, K.M. LaPorte, and T.R. Malek. 2022. Engineering IL-2 for immunotherapy of autoimmunity and cancer. *Nat Rev Immunol* 22:614-628.

Hernandez-Verdun, D., P. Roussel, M. Thiry, V. Sirri, and D.L. Lafontaine. 2010. The nucleolus: structure/function relationship in RNA metabolism. *Wiley Interdiscip Rev RNA* 1:415-431.

Hilton, J., K. Gelmon, P.L. Bedard, D. Tu, H. Xu, A.V. Tinker, R. Goodwin, S.A. Laurie, D. Jonker, A.R. Hansen, Z.W. Veitch, D.J. Renouf, L. Hagerman, H. Lui, B. Chen, D. Kellar, I. Li, S.E. Lee, T. Kono, B.Y.C. Cheng, D. Yap, D. Lai, S. Beatty, J. Soong, K.I. Pritchard, I. Soria-Bretones, E. Chen, H. Feilotter, M. Rushton, L. Seymour, S. Aparicio, and D.W. Cescon. 2022. Results of the phase I CCTG IND.231 trial of CX-5461 in patients with advanced solid tumors enriched for DNA-repair deficiencies. *Nat Commun* 13:3607.

Hoeflich, K.P., M. Merchant, C. Orr, J. Chan, D. Den Otter, L. Berry, I. Kasman, H. Koeppen, K. Rice, N.Y. Yang, S. Engst, S. Johnston, L.S. Friedman, and M. Belvin. 2012. Intermittent administration of MEK inhibitor GDC-0973 plus PI3K inhibitor GDC-0941 triggers robust apoptosis and tumor growth inhibition. *Cancer Res* 72:210-219.

Hoffmann, A., G. Natoli, and G. Ghosh. 2006. Transcriptional regulation via the NF-kappaB signaling module. *Oncogene* 25:6706-6716.

Hogquist, K.A., S.C. Jameson, W.R. Heath, J.L. Howard, M.J. Bevan, and F.R. Carbone. 1994. T cell receptor antagonist peptides induce positive selection. *Cell* 76:17-27.

Howden, A.J.M., J.L. Hukelmann, A. Brenes, L. Spinelli, L.V. Sinclair, A.I. Lamond, and D.A. Cantrell. 2019. Quantitative analysis of T cell proteomes and environmental sensors during T cell differentiation. *Nat Immunol* 20:1542-1554.

Hsieh, A.C., M. Costa, O. Zollo, C. Davis, M.E. Feldman, J.R. Testa, O. Meyuhas, K.M. Shokat, and D. Ruggero. 2010. Genetic dissection of the oncogenic mTOR pathway reveals druggable addiction to translational control via 4EBP-eIF4E. *Cancer Cell* 17:249-261.

Hudson, C.C., M. Liu, G.G. Chiang, D.M. Otterness, D.C. Loomis, F. Kaper, A.J. Giaccia, and R.T. Abraham. 2002. Regulation of hypoxia-inducible factor 1alpha expression and function by the mammalian target of rapamycin. *Mol Cell Biol* 22:7004-7014.

Hukelmann, J.L., K.E. Anderson, L.V. Sinclair, K.M. Grzes, A.B. Murillo, P.T. Hawkins, L.R. Stephens, A.I. Lamond, and D.A. Cantrell. 2016. The cytotoxic T cell proteome and its shaping by the kinase mTOR. *Nat Immunol* 17:104-112.

Iadevaia, V., R. Liu, and C.G. Proud. 2014. mTORC1 signaling controls multiple steps in ribosome biogenesis. *Semin Cell Dev Biol* 36:113-120.

Iadevaia, V., Z. Zhang, E. Jan, and C.G. Proud. 2012. mTOR signaling regulates the processing of pre-rRNA in human cells. *Nucleic Acids Res* 40:2527-2539.

Inoki, K., Y. Li, T. Xu, and K.L. Guan. 2003. Rheb GTPase is a direct target of TSC2 GAP activity and regulates mTOR signaling. *Genes Dev* 17:1829-1834.

Ishikawa, H. 1999. Mizoribine and mycophenolate mofetil. *Curr Med Chem* 6:575-597.

Iyer-Bierhoff, A., and I. Grummt. 2019. Stop-and-Go: Dynamics of nucleolar transcription during the cell cycle. *Epigenet Insights* 12:2516865719849090.

Jaako, P., J. Flygare, K. Olsson, R. Quere, M. Ehinger, A. Henson, S. Ellis, A. Schambach, C. Baum, J. Richter, J. Larsson, D. Bryder, and S. Karlsson. 2011. Mice with ribosomal protein S19 deficiency develop bone marrow failure and symptoms like patients with Diamond-Blackfan anemia. *Blood* 118:6087-6096.

Jacinto, E., V. Facchinetti, D. Liu, N. Soto, S. Wei, S.Y. Jung, Q. Huang, J. Qin, and B. Su. 2006. SIN1/MIP1 maintains rictor-mTOR complex integrity and regulates Akt phosphorylation and substrate specificity. *Cell* 127:125-137.

Jacinto, E., R. Loewith, A. Schmidt, S. Lin, M.A. Ruegg, A. Hall, and M.N. Hall. 2004. Mammalian TOR complex 2 controls the actin cytoskeleton and is rapamycin insensitive. *Nat Cell Biol* 6:1122-1128.

Janes, M.R., J.J. Limon, L. So, J. Chen, R.J. Lim, M.A. Chavez, C. Vu, M.B. Lilly, S. Mallya, S.T. Ong, M. Konopleva, M.B. Martin, P. Ren, Y. Liu, C. Rommel, and D.A. Fruman. 2010. Effective and selective targeting of leukemia cells using a TORC1/2 kinase inhibitor. *Nat Med* 16:205-213.

Janknecht, R., W.H. Ernst, V. Pingoud, and A. Nordheim. 1993. Activation of ternary complex factor Elk-1 by MAP kinases. *EMBO J* 12:5097-5104.

Jin, R., and W. Zhou. 2016. TIF-IA: An oncogenic target of pre-ribosomal RNA synthesis. *Biochim Biophys Acta* 1866:189-196.

Jorgensen, P., and M. Tyers. 2004. How cells coordinate growth and division. *Curr Biol* 14:R1014-1027.

Kaizuka, T., T. Hara, N. Oshiro, U. Kikkawa, K. Yonezawa, K. Takehana, S. Iemura, T. Natsume, and N. Mizushima. 2010. Tti1 and Tel2 are critical factors in mammalian target of rapamycin complex assembly. *J Biol Chem* 285:20109-20116.

Kalia, V., S. Sarkar, S. Subramaniam, W.N. Haining, K.A. Smith, and R. Ahmed. 2010. Prolonged interleukin-2Ralpha expression on virus-specific $CD8^+$ T cells favors terminal-effector differentiation in vivo. *Immunity* 32:91-103.

Kaminuma, O., M. Deckert, C. Elly, Y.C. Liu, and A. Altman. 2001. Vav-Rac1-mediated activation of the c-Jun N-terminal kinase/c-Jun/AP-1 pathway plays a major role in stimulation of the distal NFAT site in the interleukin-2 gene promoter. *Mol Cell Biol* 21:3126-3136.

Kang, S.M., B. Beverly, A.C. Tran, K. Brorson, R.H. Schwartz, and M.J. Lenardo. 1992. Transactivation by AP-1 is a molecular target of T cell clonal anergy. *Science* 257:1134-1138.

Kantidakis, T., B.A. Ramsbottom, J.L. Birch, S.N. Dowding, and R.J. White. 2010. mTOR associates with TFIIIC, is found at tRNA and 5S rRNA genes, and targets their repressor Maf1. *Proc Natl Acad Sci U S A* 107:11823-11828.

Kaye, J., M.L. Hsu, M.E. Sauron, S.C. Jameson, N.R. Gascoigne, and S.M. Hedrick. 1989. Selective development of $CD4^+$ T cells in transgenic mice expressing a class II MHC-restricted antigen receptor. *Nature* 341:746-749.

Khajuria, R.K., M. Munschauer, J.C. Ulirsch, C. Fiorini, L.S. Ludwig, S.K. McFarland, N.J. Abdulhay, H. Specht, H. Keshishian, D.R. Mani, M. Jovanovic, S.R. Ellis, C.P. Fulco, J.M. Engreitz, S. Schutz, J. Lian, K.W. Gripp, O.K. Weinberg, G.S. Pinkus, L. Gehrke, A. Regev, E.S. Lander, H.T. Gazda, W.Y. Lee, V.G. Panse, S.A. Carr, and V.G. Sankaran. 2018. Ribosome levels selectively regulate translation and lineage commitment in human hematopoiesis. *Cell* 173:90-103 e119.

Kim, D.H., D.D. Sarbassov, S.M. Ali, J.E. King, R.R. Latek, H. Erdjument-Bromage, P. Tempst, and D.M. Sabatini. 2002. mTOR interacts with raptor to form a nutrient-sensitive complex that signals to the cell growth machinery. *Cell* 110:163-175.

Kim, D.H., D.D. Sarbassov, S.M. Ali, R.R. Latek, K.V. Guntur, H. Erdjument-Bromage, P. Tempst, and D.M. Sabatini. 2003. GbetaL, a positive regulator of the rapamycin-sensitive pathway required for the nutrient-sensitive interaction between raptor and mTOR. *Mol Cell* 11:895-904.

Klein, J., and I. Grummt. 1999. Cell cycle-dependent regulation of RNA polymerase I transcription: the nucleolar transcription factor UBF is inactive in mitosis and early G1. *Proc Natl Acad Sci U S A* 96:6096-6101.

Klein, L., B. Kyewski, P.M. Allen, and K.A. Hogquist. 2014. Positive and negative selection of the T cell repertoire: what thymocytes see (and don't see). *Nat Rev Immunol* 14:377-391.

Klinge, S., and J.L. Woolford, Jr. 2019. Ribosome assembly coming into focus. *Nat Rev Mol Cell Biol* 20:116-131.

Kolch, W. 2005. Coordinating ERK/MAPK signalling through scaffolds and inhibitors. *Nat Rev Mol Cell Biol* 6:827-837.

Kostjukovits, S., P. Klemetti, H. Valta, T. Martelius, L.D. Notarangelo, M. Seppanen, M. Taskinen, and O. Makitie. 2017. Analysis of clinical and immunologic phenotype in a large cohort of children and adults with cartilage-hair hypoplasia. *J Allergy Clin Immunol* 140:612-614 e615.

Kunz, J., R. Henriquez, U. Schneider, M. Deuter-Reinhard, N.R. Movva, and M.N. Hall. 1993. Target of rapamycin in yeast, TOR2, is an essential phosphatidylinositol kinase homolog required for G1 progression. *Cell* 73:585-596.

Kurki, S., K. Peltonen, L. Latonen, T.M. Kiviharju, P.M. Ojala, D. Meek, and M. Laiho. 2004. Nucleolar protein NPM interacts with HDM2 and protects tumor suppressor protein p53 from HDM2-mediated degradation. *Cancer Cell* 5:465-475.

Lalvani, A., R. Brookes, S. Hambleton, W.J. Britton, A.V. Hill, and A.J. McMichael. 1997. Rapid effector function in $CD8^+$ memory T cells. *J Exp Med* 186:859-865.

Laplante, M., and D.M. Sabatini. 2009. An emerging role of mTOR in lipid biosynthesis. *Curr Biol* 19:R1046-1052.

Laplante, M., and D.M. Sabatini. 2012. mTOR signaling in growth control and disease. *Cell* 149:274-293.

Laughner, E., P. Taghavi, K. Chiles, P.C. Mahon, and G.L. Semenza. 2001. HER2 (neu) signaling increases the rate of hypoxia-inducible factor 1alpha (HIF-1alpha) synthesis: novel mechanism for HIF-1-mediated vascular endothelial growth factor expression. *Mol Cell Biol* 21:3995-4004.

Lee, P.P., D.R. Fitzpatrick, C. Beard, H.K. Jessup, S. Lehar, K.W. Makar, M. Perez-Melgosa, M.T. Sweetser, M.S. Schlissel, S. Nguyen, S.R. Cherry, J.H. Tsai, S.M. Tucker, W.M. Weaver, A. Kelso, R. Jaenisch, and C.B. Wilson. 2001. A critical role for Dnmt1 and DNA methylation in T cell development, function, and survival. *Immunity* 15:763-774.

Li, H., C.K. Tsang, M. Watkins, P.G. Bertram, and X.F. Zheng. 2006. Nutrient regulates Tor1 nuclear localization and association with rDNA promoter. *Nature* 442:1058-1061.

Li, Q., R.R. Rao, K. Araki, K. Pollizzi, K. Odunsi, J.D. Powell, and P.A. Shrikant. 2011a. A central role for mTOR kinase in homeostatic proliferation induced $CD8^+$ T cell memory and tumor immunity. *Immunity* 34:541-553.

Li, S., M.S. Brown, and J.L. Goldstein. 2010. Bifurcation of insulin signaling pathway in rat liver: mTORC1 required for stimulation of lipogenesis, but not inhibition of gluconeogenesis. *Proc Natl Acad Sci U S A* 107:3441-3446.

Li, S., W. Ogawa, A. Emi, K. Hayashi, Y. Senga, K. Nomura, K. Hara, D. Yu, and M. Kasuga. 2011b. Role of S6K1 in regulation of SREBP1c expression in the liver. *Biochem Biophys Res Commun* 412:197-202.

Li, W., C.D. Whaley, A. Mondino, and D.L. Mueller. 1996. Blocked signal transduction to the ERK and JNK protein kinases in anergic $CD4^+$ T cells. *Science* 271:1272-1276.

Liao, W., J.X. Lin, and W.J. Leonard. 2013. Interleukin-2 at the crossroads of effector responses, tolerance, and immunotherapy. *Immunity* 38:13-25.

Lin, C.Y., J. Loven, P.B. Rahl, R.M. Paranal, C.B. Burge, J.E. Bradner, T.I. Lee, and R.A. Young. 2012. Transcriptional amplification in tumor cells with elevated c-Myc. *Cell* 151:56-67.

Liu, J., J.D. Farmer, Jr., W.S. Lane, J. Friedman, I. Weissman, and S.L. Schreiber. 1991. Calcineurin is a common target of cyclophilin-cyclosporin A and FKBP-FK506 complexes. *Cell* 66:807-815.

Liu, M., J. Zhang, B.D. Pinder, Q. Liu, D. Wang, H. Yao, Y. Gao, A. Toker, J. Gao, A. Peterson, J. Qu, and K.A. Siminovitch. 2021. WAVE2 suppresses mTOR activation to maintain T cell homeostasis and prevent autoimmunity. *Science* 371:

Livermore, D.M. 2005. Tigecycline: what is it, and where should it be used? *J Antimicrob Chemother* 56:611-614.

Ljungman, M. 2007. The transcription stress response. *Cell Cycle* 6:2252-2257.

Lu, H.Y., B.M. Bauman, S. Arjunaraja, B. Dorjbal, J.D. Milner, A.L. Snow, and S.E. Turvey. 2018. The CBM-opathies-A rapidly expanding spectrum of human inborn errors of immunity caused by mutations in the CARD11-BCL10-MALT1 complex. *Front Immunol* 9:2078.

Ma, X.M., and J. Blenis. 2009. Molecular mechanisms of mTOR-mediated translational control. *Nat Rev Mol Cell Biol* 10:307-318.

Macian, F., F. Garcia-Cozar, S.H. Im, H.F. Horton, M.C. Byrne, and A. Rao. 2002. Transcriptional mechanisms underlying lymphocyte tolerance. *Cell* 109:719-731.

Mahajan, P.B. 1994. Modulation of transcription of rRNA genes by rapamycin. *Int J Immunopharmacol* 16:711-721.

Matsumoto, R., D. Wang, M. Blonska, H. Li, M. Kobayashi, B. Pappu, Y. Chen, D. Wang, and X. Lin. 2005. Phosphorylation of CARMA1 plays a critical role in T Cell receptor-mediated NF-kappaB activation. *Immunity* 23:575-585.

Mayer, C., and I. Grummt. 2006. Ribosome biogenesis and cell growth: mTOR coordinates transcription by all three classes of nuclear RNA polymerases. *Oncogene* 25:6384-6391.

Mayer, C., J. Zhao, X. Yuan, and I. Grummt. 2004. mTOR-dependent activation of the transcription factor TIF-IA links rRNA synthesis to nutrient availability. *Genes Dev* 18:423-434.

McGowan, K.A., J.Z. Li, C.Y. Park, V. Beaudry, H.K. Tabor, A.J. Sabnis, W. Zhang, H. Fuchs, M.H. de Angelis, R.M. Myers, L.D. Attardi, and G.S. Barsh. 2008. Ribosomal mutations cause p53-mediated dark skin and pleiotropic effects. *Nat Genet* 40:963-970.

McKenzie, I.F., G.M. Morgan, R.V. Blanden, R. Melvold, and H. Kohn. 1977. Studies of H-2 mutations in C57BL/6 and BALB/c mice. *Transplant Proc* 9:551-553.

McKenzie, I.F., G.M. Morgan, M.S. Sandrin, M.M. Michaelides, R.W. Melvold, and H.I. Kohn. 1979. B6.C-*H-2*^{bm12}. A new *H-2* mutation in the *I* region in the mouse. *J Exp Med* 150:1323-1338.

Meininger, I., and D. Krappmann. 2016. Lymphocyte signaling and activation by the CARMA1-BCL10-MALT1 signalosome. *Biol Chem* 397:1315-1333.

Melisi, D., and P.J. Chiao. 2007. NF-kappa B as a target for cancer therapy. *Expert Opin Ther Targets* 11:133-144.

Melnikov, S., A. Ben-Shem, N. Garreau de Loubresse, L. Jenner, G. Yusupova, and M. Yusupov. 2012. One core, two shells: bacterial and eukaryotic ribosomes. *Nat Struct Mol Biol* 19:560-567.

Meyuhas, O. 2015. Ribosomal Protein S6 Phosphorylation: Four Decades of Research. *Int Rev Cell Mol Biol* 320:41-73.

Moorefield, B., E.A. Greene, and R.H. Reeder. 2000. RNA polymerase I transcription factor Rrn3 is functionally conserved between yeast and human. *Proc Natl Acad Sci U S A* 97:4724-4729.

Moran, A.E., K.L. Holzapfel, Y. Xing, N.R. Cunningham, J.S. Maltzman, J. Punt, and K.A. Hogquist. 2011. T cell receptor signal strength in Treg and iNKT cell development demonstrated by a novel fluorescent reporter mouse. *J Exp Med* 208:1279-1289.

Narayan, P., B. Holt, R. Tosti, and L.P. Kane. 2006. CARMA1 is required for Akt-mediated NF-kappaB activation in T cells. *Mol Cell Biol* 26:2327-2336.

Nemeth, A., and I. Grummt. 2018. Dynamic regulation of nucleolar architecture. *Curr Opin Cell Biol* 52:105-111.

O'Reilly, K.E., F. Rojo, Q.B. She, D. Solit, G.B. Mills, D. Smith, H. Lane, F. Hofmann, D.J. Hicklin, D.L. Ludwig, J. Baselga, and N. Rosen. 2006. mTOR inhibition induces upstream receptor tyrosine kinase signaling and activates Akt. *Cancer Res* 66:1500-1508.

O'Sullivan, D. 2019. The metabolic spectrum of memory T cells. *Immunol Cell Biol* 97:636-646.

Obst, R. 2015. The timing of T cell priming and cycling. *Front Immunol* 6:563.

Obst, R., H.M. van Santen, R. Melamed, A.O. Kamphorst, C. Benoist, and D. Mathis. 2007. Sustained antigen presentation can promote an immunogenic T cell response, like dendritic cell activation. *Proc Natl Acad Sci U S A* 104:15460-15465.

Oh-hora, M., and A. Rao. 2008. Calcium signaling in lymphocytes. *Curr Opin Immunol* 20:250-258.

Otto, T., and P. Sicinski. 2017. Cell cycle proteins as promising targets in cancer therapy. *Nat Rev Cancer* 17:93-115.

Pan, M., W.C. Wright, R.H. Chapple, A. Zubair, M. Sandhu, J.E. Batchelder, B.C. Huddle, J. Low, K.B. Blankenship, Y. Wang, B. Gordon, P. Archer, S.W. Brady, S. Natarajan, M.J. Posgai, J. Schuetz, D. Miller, R. Kalathur, S. Chen, J.P. Connelly, M.M. Babu, M.A. Dyer, S.M. Pruett-Miller, B.B. Freeman, 3rd, T. Chen, L.A. Godley, S.C. Blanchard, E. Stewart, J. Easton, and P. Geeleher. 2021. The chemotherapeutic CX-5461 primarily targets TOP2B and exhibits selective activity in high-risk neuroblastoma. *Nat Commun* 12:6468.

Parlato, R., G. Kreiner, G. Erdmann, C. Rieker, S. Stotz, E. Savenkova, S. Berger, I. Grummt, and G. Schutz. 2008. Activation of an endogenous suicide response after perturbation of rRNA synthesis leads to neurodegeneration in mice. *J Neurosci* 28:12759-12764.

Pearce, E.L., M.C. Poffenberger, C.H. Chang, and R.G. Jones. 2013. Fueling immunity: insights into metabolism and lymphocyte function. *Science* 342:1242454.

Pearce, L.R., X. Huang, J. Boudeau, R. Pawlowski, S. Wullschleger, M. Deak, A.F. Ibrahim, R. Gourlay, M.A. Magnuson, and D.R. Alessi. 2007. Identification of Protor as a novel Rictor-binding component of mTOR complex-2. *Biochem J* 405:513-522.

Pearce, L.R., E.M. Sommer, K. Sakamoto, S. Wullschleger, and D.R. Alessi. 2011. Protor-1 is required for efficient mTORC2-mediated activation of SGK1 in the kidney. *Biochem J* 436:169-179.

Peltonen, K., L. Colis, H. Liu, S. Jaamaa, H.M. Moore, J. Enback, P. Laakkonen, A. Vaahtokari, R.J. Jones, T.M. af Hallstrom, and M. Laiho. 2010. Identification of novel p53 pathway activating small-molecule compounds reveals unexpected similarities with known therapeutic agents. *PLoS One* 5:e12996.

Peltonen, K., L. Colis, H. Liu, R. Trivedi, M.S. Moubarek, H.M. Moore, B. Bai, M.A. Rudek, C.J. Bieberich, and M. Laiho. 2014. A targeting modality for destruction of RNA polymerase I that possesses anticancer activity. *Cancer Cell* 25:77-90.

Pennavaria, S. 2019. mTORC1-dependent RNA synthesis in proliferating T cells. Dissertation. In LMU München, Medizinische Fakultät, published online at edoc.ub.uni-muenchen.de.

Percharde, M., A. Bulut-Karslioglu, and M. Ramalho-Santos. 2017. Hypertranscription in Development, Stem Cells, and Regeneration. *Dev Cell* 40:9-21.

Peterson, T.R., M. Laplante, C.C. Thoreen, Y. Sancak, S.A. Kang, W.M. Kuehl, N.S. Gray, and D.M. Sabatini. 2009. DEPTOR is an mTOR inhibitor frequently overexpressed in multiple myeloma cells and required for their survival. *Cell* 137:873-886.

Pipkin, M.E., J.A. Sacks, F. Cruz-Guilloty, M.G. Lichtenheld, M.J. Bevan, and A. Rao. 2010. Interleukin-2 and inflammation induce distinct transcriptional programs that promote the differentiation of effector cytolytic T cells. *Immunity* 32:79-90.

Pitts, S., and M. Laiho. 2022. Regulation of RNA Polymerase I Stability and Function. *Cancers (Basel)* 14:

Pitts, S., H. Liu, A. Ibrahim, A. Garg, C.M. Felgueira, A. Begum, W. Fan, S. Teh, J.Y. Low, B. Ford, D.A. Schneider, R. Hay, and M. Laiho. 2022. Identification of an E3 ligase that targets the catalytic subunit of RNA Polymerase I upon transcription stress. *J Biol Chem* 298:102690.

Pollizzi, K.N., C.H. Patel, I.H. Sun, M.H. Oh, A.T. Waickman, J. Wen, G.M. Delgoffe, and J.D. Powell. 2015. mTORC1 and mTORC2 selectively regulate $CD8^+$ T cell differentiation. *J Clin Invest* 125:2090-2108.

Pollizzi, K.N., and J.D. Powell. 2015. Regulation of T cells by mTOR: the known knowns and the known unknowns. *Trends Immunol* 36:13-20.

Popov, A., E. Smirnov, L. Kovacik, O. Raska, G. Hagen, L. Stixova, and I. Raska. 2013. Duration of the first steps of the human rRNA processing. *Nucleus* 4:134-141.

Powell, J.D., K.N. Pollizzi, E.B. Heikamp, and M.R. Horton. 2012. Regulation of immune responses by mTOR. *Annu Rev Immunol* 30:39-68.

Preston, G.C., L.V. Sinclair, A. Kaskar, J.L. Hukelmann, M.N. Navarro, I. Ferrero, H.R. MacDonald, V.H. Cowling, and D.A. Cantrell. 2015. Single cell tuning of Myc expression by antigen receptor signal strength and interleukin-2 in T lymphocytes. *EMBO J* 34:2008-2024.

Rao, R.R., Q. Li, K. Odunsi, and P.A. Shrikant. 2010. The mTOR kinase determines effector versus memory $CD8^+$ T cell fate by regulating the expression of transcription factors T-bet and Eomesodermin. *Immunity* 32:67-78.

Rickards, B., S.J. Flint, M.D. Cole, and G. LeRoy. 2007. Nucleolin is required for RNA polymerase I transcription in vivo. *Mol Cell Biol* 27:937-948.

Robertson, N., V. Shchepachev, D. Wright, T.W. Turowski, C. Spanos, A. Helwak, R. Zamoyska, and D. Tollervey. 2022. A disease-linked lncRNA mutation in RNase MRP inhibits ribosome synthesis. *Nat Commun* 13:649.

Robitaille, A.M., S. Christen, M. Shimobayashi, M. Cornu, L.L. Fava, S. Moes, C. Prescianotto-Baschong, U. Sauer, P. Jenoe, and M.N. Hall. 2013. Quantitative phosphoproteomics reveal mTORC1 activates de novo pyrimidine synthesis. *Science* 339:1320-1323.

Rollings, C.M., L.V. Sinclair, H.J.M. Brady, D.A. Cantrell, and S.H. Ross. 2018. Interleukin-2 shapes the cytotoxic T cell proteome and immune environment-sensing programs. *Sci Signal* 11:526.

Rosenberg, A.S., and A. Singer. 1992. Cellular basis of skin allograft rejection: an in vivo model of immune-mediated tissue destruction. *Annu Rev Immunol* 10:333-358.

Ross, S.H., and D.A. Cantrell. 2018. Signaling and Function of Interleukin-2 in T Lymphocytes. *Annu Rev Immunol* 36:411-433.

Rowell, E.A., L. Wang, W.W. Hancock, and A.D. Wells. 2006. The cyclin-dependent kinase inhibitor p27kip1 is required for transplantation tolerance induced by costimulatory blockade. *J Immunol* 177:5169-5176.

Rubbi, C.P., and J. Milner. 2003. Disruption of the nucleolus mediates stabilization of p53 in response to DNA damage and other stresses. *EMBO J* 22:6068-6077.

Ruland, J., and L. Hartjes. 2019. CARD-BCL-10-MALT1 signalling in protective and pathological immunity. *Nat Rev Immunol* 19:118-134.

Russo, A., and G. Russo. 2017. Ribosomal proteins control or bypass p53 during nucleolar stress. *Int J Mol Sci* 18:1.

Sabatini, D.M., H. Erdjument-Bromage, M. Lui, P. Tempst, and S.H. Snyder. 1994. RAFT1: a mammalian protein that binds to FKBP12 in a rapamycin-dependent fashion and is homologous to yeast TORs. *Cell* 78:35-43.

Sabers, C.J., M.M. Martin, G.J. Brunn, J.M. Williams, F.J. Dumont, G. Wiederrecht, and R.T. Abraham. 1995. Isolation of a protein target of the FKBP12-rapamycin complex in mammalian cells. *J Biol Chem* 270:815-822.

Salmond, R.J., R.J. Brownlie, O. Meyuhas, and R. Zamoyska. 2015. Mechanistic target of rapamycin complex 1/S6 kinase 1 signals influence T cell activation independently of ribosomal protein S6 phosphorylation. *J Immunol* 195:4615-4622.

Salmond, R.J., J. Emery, K. Okkenhaug, and R. Zamoyska. 2009. MAPK, phosphatidylinositol 3-kinase, and mammalian target of rapamycin pathways converge at the level of ribosomal protein S6 phosphorylation to control metabolic signaling in CD8 T cells. *J Immunol* 183:7388-7397.

Samelson, L.E. 2002. Signal transduction mediated by the T cell antigen receptor: the role of adapter proteins. *Annu Rev Immunol* 20:371-394.

Sancak, Y., C.C. Thoreen, T.R. Peterson, R.A. Lindquist, S.A. Kang, E. Spooner, S.A. Carr, and D.M. Sabatini. 2007. PRAS40 is an insulin-regulated inhibitor of the mTORC1 protein kinase. *Mol Cell* 25:903-915.

Sarbassov, D.D., S.M. Ali, D.H. Kim, D.A. Guertin, R.R. Latek, H. Erdjument-Bromage, P. Tempst, and D.M. Sabatini. 2004. Rictor, a novel binding partner of mTOR, defines a rapamycin-insensitive and raptor-independent pathway that regulates the cytoskeleton. *Curr Biol* 14:1296-1302.

Sawada, S., J.D. Scarborough, N. Killeen, and D.R. Littman. 1994. A lineage-specific transcriptional silencer regulates CD4 gene expression during T lymphocyte development. *Cell* 77:917-929.

Saxton, R.A., C.R. Glassman, and K.C. Garcia. 2023. Emerging principles of cytokine pharmacology and therapeutics. *Nat Rev Drug Discov* 22:21-37.

Saxton, R.A., and D.M. Sabatini. 2017. mTOR signaling in growth, metabolism, and disease. *Cell* 169:361-371.

Schnapp, A., G. Schnapp, B. Erny, and I. Grummt. 1993. Function of the growth-regulated transcription initiation factor TIF-IA in initiation complex formation at the murine ribosomal gene promoter. *Mol Cell Biol* 13:6723-6732.

Schneider, D.A., A. Michel, M.L. Sikes, L. Vu, J.A. Dodd, S. Salgia, Y.N. Osheim, A.L. Beyer, and M. Nomura. 2007. Transcription elongation by RNA polymerase I is linked to efficient rRNA processing and ribosome assembly. *Mol Cell* 26:217-229.

Schulze-Luehrmann, J., and S. Ghosh. 2006. Antigen-receptor signaling to nuclear factor kappa B. *Immunity* 25:701-715.

Schwartz, D.M., Y. Kanno, A. Villarino, M. Ward, M. Gadina, and J.J. O'Shea. 2017. JAK inhibition as a therapeutic strategy for immune and inflammatory diseases. *Nat Rev Drug Discov* 17:78.

Sengupta, S., T.R. Peterson, M. Laplante, S. Oh, and D.M. Sabatini. 2010. mTORC1 controls fasting-induced ketogenesis and its modulation by ageing. *Nature* 468:1100-1104.

Shah, K., A. Al-Haidari, J. Sun, and J.U. Kazi. 2021. T cell receptor (TCR) signaling in health and disease. *Signal Transduct Target Ther* 6:412.

Shapiro, H.M. 1981. Flow cytometric estimation of DNA and RNA content in intact cells stained with Hoechst 33342 and pyronin Y. *Cytometry* 2:143-150.

Shor, B., J. Wu, Q. Shakey, L. Toral-Barza, C. Shi, M. Follettie, and K. Yu. 2010. Requirement of the mTOR kinase for the regulation of Maf1 phosphorylation and control of RNA polymerase III-dependent transcription in cancer cells. *J Biol Chem* 285:15380-15392.

Sinclair, L.V., D. Finlay, C. Feijoo, G.H. Cornish, A. Gray, A. Ager, K. Okkenhaug, T.J. Hagenbeek, H. Spits, and D.A. Cantrell. 2008. Phosphatidylinositol-3-OH kinase and nutrient-sensing mTOR pathways control T lymphocyte trafficking. *Nat Immunol* 9:513-521.

Skrtic, M., S. Sriskanthadevan, B. Jhas, M. Gebbia, X. Wang, Z. Wang, R. Hurren, Y. Jitkova, M. Gronda, N. Maclean, C.K. Lai, Y. Eberhard, J. Bartoszko, P. Spagnuolo, A.C. Rutledge, A. Datti, T. Ketela, J. Moffat, B.H. Robinson, J.H. Cameron, J. Wrana, C.J. Eaves, M.D. Minden, J.C. Wang, J.E. Dick, K. Humphries, C. Nislow, G. Giaever, and A.D. Schimmer. 2011. Inhibition of mitochondrial translation as a therapeutic strategy for human acute myeloid leukemia. *Cancer Cell* 20:674-688.

So, T., and M. Croft. 2012. Regulation of the PKCtheta-NF-kappaB axis in T lymphocytes by the tumor necrosis factor receptor family member OX40. *Front Immunol* 3:133.

Sowell, R.T., M. Rogozinska, C.E. Nelson, V. Vezys, and A.L. Marzo. 2014. Cutting edge: generation of effector cells that localize to mucosal tissues and form resident memory CD8 T cells is controlled by mTOR. *J Immunol* 193:2067-2071.

Srivastava, M., and H.B. Pollard. 1999. Molecular dissection of nucleolin's role in growth and cell proliferation: new insights. *FASEB J* 13:1911-1922.

Steitz, T.A. 2008. A structural understanding of the dynamic ribosome machine. *Nat Rev Mol Cell Biol* 9:242-253.

Storck, S., M. Thiry, and P. Bouvet. 2009. Conditional knockout of nucleolin in DT40 cells reveals the functional redundancy of its RNA-binding domains. *Biol Cell* 101:153-167.

Suchin, E.J., P.B. Langmuir, E. Palmer, M.H. Sayegh, A.D. Wells, and L.A. Turka. 2001. Quantifying the frequency of alloreactive T cells in vivo: new answers to an old question. *J Immunol* 166:973-981.

Sulic, S., L. Panic, M. Barkic, M. Mercep, M. Uzelac, and S. Volarevic. 2005. Inactivation of S6 ribosomal protein gene in T lymphocytes activates a p53-dependent checkpoint response. *Genes Dev* 19:3070-3082.

Sun, L., L. Deng, C.K. Ea, Z.P. Xia, and Z.J. Chen. 2004. The TRAF6 ubiquitin ligase and TAK1 kinase mediate IKK activation by BCL10 and MALT1 in T lymphocytes. *Mol Cell* 14:289-301.

Sun, S., X. Zhang, D.F. Tough, and J. Sprent. 1998. Type I interferon-mediated stimulation of T cells by CpG DNA. *J Exp Med* 188:2335-2342.

Szaflarski, W., M. Lesniczak-Staszak, M. Sowinski, S. Ojha, A. Aulas, D. Dave, S. Malla, P. Anderson, P. Ivanov, and S.M. Lyons. 2022. Early rRNA processing is a stress-dependent regulatory event whose inhibition maintains nucleolar integrity. *Nucleic Acids Res* 50:1033-1051.

Szymanski, J., C. Mayer, U. Hoffmann-Rohrer, C. Kalla, I. Grummt, and M. Weiss. 2009. Dynamic subcellular partitioning of the nucleolar transcription factor TIF-IA under ribotoxic stress. *Biochim Biophys Acta* 1793:1191-1198.

Tan, H., K. Yang, Y. Li, T.I. Shaw, Y. Wang, D.B. Blanco, X. Wang, J.H. Cho, H. Wang, S. Rankin, C. Guy, J. Peng, and H. Chi. 2017. Integrative proteomics and phosphoproteomics profiling reveals dynamic signaling networks and bioenergetics pathways underlying T cell activation. *Immunity* 46:488-503.

Tang, F., Q. Wu, T. Ikenoue, K.L. Guan, Y. Liu, and P. Zheng. 2012. A critical role for Rictor in T lymphopoiesis. *J Immunol* 189:1850-1857.

Taylor, A.M., J.M. Humphries, R.M. White, R.D. Murphey, C.E. Burns, and L.I. Zon. 2012. Hematopoietic defects in rps29 mutant zebrafish depend upon p53 activation. *Exp Hematol* 40:228-237 e225.

Tee, A.R., B.D. Manning, P.P. Roux, L.C. Cantley, and J. Blenis. 2003. Tuberous sclerosis complex gene products, Tuberin and Hamartin, control mTOR signaling by acting as a GTPase-activating protein complex toward Rheb. *Curr Biol* 13:1259-1268.

Terada, N., R.A. Franklin, J.J. Lucas, J. Blenis, and E.W. Gelfand. 1993a. Failure of rapamycin to block proliferation once resting cells have entered the cell cycle despite inactivation of p70 S6 kinase. *J Biol Chem* 268:12062-12068.

Terada, N., J.J. Lucas, A. Szepesi, R.A. Franklin, J. Domenico, and E.W. Gelfand. 1993b. Rapamycin blocks cell cycle progression of activated T cells prior to events characteristic of the middle to late G1 phase of the cycle. *J Cell Physiol* 154:7-15.

Thedieck, K., P. Polak, M.L. Kim, K.D. Molle, A. Cohen, P. Jeno, C. Arrieumerlou, and M.N. Hall. 2007. PRAS40 and PRR5-like protein are new mTOR interactors that regulate apoptosis. *PLoS One* 2:e1217.

Thielmann, H.W., O. Popanda, and H.J. Staab. 1999. Subnuclear distribution of DNA topoisomerase I and Bax protein in normal and xeroderma pigmentosum fibroblasts after irradiation with UV light and gamma rays or treatment with topotecan. *J Cancer Res Clin Oncol* 125:193-208.

Thiry, M., F. Lamaye, and D.L. Lafontaine. 2011. The nucleolus: when 2 became 3. *Nucleus* 2:289-293.

Thoreen, C.C., L. Chantranupong, H.R. Keys, T. Wang, N.S. Gray, and D.M. Sabatini. 2012. A unifying model for mTORC1-mediated regulation of mRNA translation. *Nature* 485:109-113.

Thoreen, C.C., S.A. Kang, J.W. Chang, Q. Liu, J. Zhang, Y. Gao, L.J. Reichling, T. Sim, D.M. Sabatini, and N.S. Gray. 2009. An ATP-competitive mammalian target of rapamycin inhibitor reveals rapamycin-resistant functions of mTORC1. *J Biol Chem* 284:8023-8032.

Tsang, C.K., H. Liu, and X.F. Zheng. 2010. mTOR binds to the promoters of RNA polymerase I- and III-transcribed genes. *Cell Cycle* 9:953-957.

Turner, A.P., V.O. Shaffer, K. Araki, C. Martens, P.L. Turner, S. Gangappa, M.L. Ford, R. Ahmed, A.D. Kirk, and C.P. Larsen. 2011. Sirolimus enhances the magnitude and quality of viral-specific $CD8^+$ T-cell responses to vaccinia virus vaccination in rhesus macaques. *Am J Transplant* 11:613-618.

Tzur, A., J.K. Moore, P. Jorgensen, H.M. Shapiro, and M.W. Kirschner. 2011. Optimizing optical flow cytometry for cell volume-based sorting and analysis. *PLoS One* 6:e16053.

Um, S.H., D. D'Alessio, and G. Thomas. 2006. Nutrient overload, insulin resistance, and ribosomal protein S6 kinase 1, S6K1. *Cell Metab* 3:393-402.

Vakkilainen, S., M. Taskinen, and O. Makitie. 2020. Immunodeficiency in cartilage-hair hypoplasia: Pathogenesis, clinical course and management. *Scand J Immunol* 92:e12913.

Valvezan, A.J., M. Turner, A. Belaid, H.C. Lam, S.K. Miller, M.C. McNamara, C. Baglini, B.E. Housden, N. Perrimon, D.J. Kwiatkowski, J.M. Asara, E.P. Henske, and B.D. Manning. 2017. mTORC1 couples nucleotide synthesis to nucleotide demand resulting in a targetable metabolic vulnerability. *Cancer Cell* 32:624-638 e625.

van Riggelen, J., A. Yetil, and D.W. Felsher. 2010. MYC as a regulator of ribosome biogenesis and protein synthesis. *Nat Rev Cancer* 10:301-309.

Vander Haar, E., S.I. Lee, S. Bandhakavi, T.J. Griffin, and D.H. Kim. 2007. Insulin signalling to mTOR mediated by the Akt/PKB substrate PRAS40. *Nat Cell Biol* 9:316-323.

Vlachos, A., P.S. Rosenberg, E. Atsidaftos, B.P. Alter, and J.M. Lipton. 2012. Incidence of neoplasia in Diamond Blackfan anemia: a report from the Diamond Blackfan Anemia Registry. *Blood* 119:3815-3819.

Wang, B.T., G.S. Ducker, A.J. Barczak, R. Barbeau, D.J. Erle, and K.M. Shokat. 2011a. The mammalian target of rapamycin regulates cholesterol biosynthetic gene expression and exhibits a rapamycin-resistant transcriptional profile. *Proc Natl Acad Sci U S A* 108:15201-15206.

Wang, L., T.E. Harris, R.A. Roth, and J.C. Lawrence, Jr. 2007. PRAS40 regulates mTORC1 kinase activity by functioning as a direct inhibitor of substrate binding. *J Biol Chem* 282:20036-20044.

Wang, R., C.P. Dillon, L.Z. Shi, S. Milasta, R. Carter, D. Finkelstein, L.L. McCormick, P. Fitzgerald, H. Chi, J. Munger, and D.R. Green. 2011b. The transcription factor Myc controls metabolic reprogramming upon T lymphocyte activation. *Immunity* 35:871-882.

Wang, Y., X.Y. Wang, J.R. Subjeck, P.A. Shrikant, and H.L. Kim. 2011c. Temsirolimus, an mTOR inhibitor, enhances anti-tumour effects of heat shock protein cancer vaccines. *Br J Cancer* 104:643-652.

Warner, J.R. 1999. The economics of ribosome biosynthesis in yeast. *Trends Biochem Sci* 24:437-440.

Wei, T., S.M. Najmi, H. Liu, K. Peltonen, A. Kucerova, D.A. Schneider, and M. Laiho. 2018. Small-Molecule Targeting of RNA Polymerase I Activates a Conserved Transcription Elongation Checkpoint. *Cell Rep* 23:404-414.

Weil, R., and A. Israel. 2006. Deciphering the pathway from the TCR to NF-kappaB. *Cell Death Differ* 13:826-833.

Wells, A.D., and P.A. Morawski. 2014. New roles for cyclin-dependent kinases in T cell biology: linking cell division and differentiation. *Nat Rev Immunol* 14:261-270.

Wolf, T., W. Jin, G. Zoppi, I.A. Vogel, M. Akhmedov, C.K.E. Bleck, T. Beltraminelli, J.C. Rieckmann, N.J. Ramirez, M. Benevento, S. Notarbartolo, D. Bumann, F. Meissner, B. Grimbacher, M. Mann, A. Lanzavecchia, F. Sallusto, I. Kwee, and R. Geiger. 2020. Dynamics in protein translation sustaining T cell preparedness. *Nat Immunol* 21:927-937.

Xia, F., C.R. Qian, Z. Xun, Y. Hamon, A.M. Sartre, A. Formisano, S. Mailfert, M.C. Phelipot, C. Billaudeau, S. Jaeger, J.A. Nunes, X.J. Guo, and H.T. He. 2018. TCR and CD28 concomitant stimulation elicits a distinctive calcium response in naive T cells. *Front Immunol* 9:2864.

Yang, K., G. Neale, D.R. Green, W. He, and H. Chi. 2011. The tumor suppressor Tsc1 enforces quiescence of naive T cells to promote immune homeostasis and function. *Nat Immunol* 12:888-897.

Yang, K., S. Shrestha, H. Zeng, P.W. Karmaus, G. Neale, P. Vogel, D.A. Guertin, R.F. Lamb, and H. Chi. 2013. T cell exit from quiescence and differentiation into Th2 cells depend on Raptor-mTORC1-mediated metabolic reprogramming. *Immunity* 39:1043-1056.

Yang, K., M. Wang, Y. Zhao, X. Sun, Y. Yang, X. Li, A. Zhou, H. Chu, H. Zhou, J. Xu, M. Wu, J. Yang, and J. Yi. 2016. A redox mechanism underlying nucleolar stress sensing by nucleophosmin. *Nat Commun* 7:13599.

Yogev, O., K. Saadon, S. Anzi, K. Inoue, and E. Shaulian. 2008. DNA damage-dependent translocation of B23 and p19 ARF is regulated by the Jun N-terminal kinase pathway. *Cancer Res* 68:1398-1406.

Yoon, H., T.S. Kim, and T.J. Braciale. 2010. The cell cycle time of $CD8^+$ T cells responding in vivo is controlled by the type of antigenic stimulus. *PLoS One* 5:e15423.

Youngblood, B., J.S. Hale, H.T. Kissick, E. Ahn, X. Xu, A. Wieland, K. Araki, E.E. West, H.E. Ghoneim, Y. Fan, P. Dogra, C.W. Davis, B.T. Konieczny, R. Antia, X. Cheng, and R. Ahmed. 2017. Effector CD8 T cells dedifferentiate into long-lived memory cells. *Nature* 552:404-409.

Yuan, X., Y. Zhou, E. Casanova, M. Chai, E. Kiss, H.J. Grone, G. Schutz, and I. Grummt. 2005. Genetic inactivation of the transcription factor TIF-IA leads to nucleolar disruption, cell cycle arrest, and p53-mediated apoptosis. *Mol Cell* 19:77-87.

Yung, B.Y., R.K. Busch, H. Busch, A.B. Mauger, and P.K. Chan. 1985. Effects of actinomycin D analogs on nucleolar phosphoprotein B23 (37,000 daltons/pI 5.1). *Biochem Pharmacol* 34:4059-4063.

Zhong, X.P., R. Guo, H. Zhou, C. Liu, and C.K. Wan. 2008. Diacylglycerol kinases in immune cell function and self-tolerance. *Immunol Rev* 224:249-264.

Zhou, X., Q. Hao, J.M. Liao, P. Liao, and H. Lu. 2013. Ribosomal protein S14 negatively regulates c-Myc activity. *J Biol Chem* 288:21793-21801.

Zhu, Z., and G.K.K. Leung. 2020. More than a metabolic enzyme: MTHFD2 as a novel target for anticancer therapy? *Front Oncol* 10:658.

Zikherman, J., R. Parameswaran, and A. Weiss. 2012. Endogenous antigen tunes the responsiveness of naive B cells but not T cells. *Nature* 489:160-164.

Acknowledgements

First, I want to thank my supervisor PD Dr. Reinhard Obst for the opportunity to work on this project in his lab and for all the constant support, discussions, and ideas during my whole doctoral study. At the same time my thanks go to Prof. Dr. Thomas Brocker for giving me the opportunity to work at the Institute for Immunology.
Furthermore, I would like to thank the SFB1054 and the associated IRTG for financial support, excellent training opportunities and workshops, as well as professional and informative, but as well enjoyable retreats.
I also want to thank all the animal caretakers in the Core Facility Animal Models at the BMC for animal husbandry and their quick and reliable work.
I want to thank the whole AG Obst with Stefanie Pennavaria, for introducing me into the project, Anne Trefzer, Pallavi Kadam, Simone Pentz, Anna Kollar and Josephine Wieland for nice discussions, great coffee breaks and constant emotional and professional support and all the fun that we had over all the years.
Special thanks also go to Jan Kranich and Lisa Rausch for instructing me at the Amnis, especially Jan for performing Amnis analyses on cellular structures and spot counts of nucleoli.
Thanks to Gesine Behrens and Timsse Raj for helping me with Western Blotting.
Special thanks also go to Lisa Richter and Pardis Khosravani from the FACS Core Facility for all the introductions and support at the FACS machines, as well as performing cell sorting for my experiments.
My overall thanks go to all colleagues at the Institute for Immunology for great discussions, lunch breaks, parties, and a great working atmosphere. Especially to Anne Trefzer, Pallavi Kadam, Sebastian Teschner, Tilman Kurz and Lisa Rausch for all the fun and making it an overall great and memorable time!
Finally, I want to thank my family and my husband Julian for continuous support during this challenging and exciting phase.

Affidavit

LMU LUDWIG-MAXIMILIANS-UNIVERSITÄT MÜNCHEN

Dekanat Medizinische Fakultät
Promotionsbüro

Affidavit

Rosenlehner, Teresa

Surname, first name

I hereby declare, that the submitted thesis entitled

Reciprocal regulation of mTORC1 and ribosomal biosynthesis determines cell cycle progression in activated T cells.

is my own work. I have only used the sources indicated and have not made unauthorised use of services of a third party. Where the work of others has been quoted or reproduced, the source is always given.

I further declare that the dissertation presented here has not been submitted in the same or similar form to any other institution for the purpose of obtaining an academic degree.

München, 18.10.2024

Place, Date

Teresa Rosenlehner

Signature doctoral candidate

Confirmation of congruency

LMU LUDWIG-MAXIMILIANS-UNIVERSITÄT MÜNCHEN

Dekanat Medizinische Fakultät
Promotionsbüro

Confirmation of congruency between printed and electronic version of the doctoral thesis

Doctoral candidate: Teresa Rosenlehner

Address: Josef-Frankl-Str., 17a, 80995 München

I hereby declare that the electronic version of the submitted thesis, entitled

Reciprocal regulation of mTORC1 and ribosomal biosynthesis determines cell cycle progression in activated T cells.

is congruent with the printed version both in content and format.

München, 18.10.2024
Place, Date

Teresa Rosenlehner
Signature doctoral candidate

List of publications

First author publication

“Reciprocal regulation of mTORC1 and ribosomal biosynthesis determines cell cycle progression in activated T cells”, Teresa Rosenlehner*, Stefanie Pennavaria*, Batuhan Akçabozan, Tobias Straub, Jan Kranich, Reinhard Obst, *submitted for publication*

Congress contribution

“Reciprocal regulation of mTORC1 and ribosomal biosynthesis determines cell cycle progression in activated T cells”, AAI Meeting 2021, Teresa Rosenlehner*, Stefanie Pennavaria, Tobias Straub, Jan Kranich, Reinhard Obst (presentation and poster)